Title
Adenovirus: A Versatile Tool for Studying and Treating Diseases

Author
Moberg Parker, Jordan

Publication Date
2012

Peer reviewed|Thesis/dissertation

UNIVERSITY OF CALIFORNIA

Los Angeles

Adenovirus:
A Versatile Tool for Studying and Treating Diseases

A dissertation submitted in partial satisfaction of the
requirements for the degree Doctor of Philosophy in
Molecular Biology

by

Jordan Moberg Parker

2012

ABSTRACT OF THE DISSERTATION

Adenovirus: A Versatile Tool for Studying and Treating Diseases

by

Jordan Moberg Parker

Doctor of Philosophy in Molecular Biology

University of California, Los Angeles, 2012

Professor Arnold J. Berk, Chair

Adenoviruses have taught us much about transcriptional regulation and cell cycle control because the cells they commonly infect are end-differentiated non-cycling cells. In order for these cells to be adequate hosts for viral replication, the virus must force the cells into the cell cycle. Adenoviruses express the small e1a protein immediately upon infection, which is responsible for initiating cell replication. Small e1a interacts with both the transcriptional co-activators p300/CBP and the transcriptional repressor RB-family proteins in order to induce epigenetic reprogramming that results in activation of cell cycle genes and inactivation of genes detrimental to adenoviral replication.

This work investigated how the specific interactions between e1a and p300/CBP or e1a and RB-family proteins affect the distribution of the H3K18ac marker throughout the genome and the subsequent changes in expression.

Cell cycle arrested cells were infected with adenovirus e1a mutants that either cannot interact with p300/CBP, or cannot interact with RB-family proteins. The genome wide distribution of the histone marker H3K18ac following infection with wild-type e1a or the e1a

mutants, compared to mock infected cells, was determined by chromatin immunoprecipitation with anti-H3K18ac antibody followed by massive parallel sequencing (ChIP-seq). Correlations between H3K18ac and expression levels were established through whole transcriptome sequencing (RNA-seq).

We have found that a simple model can only begin to describe the complex interactions between e1a and it's cellular partners. The e1a interaction with p300/CBP appears to be more important for global hypoacetylation than the interaction with RB-family proteins, but surprisingly, the e1a and RB interaction is required for hyperacetylation and activation of cell cycle promoters.

The second half of this work focuses on the construction and validation of an adenovirus "helper virus" for targeting the Helper Dependent Adenovirus/Epstein Barr virus (HDAd/EBV) hybrid system targeted to Hematopoietic stem cells by a chimeric Ad5/35 fiber. The challenges associated with developing an adenovirus replication permissive cell line (HEK293) with adequate levels of FLPe expression to limit helper virus contamination in the HDAd/EBV vector stock are also discussed.

The dissertation of Kristina May Clark is approved.

Lily Wu

Matteo Pellegrini

Siavash K. Kurdistani

Harvey R. Herschman

Arnold J. Berk, Committee Chair

University of California, Los Angeles

2012

TABLE OF CONTENTS

TABLES AND FIGURES

CHAPTER 1

CHAPTER 2

CHAPTER 3

ACKNOWLEDGMENTS

As a high school student I was fascinated with the idea of gene therapy. I decided I had to be a scientist so I could so I could cure diseases in such a cool and elegant way. So, much credit must go to Mr. John Hayes, the one and only science teacher at Freeman High School, for setting me on the path that has led me here.

Dr. Susan Elrod at Cal Poly, San Luis Obispo, and Dr. Erin Sanders at UCLA have not only been mentors, but also role models who's dedication to education continues to inspire me.

I could not have survived grad school without my friends! Mara Sherman and Meghan Mclean have been with me since the first day and are the key characters in all of my best grad school memories. Many bottles of wine have met their end at our hands. Our stint as International Scientists in Japan was one of the most incredible experiences of my life! MFK!!!

I would like to thank all of my friends and colleagues in the Berk Lab who made the day-to-day bearable and even entertaining. Carol is the heart of the lab and none of us would have been able to do our jobs without her. Miguel Nava and Dawei Guo helped me transition to the new and terrifying realm of transcription. I have picked on Sarah Johnson like a little sister, but she was always there to lend me an ear and buy me a beer.

I have been truly fortunate to be a member of Arnie Berk's lab. Not only is he an uncannily talented scientist and a cultured opera lover, but a supportive mentor and really nice guy. There were people at each stage of my research without whom my dissertation would not have been possible. Sean Gallaher, friend and mentor extraordinaire, has been instrumental in shaping my grad school career. His excellent advice and guidance on the gene therapy vector project were second only to his unwavering friendship. He also makes a mean mai tai. Odisse

Azizgolshani provided the inspiration and know-how for the Sindbis aspects of the FLPe project. Her meticulous attention to detail and extremely giving nature make her an ideal collaborator, and her big heart makes her a wonderful friend.

The ChIP-seq project would not have been possible without the bioinformatics analysis, technical expertise, and guidance of Roberto Ferrari. I am extremely grateful for the countless hours he dedicated to helping me.

I think this is also the appropriate place to thank Dr. John Timmerman and all the staff of the UCLA Lymphoma Clinic for the amazing treatment and care I received at their hands. This year marks my fourth year in complete remission. I would also like to thank everyone for their support during that difficult time. My dedicated family and friends never let me go through chemo alone and saved me from hospital food. I would especially like to thank Arnie and Sally for being so supportive of me though the whole process and ungrudgingly giving me the time I needed to recover.

Finally, and most importantly, no words could ever express my love and gratitude for my incredible husband. We have been through so much together to get to this place, and I could not have done this without him. We survived long distance, cancer, and my dissertation, so I think that together we can face any challenges.

Funding

I received funding from the Cellular and Molecular Biology Training Grant from 2006-2009 and the Philip J. Whitcome Molecular Biology Interdepartmental Program Award in 2008. I was awarded a National Science Foundation Graduate Teaching Fellowship in K-12 Education for 2010-2011.

VITA

2003	B.S. in Microbiology, Minor in Biotechnology California Polytechnic State University, San Luis Obispo
2003 - 2005	Research Associate Center for Environmental Biotechnology, Earth Sciences Division Lawrence Berkeley National Laboratory, Berkeley, CA
2005-2012	Graduate Student Researcher Molecular Biology Interdepartmental Graduate Program University of California, Los Angeles
2006 - 2009	Undergraduate Research Mentor Undergraduate Research Center/Center for Academic and Research Excellence University of California, Los Angeles
2007, 2008	Teaching Assistant - Cell Biology of the Nucleus Microbiology, Immunology, and Molecular Genetics Department University of California, Los Angeles
2009-2010	Undergraduate Research Mentor Microbiology, Immunology, and Molecular Genetics Department University of California, Los Angeles
2010-2011	National Science Foundation GK-12 Graduate Teaching Fellow Science and Engineering of the Environment of Los Angeles University of California, Los Angeles
2011-2012	Teaching Assistant Consultant Microbiology, Immunology, and Molecular Genetics University of California, Los Angeles
2012	Expert Content Evaluator Office of Instructional Development University of California, Los Angeles

PRESENTATIONS AND PUBLICATIONS

Tokyo Institute of Technology Global Centers of Excellence (GCOE) Summer School
July 16-17, 2009 in Hayama, Kanagawa, Japan
"Evolving Education and Research Center for Spatio-Temporal Biological Network"

Shapiro, C., Ayon, C., Moberg-Parker, J., Levis-Fitzgerald, M., and Sanders, E.R. (2012). Strategies for Using Peer-Assisted Learning Effectively in an Undergraduate Bioinformatics Course. Biochemistry and Molecular Biology Education *In Press*.

Brodie, E.L., DeSantis, T.Z., Parker, J.P.M., Zubietta, I.X., Piceno, Y.M., and Andersen, G.L. (2007). Urban aerosols harbor diverse and dynamic bacterial populations. Proceedings of the National Academy of Sciences *104*, 299–304.

DeSantis, T.Z., Brodie, E.L., Moberg, J.P., Zubieta, I.X., Piceno, Y.M., and Andersen, G.L. (2007). High-density universal 16S rRNA microarray analysis reveals broader diversity than typical clone library when sampling the environment. Microbial Ecology *53*, 371–383.

DeSantis, T.Z., Stone, C.E., Murray, S.R., Moberg, J.P., and Andersen, G.L. (2006). Rapid quantification and taxonomic classification of environmental DNA from both prokaryotic and eukaryotic origins using a microarray. FEMS Microbiology Letters *245*, 271–278.

Chapter 1

INTRODUCTION

CHAPTER 1: ADENOVIRUS – A VERSATILE TOOL FOR MOLECULAR BIOLOGY

Viruses are thought of, first and foremost, as infectious agents that cause diseases ranging from the common cold to HIV/AIDS, but viruses are much more than that. Many different viruses have become powerful tools in the scientific arsenal. In 1952, Alfred Hershey and Martha Chase used bacteriophage to help confirm DNA as the genetic material (1). The ability of bacteriophages and other viruses to deliver their genetic material to a large variety of cell types make them useful for studying everything from basic biological processes to complex disease models (2). Adenoviruses in particular emerged as a very versatile tool for a variety of applications in molecular biology, such as the study of gene expression and regulation, cell cycle control and oncogenesis, and delivery of DNA for gene replacement therapy (3). This work focuses on the use of adenovirus as a model system for studying cancer and as a gene delivery vector for hematopoietic, or blood, diseases.

Adenoviruses make an attractive experimental system for a number of reasons:

1. They can be grown to high titers in the laboratory. Replication incompetent mutants deleted for E1 (discussed below) can be propagated in human embryonic kidney (HEK293 or 293) cells that are transformed with the left end of the Adenovirus type 5 (Ad5) genome and express the adenoviral E1A and E1B proteins (4).
2. They can initiate synchronous infections in cell culture (3).
3. The linear double stranded DNA genome is easy to manipulate (5–7).
4. They are able to infect both dividing and non-dividing cells in a wide variety of vertebrate hosts (3) through variable globular domains on fiber proteins extending from the icosahedral capsid shell (8–10).

ADENOVIRUS AS A CANCER MODEL SYSTEM

Although adenoviruses were first isolated in 1953 from human adenoid tissue as an etiological agent of acute respiratory illness (11–13), they have since been determined to only be responsible for a small percentage of cases (3). Just less than 10 years later, it was discovered that human adenovirus type 12 could induce malignant tumors in newborn hamsters, launching DNA tumor viruses as a specific field of study (14). Although adenoviruses have not been linked to tumors in humans (15), the ability to induce rodent tumors and transform human cell in culture has made adenoviruses ideal models system for studying the process of oncogenesis.

In the normal transmission of an adenovirus respiratory infection, adenovirus infects end-differentiated, G_0-arrested, respiratory epithelium cells. These cells have both low concentration of dNTPs and low rates of protein synthesis. Immediately upon infection, adenovirus must stimulate the infected cell to be a better host by re-entering the cell cycle, a process remarkably similar to oncogenic transformation. Adenovirus must transform the non-dividing respiratory cells into environments conducive to viral replication by inducing transcription of viral genes and forcing the cell into S-phase to supply the precursors needed for viral DNA, mRNA, and protein synthesis, as well as protecting the host cell from apoptosis (16). Adenovirus has evolved to accomplish this by interacting with and exploiting host proteins (3). We can apply what we learn by dissecting the mechanisms of these virus-host interactions to help us understand parallel processes that result in human cancers.

Adenovirus E1A

The adenovirus early region 1A (E1A) proteins have several important roles early in the infection process, including stimulating transcription of the other early expressed viral genes and

stimulating host cells into S-phase and through the cell cycle (17). Upon infection the adenoviral genome is transported to the nucleus, where the early region 1A (E1A) is the first transcriptional unit to be expressed (18) from a constitutively active enhancer (19). This transcript is processed into two main alternatively spliced mRNAs, the 13S and 12S, early in the infectious cycle (20). The 13S transcript encodes the "large E1A" 289 amino acid residue protein, and the 12S transcript encodes the "small e1a" 243 amino acid protein, which differs by 46 internal amino acids (21). E1A has five conserved regions (CR): the N-terminal region, CR1, CR2, CR3, and CR4 (22–25). The small e1a protein results from an alternative splicing that excludes CR3 (Fig. 1.1) (26).

E1A can stimulate G_0 and G_1 arrested cells to enter S-phase even without the presence of other mitogenic signals (17, 21, 27–29), but stable transformation of rodent cells requires cooperation with the adenoviral protein E1B, or the cellular oncoprotein activated (G12V) H-Ras (17, 28, 30). E1A cannot bind DNA directly, through the conserved domains, it interacts with an array of different cellular proteins that bind DNA (Fig. 1.2) (25, 31–34).

The CR3 region of large E1A is a strong transcriptional activator of the early and late viral promoters (21, 35, 36), and does so by interacting with host cellular transcription factors (36). The small e1a protein can stimulate low levels of early viral transcription (37), but it is primarily responsible for forcing G_0 arrested cells into the cell cycle (21, 27, 38).

Small e1a drives contact inhibited primary cells into S-phase

Small e1a lacks the CR3 transcriptional activator of viral promoters present in large E1A, but it is able to drive contact inhibited primary fibroblasts to not only begin DNA synthesis, but also to progress through the cell cycle (27, 39). This makes adenoviral mutants that only express

small e1a the ideal candidates to use in an adenoviral model of oncogenesis, since they would stimulate host cell replication without the interference of viral gene expression.

Both CR1 and CR2 of small e1a are required to transform primary cells in cooperation with E1B or activated RAS, but either CR1 or CR2 alone can drive G0 arrested cells into S-phase (28, 30). This ability of e1a to overcome the repressive mechanisms that maintain cells in a quiescent state, or "immortalize" cells to continue to divide, is a function of the interactions of e1a CR1 and CR2 with cellular host proteins (17).

Cell cycle induction by small e1a requires interaction with both RB and p300/CBP

CR1 and CR2 of E1A interact with a number of host proteins that were found to have important roles in the control of transcription and the cell cycle (28), including the product of the retinoblastoma tumor suppressor gene RB1 (40, 41) and the closely related paralogs RBL1 (p107) and RBL2 (p130), referred to collectively as RB-family proteins (42–44). CR1 also binds to the closely related transcriptional co-activators p300 (30, 42, 45, 46) and CBP (CREB binding protein) (32), referred to collectively as p300/CBP.

The e1a interaction with the retinoblastoma (RB) family proteins removes them from E2F-family transcription factors that regulate the genes needed to drive cells into S-phase (47–49). The p300/CBP proteins are multi-domain proteins that combine histone acetyltransferase (HAT) activity with specific transcriptional activation domains to regulate transcription through control of the chromatin condensation state (50–55).

Induction of cellular DNA synthesis requires interactions of both an RB-family protein and p300/CBP with e1a (28, 31, 40, 41, 47, 56). Formation of an e1a-RB-p300/CBP tri-molecular complex is closely correlated with the ability of e1a to induce proliferation in

quiescent primary cells (57).

Small e1a disrupts the binding of RB-family proteins to E2F transcription factors through the high affinity binding of the Leucine-X-Cysteine-X-Glutamic acid (LxCxE) motif between residues 122-126 of CR2, which is shared by HPV E7 and SV40 T-antigen (58), to the outside of the B-domain of RB (56, 59). This keeps the e1a in a high local concentration and allows the N-terminal amino acids of CR1 to bind to the "pocket domain" between the A and B domains and compete for binding with E2F (56, 58–60). The N-terminal region and the C-terminal region of CR1 of e1a interact with opposite faces of the transcriptional adaptor Zn-finger 2 (TAZ2) domain of CBP (60). The model by Ferreon et al. (Fig. 1.3) demonstrates that in the tri-molecular protein complex, e1a in effect clips CBP to RB in order to regulate their activities.

The interaction of e1a with RB proteins and p300/CBP was found to cause the re-localization of both RB proteins and p300/CBP histone acetyltransferases on promoters, with the result of epigenetic changes to the chromatin state and stimulation of cell cycle genes (61).

Chromatin structure effects transcriptional control

Small e1a must reconfigure the chromatin structure of host cells if it is to activate transcription of the genes needed to overcome the repressive mechanism that maintains cells in a quiescent state (29). The basic structure of chromatin consists of approximately 147 base pairs (bp) of DNA wrapped around an octamer of histone core proteins composed of two of each H2A, H2B, H3, and H4. The N-termini, and C-termini of H2A and H2B, tail domains of the histones extend out from the core octamer and are subject to a wide variety of covalent modifications that include: lysine acetylation, lysine and arginine methylation, serine and threonine phosphorylation, ADP- ribosylation, ubiquitination, and sumolation (62). Mis-targeting of these

chromatin modifications was found to be linked to cancer (62–64).

Histone acetylation, which occurs at lysines in the N-termini of histone tails, is closely tied to the transcriptional availability of genes. High levels of histone acetylation (hyperacetylation) are associated with decondensed transcriptionally active chromatin, while condensed transcriptionally silent chromatin usually has low levels of acetylation (hypoacetylation) (62, 65, 66). The acetylation state of histones affects transcription by modulating the physical accessibility of DNA, as well as by providing binding sites for specific activators and repressors of gene activity (67–69). The targeted histone acetylations and deacetylations involved in control of transcription occur in a background of global histone modifications that controls the basal level of transcription (70).

Small e1a retargets p300/CBP and RB to alter epigenetic and transcriptional patterns

The p300/CBP proteins are multi-domain proteins that combine histone acetyltransferase (HAT) activity with specific transcriptional activation domains to regulate transcription through control of the chromatin condensation state (53–55) The p300/CBP proteins facilitate chromatin remodeling in order to activate gene transcription by acting as a histone acetyltransferase, a transcription factor acetyltransferase, a scaffold for transcription factors to interact with chromatin, and a bridge between transcription factors and basal transcription machinery (71). Modulating all of these possible functions makes regulation of p300/CBP a selective mechanism for determining which sets of genes are expressed (72).

Several different lysines are acetylated by p300/CBP (73), but experiments knocking down or deleting both p300 and CBP, but not each individually, have shown that lysine 18 on histone H3 (H3K18) is specifically hypoacetylated in the absence of both p300 and CBP (74,

75), indicating H3K18 is a specific target of p300/CBP for acetylation. Interestingly, the interaction of e1a with p300/CBP causes a three-fold reduction in the total H3K18ac (74). Low levels of H3K18 acetylation (H3K18ac) correlate to poorer prognosis in prostate, lung, and kidney cancers (63, 64). Mutations in p300/CBP are associated with various forms of cancer (76), perhaps due to p300/CBP's inability to maintain H3K18ac at levels that activate appropriate transcription.

Small e1a can inhibit transcriptional activation by sequestering p300/CBP and preventing histone acetylation (72, 77), and directly repressing the HAT activity of both p300/CBP and the transcriptional activator p300/CBP associating factor (PCAF). This happens in part due to the displacement of PCAF from an activation complex critical for RNA polymerase II-dependent transcription by the binding of e1a to p300/CBP (34, 78).

RB proteins, which are inactivated in approximately one third of human tumors, (79) repress E2F activation and help maintain cells in a quiescent state. They do this in part by modifying chromatin to inhibit transcription through binding of repressive complexes that include histone deacetylase complexes (HDACs) and histone methylatransferases (80, 81). It has been demonstrated that RB proteins associate with HDAC1 and E2Fs at promoters to silence cell cycle genes by continually deacetylating their associated histones (82, 83).

The E1A interaction with RB-family proteins removes them from E2F-family transcription factors that regulate the genes needed to drive the cells into S-phase, including cyclin dependent kinase (*CDK2*) and cyclins E and A (*CCNE, CCNA*) (29, 47, 49, 59, 84, 85). This bypassing of the normal regulation of E2Fs causes promoters with E2F sites to be constitutively active, illustrating at least in part, how small e1a drives G_0 cells into S-phase (17, 29).

Collaborative work between the labs of Drs. Berk and Kurdistani at UCLA have begun to shed additional light on how small e1a alters the transcriptional and epigenetic patterns of quiescent cells to re-enter the cell cycle (61). The distribution patterns of e1a, RB-family proteins, p300, PCAF, and H3K18ac around the promoters of ~17,000 human genes were analyzed by chromatin immunoprecipitation (ChIP) and microarray (ChIP-on-chip) experiments (86). They found that e1a displaced the RB-family proteins from promoter regions of a large number of genes, likely corresponding to the large numbers of cellular promoters that are bound by E2F-family transcription factors, including cell cycle control and DNA synthesis genes expected to be induced by e1a. The promoter regions of these genes were also enriched for p300 and PCAF, and were hyperacetylated at H3K18ac resulting in transcriptional activation. Small e1a also associated with the promoters of anti-viral, development and differentiation genes, causing enrichment of RB-family members and repressing transcription. These patterns of chromatin modifications and transcriptional activation and repression were dependent on the ability of e1a to interact with RB and p300 (61).

Next generation sequencing for transcriptional and genomic analysis

Ultra-high throughput or next-generation sequencing is rapidly replacing microarray analysis for both genomic and transcriptomic analysis (87). Next-generation sequencing of cDNA (RNA-seq) allows for identification and quantification of transcripts, including alternative splicing products, without prior knowledge of particular genes (87, 88). RNA-seq has recently identified ~3800 genes that are differentially expressed more than 2-fold in adenovirus infected human primary cells (89). Chromatin immunoprecipitation followed by next-generation sequencing (ChIP-seq) (Fig. 1.4) (90) has been used extensively to map protein-DNA

interactions in vivo, and has been of particular use in identifying transcription factor binding sites (91) and profiling histone modifications (92).

The epigenetic profile that began to emerge with the ChIP-on-chip study by Ferrari et al. told us a great deal about how e1a's interaction with RB proteins and p300/CBP reconfigures chromatin at promoters, but the limited coverage of 8 kilobases (kb) around transcription start sites (TSS) (61) could not explain the global reduction of H3K18ac to ~1/3 of normal levels observed upon expression of e1a (74). Recent work by Ferrari et al. (93) used RNA-seq and ChIP-seq to investigate the small e1a induced transcriptional and epigenetic changes in growth arrested primary human lung fibroblasts (IMR90) (94).

They found that the number of significant peaks of H3K18ac in e1a expressing cells was reduced to about a third of normal levels, and that most peaks were in new positions. These results not only confirmed the observations of a previous study (74), but elucidated the genomic localization of the peaks of H3K18ac. We observed that peaks of H3K18ac in intergenic regions and in the promoter regions of many repressed genes were greatly reduced or eliminated. Most peaks of H3K18ac were located at promoters, but some peaks were still found within genes and intergenic regions, although these were greatly reduced in number. Significantly, peaks of H3K18ac were found at promoters of genes activated as cells enter S-phase, such as *CCNE*, and these peaks corresponded to induction of transcription. Throughout the genome overall, most peaks associated with e1a expression were redistributed compared to normal growth arrested cells (93).

How the interaction of e1a with p300/CBP and the RB-family proteins affects this rearrangement of H3K18ac peaks, and the subsequent changes in transcription, is the subject of Chapter 2 of this work.

ADENOVIRUS AS A GENE THERAPY VECTOR

Gene therapy for hematopoietic diseases

Hematopoietic stem cells (HSC) are a very important target for gene replacement therapy due to the number and variety of human genetic diseases that manifest in differentiated blood cells (95). Gene therapy has been used to treat hemaglobinopathies like sickle cell anemia and β-thalassemias, in addition to X-linked severe combined immunodeficiency (X-SCID) and adenosine deaminase (ADA)-deficient SCID (96, 97). Recently much interest has arisen in the use of gene therapy for treatment and prophylaxis of HIV/AIDS (98).

Many of the early successful gene therapy trials used retrovirus vectors for delivery into hematopoietic stem cells (99–101). Retroviruses have the benefit of integrating into the host genome to provide long-term expression of the therapeutic gene (102). However, insertion into the genome can have serious detrimental effects by disrupting or activating cellular genes, such as when patients developed leukemia through the activation of the *LMO2* proto-ontogene by the integration of the retrovirus (103–106).

First generation adenovirus vectors

Adenoviral vectors account for roughly one quarter of all gene therapy trials world-wide (107, 108), with the majority of adenovirus trials targeted toward uses where only transient gene expression is required, such as cancer treatment and vaccinations (102). Adenovirus vectors have the advantage of infecting both dividing and non-dividing cell types in culture and *in vivo* to deliver high levels of transient gene expression from the linear, non-integrating dsDNA genome (3, 102). Absence of chromosomal integration makes adenoviral vectors an attractive system for gene therapy since there is reduced risk of insertional mutagenesis.

"First generation" adenoviral vectors are defective for replication by deletion of the E1, and often E3, regions of the genome, allowing the accommodation of ~8kb of exogenous DNA (109, 110). Adenovirus E1 mutants can be propagated in human embryonic kidney cells that have been transformed with the left end of the adenovirus type 5 (Ad5) genome (HEK293 or 293) and express E1A and E1B (4, 110). First generation adenoviral vectors can be constructed by transfection of overlapping DNA fragments into *Escherichia coli* or 293 cells for *in vivo* recombination. Alternately, 293 cells expressing Cre recombinase can be used for Cre mediated recombination, or a plasmid containing the entire adenovirus genome that can be excised by restriction digest (6, 109, 111–114).

E1A, as discussed previously, is important for viral gene expression and replication (17, 21). E1–deleted adenoviral vectors, however, express low levels of viral proteins that can be presented as antigens, resulting in immune response and cellular toxicity (102, 115–117). Synthesis of adenoviral gene products often stimulates an immune response in the infected cells and results in a loss of therapeutic gene expression (118, 119). In an extreme example, pro-inflammatory immune response contributed to the death of a gene therapy patient infused with a high titer E1/E4 deleted Ad5 vector in one of the earliest gene therapy trials (120).

The immunogenic and toxic effects of the first generation adenovirus vectors, in addition to their limited capacity for exogenous DNA, led researchers to develop adenovirus vectors deleted for all viral coding regions.

Helper Dependent Adenovirus (HDAd) vectors for gene therapy

High capacity "gutless" Helper Dependent Adenovirus (HDAd) vectors lacking viral coding regions have been demonstrated to have efficient long term expression and lower toxicity

in vivo (121–125). HDAd vectors contain only the adenovirus inverted terminal repeats (ITR) that act as origins of replication (126) and the *cis*-acting DNA packaging signal (ψ) (127), but no viral coding regions. An E1/E3-deleted helper virus provides, in *trans*, all the proteins needed for HDAd vectors to be replicated and packaged when both are introduced into a permissive cell line such as 293 (102, 114, 128).

HDAd vectors have capacity of up to ~37kb (128), allowing the vector to deliver whole genomic regions that include a gene of interest and endogenous regulation elements (129, 130). If traditional expression cassettes are used, "stuffer DNA" must be incorporated in the HDAd vector bring the size up to the ~28kb to ~39kb range that can be efficiently packaged (131–133).

A key feature of the HDAd vector system is that contaminating helper virus must be minimized because the E1/E3-deleted helper can cause the immunogenic and toxic effects problematic in the first generation vectors. The most common method for limiting helper contamination employs the phage Cre site-specific recombinase (134) to excise the packaging signal from the helper, leaving other viral functions intact. To accomplish this the viral packaging signal (ψ) is constructed with flanking Cre recognition (loxP) sites, and HDAd vectors are propagated in 293 cells that express Cre recombinase (111, 135, 136). An alternate system was developed to use 293 cells expressing the yeast FLP recombinase (137) and a helper virus with FLP recognition target (FRT) sites flanking ψ (138). Use of an *in vitro* evolved thermostable FLP (FLPe) (139) further reduced helper contamination in the FLP/FRT system (140). Vector stocks can be further purified by cesium chloride (CsCl) ultra-centrifugation gradients, due to the different densities of the HDAd vector and the helper virus (128, 138, 141).

Even if the recombinase mediated excision of ψ is 100% efficient, helper virus DNA, even lacking ψ, is packaged at a low frequency (~0.1%) (142). Unfortunately, expression level of

the recombinase used seems to be the limiting factor for the level of helper virus contamination (143). Insufficient Cre or FLPe expression results in high levels of helper contamination, but it has been demonstrated that higher expression of Cre recombinase increased the efficiency of the excision of ψ to near 100% (144).

Chapter 3 of this work addresses the challenges of developing a 293 cell line expressing high levels of FLPe recombinase.

Helper Dependent Adenovirus/Epstein Barr Virus (HDAd/EBV) hybrid vector

In order for gene replacement therapy to be effective, the therapeutic gene needs to persist in the target cells. Current vector systems using adenovirus are not suitable for transduction of hematopoietic stem cells because non-integrating adenovirus vectors are not well maintained in actively dividing cells (145, 146).

The Helper Dependent Adenovirus/Epstein-Barr Virus (HDAd/EBV) hybrid system developed by the Berk lab (Fig. 1.5) combines the well-characterized benefits of an HDAd vector, which lacks all adenovirus coding regions, with Epstein-Barr Virus (EBV), which is capable of life-long persistence (147). EBV episomes, circular extra-chromosomal DNA capable of replication and segregation, have been used in model systems to treat diseases such as diabetes and hemophilia (148, 149), but were delivered via low efficiency non-viral means. The HDAd/EBV hybrid vector uses a high capacity adenovirus vector to deliver an episome with critical EBV elements that allow therapeutic DNA to be maintained in replicating cells (150).

The deletion of the adenovirus coding regions from the HDAd vector reduces immune response and provides sufficient space to include a human origin of replication sequence (hORI). This enables the episome to replicate during S-phase, and the addition of the EBV EBNA-1

coding region and binding sites causes mitotic segregation of the episome by tethering it to chromosomes (151, 152). Lastly, the presence of loxP sites near the termini of the linear HDAd/EBV vector allows circularization of the episome, which is required for tethering to chromosomes.

In vivo, Cre recombinase can be delivered by co-infection of a second HDAd vector expressing Cre (153), or the episome can be engineered to be self-circularizing through the expression of Cre from a tissue specific promoter (154). Persistence of expression *in vivo* of a luciferase reporter gene has been demonstrated using this HDAd/EBV vector system targeted to hepatocytes using both the two-virus vector and the single self-circularizing systems (153, 154).

The use of Cre recombinase to generate the circular episome in the HDAd/EBV hybrid system necessitates the vector being propagated in 293FLPe cells with a helper virus that has FRT sites flanking the packaging signal.

Targeting the HDAd/EBV vector system to hematopoietic stem cells

Although experiments using the HDAd/EBV vector system in mouse hepatocytes *in vivo* demonstrated long-term expression, the low cell division rate of hepatocytes (154) makes them a less than optimal model system for testing the maintenance of the vector in rapidly dividing cells. Hematopoietic stems cells (HSC), however, are a rapidly dividing cell population that differentiate into a number of different cell types that manifest diseases (94). In addition, systems have already been developed for lentiviruses to deliver selective advantage to transduced HSCs, which could be easily adapted to the HDAd/EBV hybrid system (155, 156).

Commonly used adenovirus vectors, such as adenovirus serotype 5 (Ad5) used for targeting hepatocytes, primarily recognize the coxsackievirus-adenovirus receptor (CAR) (157,

158). Ad5 only poorly transduces HSCs due to the scarcity of the CAR receptor (159, 160) on hematopoietic cells. Adenovirus serotype 35 (Ad35) however, efficiently infects human HSCs and hematopoietic lineage cells (161–165) via the ubiquitously expressed receptor membrane cofactor protein CD46 (166–170). Since a helper virus provides all of the proteins that comprise HDAd vectors, the HDAd vector would necessarily have the same capsid and fiber proteins, and therefore cell specificity, as the helper virus. HDAd vectors can thus be targeted to different cell types based on the helper virus used for propagation. The tropism, or cell type specificity, of adenoviral vectors can be altered through modification of the fiber knob responsible for interacting with cellular receptors (9, 163, 171–173). For this reason, chimeric Ad5/35 helper viruses with the Ad35 fiber knob have been created to target Ad5 based HDAd vectors to hematopoietic cells (174–176), however, these helper viruses designed for use in the Cre/lox system and could not be used for HDAd/EBV hybrid vector propagation.

Chapter 3 of this work describes the construction of a helper virus with an Ad5/35 chimeric fiber, and FRT sites flanking the packaging signal, for targeting of the HDAd/EBV vector to hematopoietic stem cells.

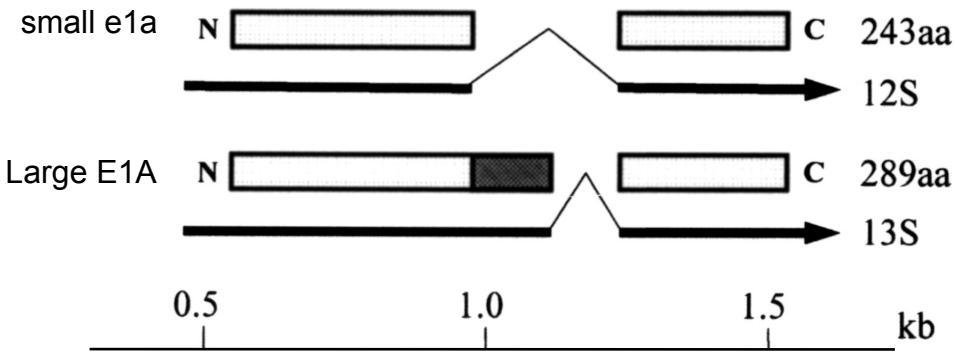

Figure 1.1. Structure of early E1A mRNAs. The bottom line represents the adenovirus genome annotated with distance from the left end in kilobases (kb). The exons of the E1A mRNAs are represented as thick solid lines joined by a single intron with alternate 5' slice sites for the 12S and 13S mRNAs. The arrowheads indicate the polyadenylated 3'-ends. Open rectangles represent regions in common between the 243aa and 289aa proteins; the solid rectangle represents the 46aa unique to Large E1A.

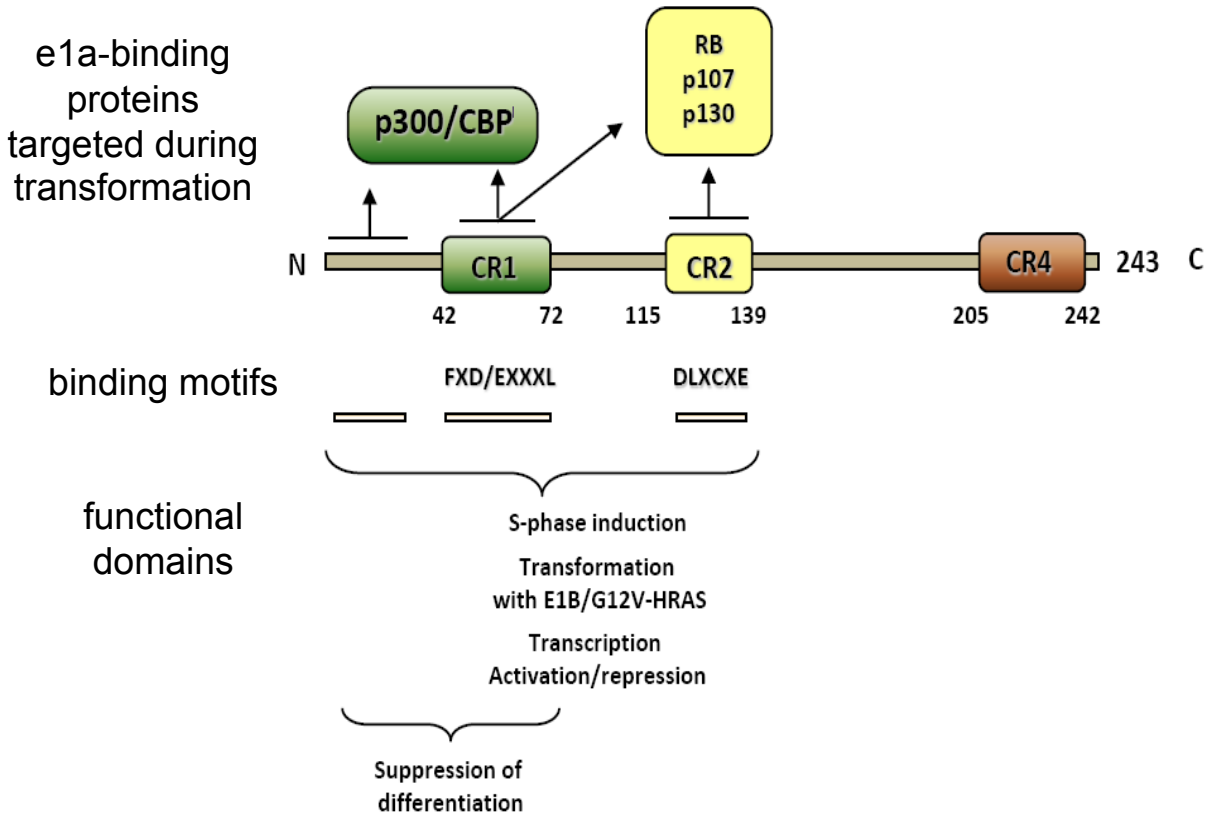

Figure 1.2. Schematic structure of small e1a and its interactions with cellular proteins required for oncogenic transformation. Small e1a has three conserved regions (CRs), the N-terminus-CR1, CR2 and CR4, and lacks CR3, which is present in large E1A. The domains required for various e1a functions are indicated as bars beneath the map. The location and consensus sequences of binding motifs necessary for interaction with p300/CBP and RB are as indicated (small e1a CRs have additional interactions and functions not discussed here). CR1 and conserved residues in the N-terminus are required for interaction with p300/CBP. CR2 binds to the RB protein family, primarily through an LXCXE-motif in CR2 but residues in CR1 also contribute to the binding affinity.

Modified from Ferrari et al., 2008.

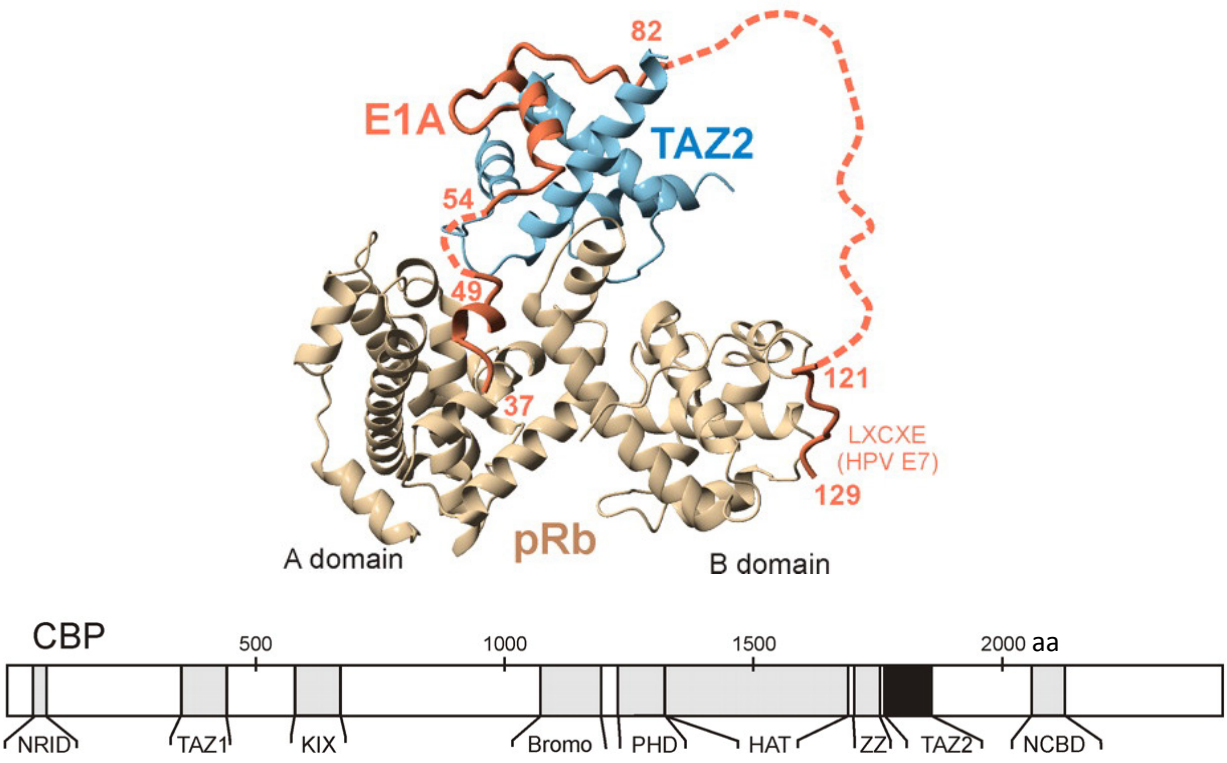

Figure 1.3. Model for the trimolecular complex between E1A residues 37 to 129 with the RB1 pocket domain and the CBP TAZ2 domain. Ribbon diagrams of the RB1 pocket domain (brown), the TAZ2 domain of CBP (blue) and regions of E1A for which the structure has been determined in complex with the RB pocket domain or the CBP TAZ2 domain (orange) are shown. Linker regions of E1A that may be unstructured are shown as a dashed orange line. The structure of the LxCxE containing region in CR2 is based on the structure of the homologous LxCxE region of HPV E7 bound to the pocket. The sequence of CBP is diagrammed at the bottom with HAT representing the lysine acetyl transferase catalytic domain, protein interaction domains indicated with TAZ2 shown in black.

Figure from Ferreon et al., 2009.

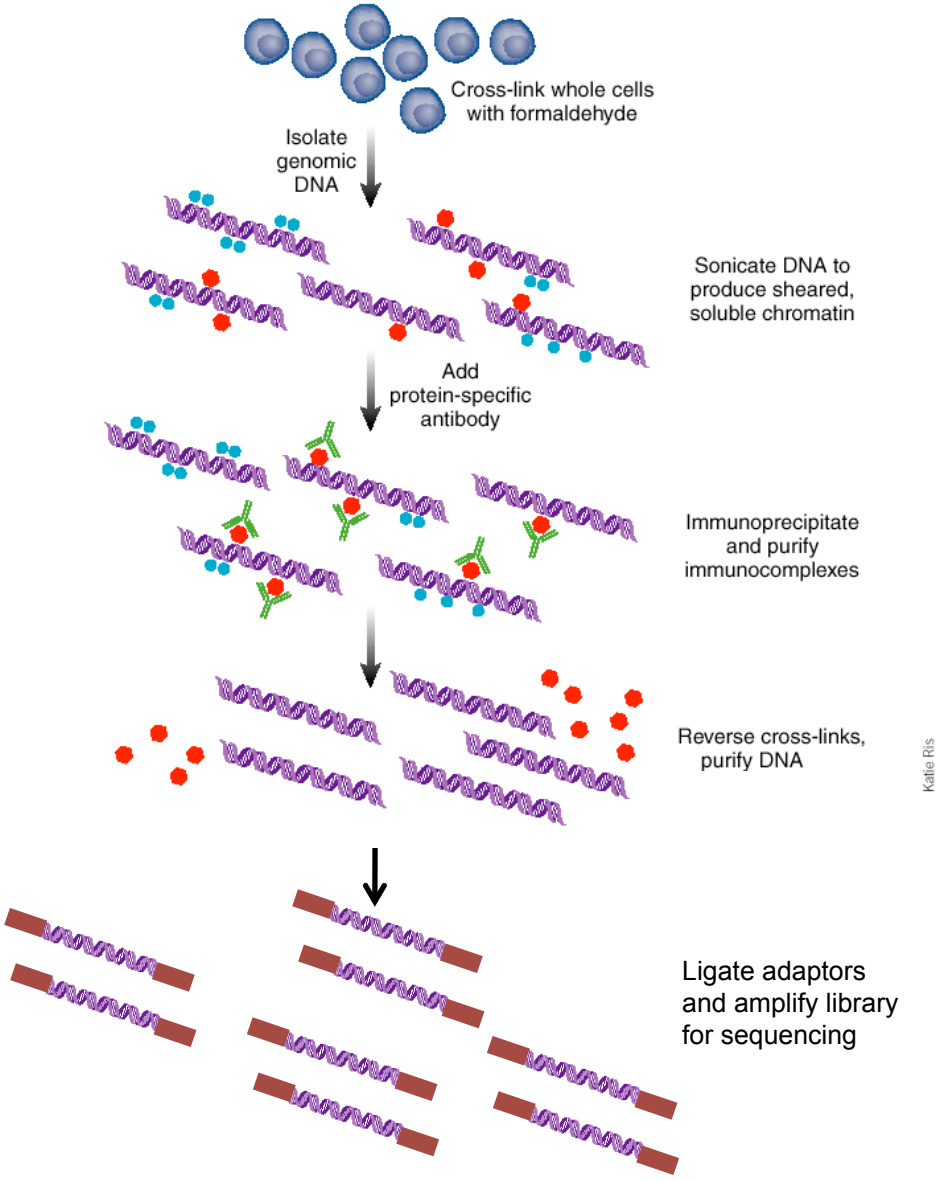

Figure 1.4. Chromatin immunoprecipitation and massive parallel sequencing (ChIP-seq). DNA and proteins are cross-linked *in vivo,* then chromatin is sheared by sonication. A protein specific antibody is used to immunoprecipitate DNA-protein complexes. Cross-links are reversed and" barcoded" adaptors with specific sequences and primer binding sites are ligated to immunoprecipitated DNA fragments. Barcoded libraries are amplified by PCR prior to sequencing.

Modified from Mardis, 2007 (Figure by Katie Ris).

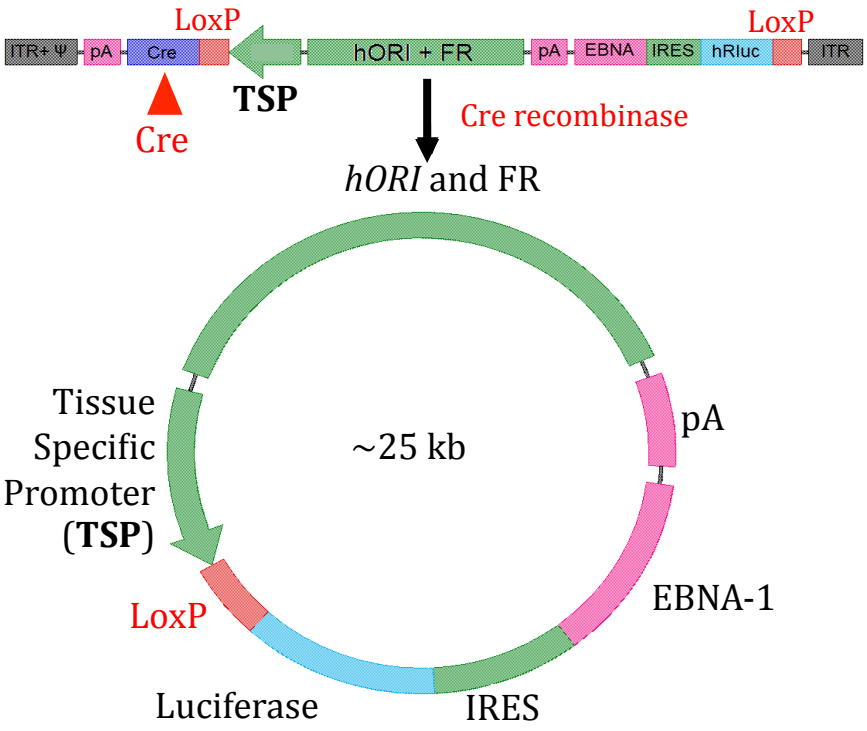

Figure 1.5. Single vector system for *in vivo* conversion of helper-dependent Ad (HDAd) linear DNA into an EBV-episome in nuclei of transduced cells. The linear DNA delivered by a HDAd vector is circularized upon transduction to the nuclei of target cells, where the tissue specific promoter drives expression of Cre recombinase. In the two-vector system, Cre is delivered by a second HDAd vector. Cre binds to the loxP sites and circularizes the intervening DNA. Circularization of the episome places the tissue specific promoter (TSP) in front of a bicistronic expression cassette for the expression of a gene of interest (in this case, a luciferase reporter gene) followed by an IRES for the expression of EBNA-1. During S-phase of the cell-cycle the episome is replicated from the human origin of replication sequence (hORI). EBNA-1 binds to the Family of Repeats (FR) and tethers the episome to a daughter cell chromosome for segregation during subsequent mitosis steps.

REFERENCES

1. Hershey AD, Chase M (1952) INDEPENDENT FUNCTIONS OF VIRAL PROTEIN AND NUCLEIC ACID IN GROWTH OF BACTERIOPHAGE. *J Gen Physiol* 36:39–56.

2. Lodish H et al. (2000) in *Molecular Cell Biology* (W. H. Freeman and Company, New York).. 4th Ed.

3. Berk AJ (2007) in *Fields Virology*, eds Knipe DM, Howley PM (Lippincott Williams & Wilkins).Fifth.

4. Graham FL, Smiley J, Russell WC, Nairn R (1977) Characteristics of a human cell line transformed by DNA from human adenovirus type 5. *J Gen Virol* 36:59–74.

5. Stow ND (1981) Cloning of a DNA fragment from the left-hand terminus of the adenovirus type 2 genome and its use in site-directed mutagenesis. *J Virol* 37:171–80.

6. Chartier C et al. (1996) Efficient generation of recombinant adenovirus vectors by homologous recombination in Escherichia coli. *J Virol* 70:4805–10.

7. Crouzet J et al. (1997) Recombinational construction in Escherichia coli of infectious adenoviral genomes. *Proc Natl Acad Sci U S A* 94:1414–9.

8. Horne R (1959) The icosahedral form of an adenovirus. *J Mol Biol* 1:84–86.

9. Devaux C, Caillet-Boudin ML, Jacrot B, Boulanger P (1987) Crystallization, enzymatic cleavage, and the polarity of the adenovirus type 2 fiber. *Virology* 161:121–8.

10. Tomko RP et al. (2000) Expression of the adenovirus receptor and its interaction with the fiber knob. *Exp Cell Res* 255:47–55.

11. Rowe WP, Huebner RJ, Gilmore LK, Parrott RH, Ward TG (1953) Isolation of a cytopathogenic agent from human adenoids undergoing spontaneous degeneration in tissue culture. *Proc Soc Exp Biol Med* 84:570–3.

12. Hilleman MR, Werner JH (1954) Recovery of new agent from patients with acute respiratory illness. *Proc Soc Exp Biol Med* 85:183–8.

13. Enders JF et al. (1956) Adenoviruses: group name proposed for new respiratory-tract viruses. *Science* 124:119–20.

14. Trentin JJ, Yabe Y, Taylor G (1962) The quest for human cancer viruses. *Science* 137:835–41.

15. Mackey JK, Rigden PM, Green M (1976) Do highly oncogenic group A human adenoviruses cause human cancer? Analysis of human tumors for adenovirus 12 transforming DNA sequences. *Proc Natl Acad Sci U S A* 73:4657–61.

16. Miller DL, Myers CL, Rickards B, Coller HA, Flint SJ (2007) Adenovirus type 5 exerts genome-wide control over cellular programs governing proliferation, quiescence, and survival. *Genome Biol* 8:R58.

17. Berk AJ (2005) Recent lessons in gene expression, cell cycle control, and cell biology from adenovirus. *Oncogene* 24:7673–7685.

18. Nevins JR, Ginsberg HS, Blanchard JM, Wilson MC, Darnell JE (1979) Regulation of the primary expression of the early adenovirus transcription units. *J Virol* 32:727–33.

19. Hearing P, Shenk T (1983) The adenovirus type 5 E1A transcriptional control region contains a duplicated enhancer element. *Cell* 33:695–703.

20. Perricaudet M, Akusjarvi G, Virtanen A, Pettersson U (1979) Structure of two spliced mRNAs from the transforming region of human subgroup C adenoviruses. *Nature* 281:694–6.

21. Montell C, Courtois G, Eng C, Berk A (1984) Complete transformation by adenovirus 2 requires both E1A proteins. *Cell* 36:951–961.

22. van Ormondt H, Maat J, Dijkema R (1980) Comparison of nucleotide sequences of the early E1a regions for subgroups A, B and C of human adenoviruses. *Gene* 12:63–76.

23. Kimelman D, Miller JS, Porter D, Roberts BE (1985) E1a regions of the human adenoviruses and of the highly oncogenic simian adenovirus 7 are closely related. *J Virol* 53:399–409.

24. Chinnadurai G (2004) Modulation of oncogenic transformation by the human adenovirus E1A C-terminal region. *Curr Top Microbiol Immunol* 273:139–61.

25. Rasti M, Grand RJ, Mymryk JS, Gallimore PH, Turnell AS (2005) Recruitment of CBP/p300, TATA-binding protein, and S8 to distinct regions at the N terminus of adenovirus E1A. *J Virol* 79:5594–605.

26. Berk AJ, Sharp PA (1978) Structure of the adenovirus 2 early mRNAs. *Cell* 14:695–711.

27. Spindler KR, Eng CY, Berk AJ (1985) An adenovirus early region 1A protein is required for maximal viral DNA replication in growth-arrested human cells. *J Virol* 53:742–750.

28. Howe JA, Mymryk JS, Egan C, Branton PE, Bayley ST (1990) Retinoblastoma growth suppressor and a 300-kDa protein appear to regulate cellular DNA synthesis. *Proc Natl Acad Sci U S A* 87:5883–5887.

29. Ghosh MK, Harter ML (2003) A Viral Mechanism for Remodeling Chromatin Structure in G0 Cells. *Molecular Cell* 12:255–260.

30. Stein RW, Corrigan M, Yaciuk P, Whelan J, Moran E (1990) Analysis of E1A-mediated growth regulation functions: binding of the 300-kilodalton cellular product correlates with

E1A enhancer repression function and DNA synthesis-inducing activity. *J Virol* 64:4421–7.

31. Barbeau D, Charbonneau R, Whalen SG, Bayley ST, Branton PE (1994) Functional interactions within adenovirus E1A protein complexes. *Oncogene* 9:359–73.

32. Arany Z, Newsome D, Oldread E, Livingston DM, Eckner R (1995) A family of transcriptional adaptor proteins targeted by the E1A oncoprotein. *Nature* 374:81–4.

33. Boyer TG, Martin ME, Lees E, Ricciardi RP, Berk AJ (1999) Mammalian Srb/Mediator complex is targeted by adenovirus E1A protein. *Nature* 399:276–9.

34. Chakravarti D et al. (1999) A viral mechanism for inhibition of p300 and PCAF acetyltransferase activity. *Cell* 96:393–403.

35. Berk AJ, Lee F, Harrison T, Williams J, Sharp PA (1979) Pre-early adenovirus 5 gene product regulates synthesis of early viral messenger RNAs. *Cell* 17:935–44.

36. Lillie JW, Green MR (1989) Transcription activation by the adenovirus E1a protein. *Nature* 338:39–44.

37. Winberg G, Shenk T (1984) Dissection of overlapping functions within the adenovirus type 5 E1A gene. *Embo J* 3:1907–12.

38. Montell C, Fisher EF, Caruthers MH, Berk AJ (1982) Resolving the functions of overlapping viral genes by site-specific mutagenesis at a mRNA splice site. *Nature* 295:380–4.

39. Zerler B, Roberts RJ, Mathews MB, Moran E (1987) Different functional domains of the adenovirus E1A gene are involved in regulation of host cell cycle products. *Mol Cell Biol* 7:821–9.

40. Whyte P et al. (1988) Association between an oncogene and an anti-oncogene: the adenovirus E1A proteins bind to the retinoblastoma gene product. *Nature* 334:124–9.

41. Egan C, Bayley ST, Branton PE (1989) Binding of the Rb1 protein to E1A products is required for adenovirus transformation. *Oncogene* 4:383–8.

42. Barbeau D, Marcellus RC, Bacchetti S, Bayley ST, Branton PE (1992) Quantitative analysis of regions of adenovirus E1A products involved in interactions with cellular proteins. *Biochem Cell Biol* 70:1123–34.

43. Dyson N, Harlow E (1992) Adenovirus E1A targets key regulators of cell proliferation. *Cancer Surv* 12:161–195.

44. Li Y, Graham C, Lacy S, Duncan AM, Whyte P (1993) The adenovirus E1A-associated 130-kD protein is encoded by a member of the retinoblastoma gene family and physically interacts with cyclins A and E. *Genes Dev* 7:2366–77.

45. Wang HG et al. (1993) Identification of specific adenovirus E1A N-terminal residues critical to the binding of cellular proteins and to the control of cell growth. *Journal of virology* 67:476–488.

46. Eckner R et al. (1994) Molecular cloning and functional analysis of the adenovirus E1A-associated 300-kD protein (p300) reveals a protein with properties of a transcriptional adaptor. *Genes Dev* 8:869–84.

47. Bagchi S, Raychaudhuri P, Nevins JR (1990) Adenovirus E1A proteins can dissociate heteromeric complexes involving the E2F transcription factor: A novel mechanism for E1A trans-activation. *Cell* 62:659–669.

48. Cao L et al. (1992) Independent binding of the retinoblastoma protein and p107 to the transcription factor E2F. *Nature* 355:176–179.

49. Blais A, Dynlacht BD (2004) Hitting their targets: an emerging picture of E2F and cell cycle control. *Current Opinion in Genetics & Development* 14:527–532.

50. Bannister AJ, Kouzarides T (1996) The CBP co-activator is a histone acetyltransferase. *Nature* 384:641–3.

51. Ait-Si-Ali S et al. (2000) CBP/p300 histone acetyl-transferase activity is important for the G1/S transition. *Oncogene* 19:2430–2437.

52. Goodman RH, Smolik S (2000) CBP/p300 in cell growth, transformation, and development. *Genes Dev* 14:1553–1577.

53. Chan HM, La Thangue NB (2001) p300/CBP proteins: HATs for transcriptional bridges and scaffolds. *J Cell Sci* 114:2363–73.

54. Vo N, Goodman RH (2001) CREB-binding protein and p300 in transcriptional regulation. *J Biol Chem* 276:13505–8.

55. Iyer NG et al. (2007) p300 is required for orderly G1/S transition in human cancer cells. *Oncogene* 26:21–29.

56. Whyte P, Williamson NM, Harlow E (1989) Cellular targets for transformation by the adenovirus E1A proteins. *Cell* 56:67–75.

57. Wang HG, Moran E, Yaciuk P (1995) E1A promotes association between p300 and pRB in multimeric complexes required for normal biological activity. *J Virol* 69:7917–7924.

58. Lee JO, Russo AA, Pavletich NP (1998) Structure of the retinoblastoma tumour-suppressor pocket domain bound to a peptide from HPV E7. *Nature* 391:859–865.

59. Liu X, Marmorstein R (2007) Structure of the retinoblastoma protein bound to adenovirus E1A reveals the molecular basis for viral oncoprotein inactivation of a tumor suppressor. *Genes Dev* 21:2711–2716.

60. Ferreon JC, Martinez-Yamout MA, Dyson HJ, Wright PE (2009) Structural basis for subversion of cellular control mechanisms by the adenoviral E1A oncoprotein. *Proc Natl Acad Sci U S A* 106:13260–13265.

61. Ferrari R et al. (2008) Epigenetic reprogramming by adenovirus e1a. *Science* 321:1086–1088.

62. Hake SB, Xiao A, Allis CD (2004) Linking the epigenetic "language" of covalent histone modifications to cancer. *British Journal of Cancer* 90:761–769.

63. Seligson DB et al. (2005) Global histone modification patterns predict risk of prostate cancer recurrence. *Nature* 435:1262–1266.

64. Seligson DB et al. (2009) Global Levels of Histone Modifications Predict Prognosis in Different Cancers. *The American Journal of Pathology* 174:1619–1628.

65. Grunstein M (1997) Histone acetylation in chromatin structure and transcription. *Nature* 389:349–352.

66. Wolffe AP, Kurumizaka H (1998) The nucleosome: a powerful regulator of transcription. *Prog Nucleic Acid Res Mol Biol* 61:379–422.

67. Horn PJ, Peterson CL (2002) Chromatin higher order folding–wrapping up transcription. *Science* 297:1824–1827.

68. Kurdistani SK, Grunstein M (2003) Histone acetylation and deacetylation in yeast. *Nature Reviews Molecular Cell Biology* 4:276–284.

69. Kurdistani SK, Tavazoie S, Grunstein M (2004) Mapping Global Histone Acetylation Patterns to Gene Expression. *Cell* 117:721–733.

70. Vogelauer M, Wu J, Suka N, Grunstein M (2000) Global histone acetylation and deacetylation in yeast. *Nature* 408:495–498.

71. Chen J, Li Q (2011) Life and death of transcriptional co-activator p300. *Epigenetics* 6:957–961.

72. Giles RH, Peters DJ., Breuning MH (1998) Conjunction dysfunction: CBP/p300 in human disease. *Trends in Genetics* 14:178–183.

73. Kouzarides T (2007) Chromatin modifications and their function. *Cell* 128:693.

74. Horwitz GA et al. (2008) Adenovirus small e1a alters global patterns of histone modification. *Science* 321:1084–1085.

75. Jin Q et al. (2011) Distinct roles of GCN5/PCAF-mediated H3K9ac and CBP/p300-mediated H3K18/27ac in nuclear receptor transactivation. *EMBO J* 30:249–262.

76. Iyer NG, Ozdag H, Caldas C (2004) p300/CBP and cancer. *Oncogene* 23:4225–31.

77. Pelka P et al. (2009) Transcriptional Control by Adenovirus E1A Conserved Region 3 Via P300/CBP. *Nucl Acids Res* 37:1095–1106.

78. Yang XJ, Ogryzko VV, Nishikawa J, Howard BH, Nakatani Y (1996) A p300/CBP-associated factor that competes with the adenoviral oncoprotein E1A. *Nature* 382:319–24.

79. Burkhart DL, Sage J (2008) Cellular mechanisms of tumour suppression by the retinoblastoma gene. *Nat Rev Cancer* 8:671–682.

80. Zhang HS, Dean DC (2001) Rb-mediated chromatin structure regulation and transcriptional repression. *Oncogene* 20:3134–8.

81. Frolov MV, Dyson NJ (2004) Molecular mechanisms of E2F-dependent activation and pRB-mediated repression. *J Cell Sci* 117:2173–81.

82. Brehm A et al. (1998) Retinoblastoma protein recruits histone deacetylase to repress transcription. *Nature* 391:597–601.

83. Rayman JB et al. (2002) E2F mediates cell cycle-dependent transcriptional repression in vivo by recruitment of an HDAC1/mSin3B corepressor complex. *Genes Dev* 16:933–947.

84. Yee SP, Branton PE (1985) Detection of cellular proteins associated with human adenovirus type 5 early region 1A polypeptides. *Virology* 147:142–53.

85. van den Heuvel S, Dyson NJ (2008) Conserved functions of the pRB and E2F families. *Nat Rev Mol Cell Biol* 9:713–24.

86. Ren B et al. (2000) Genome-Wide Location and Function of DNA Binding Proteins. *Science* 290:2306–2309.

87. Metzker ML (2010) Sequencing technologies — the next generation. *Nature Reviews Genetics* 11:31–46.

88. Wang Z, Gerstein M, Snyder M (2009) RNA-Seq: a revolutionary tool for transcriptomics. *Nature Reviews Genetics* 10:57–63.

89. Zhao H, Dahlo M, Isaksson A, Syvanen A-C, Pettersson U (2012) The transcriptome of the adenovirus infected cell. *Virology* 424:115–128.

90. Mardis ER (2007) ChIP-seq: welcome to the new frontier. *Nature Methods* 4:613–614.

91. Johnson DS, Mortazavi A, Myers RM, Wold B (2007) Genome-Wide Mapping of in Vivo Protein-DNA Interactions. *Science* 316:1497–1502.

92. Mikkelsen TS et al. (2007) Genome-wide maps of chromatin state in pluripotent and lineage-committed cells. *Nature* 448:553–560.

93. Ferrari R et al. (2012) Reorganization of the Host Epigenome by a Viral Oncogene. *Genome Res*. Available at: http://genome.cshlp.org/content/early/2012/05/20/gr.132308.111 [Accessed June 6, 2012].

94. Nichols WW et al. (1977) Characterization of a new human diploid cell strain, IMR-90. *Science* 196:60–63.

95. Graf T (2002) Differentiation plasticity of hematopoietic cells. *Blood* 99:3089–3101.

96. Kohn DB (2001) Gene therapy for genetic haematological disorders and immunodeficiencies. *J Intern Med* 249:379–90.

97. Watts KL, Adair J, Kiem H-P (2011) Hematopoietic Stem Cell Expansion and Gene Therapy. *Cytotherapy* 13:1164–1171.

98. Dropulic B, June CH (2006) Gene-based immunotherapy for human immunodeficiency virus infection and acquired immunodeficiency syndrome. *Hum Gene Ther* 17:577–88.

99. Rosenberg SA et al. (1990) Gene transfer into humans--immunotherapy of patients with advanced melanoma, using tumor-infiltrating lymphocytes modified by retroviral gene transduction. *N Engl J Med* 323:570–578.

100. Blaese RM et al. (1995) T lymphocyte-directed gene therapy for ADA- SCID: initial trial results after 4 years. *Science* 270:475–480.

101. Cavazzana-Calvo M et al. (2000) Gene therapy of human severe combined immunodeficiency (SCID)-X1 disease. *Science* 288:669–672.

102. Robbins PD, Ghivizzani SC (1998) Viral Vectors for Gene Therapy. *Pharmacology & Therapeutics* 80:35–47.

103. Rabbitts TH et al. (1999) The effect of chromosomal translocations in acute leukemias: the LMO2 paradigm in transcription and development. *Cancer Res* 59:1794s–1798s.

104. Hacein-Bey-Abina S et al. (2003) A serious adverse event after successful gene therapy for X-linked severe combined immunodeficiency. *N Engl J Med* 348:255–6.

105. Hacein-Bey-Abina S et al. (2003) LMO2-associated clonal T cell proliferation in two patients after gene therapy for SCID-X1. *Science* 302:415–9.

106. Davé UP et al. (2009) Murine Leukemias with Retroviral Insertions at Lmo2 Are Predictive of the Leukemias Induced in SCID-X1 Patients Following Retroviral Gene Therapy. *PLoS Genet* 5:e1000491.

107. Gene Therapy Clinical Trials Worldwide Available at: http://www.wiley.com//legacy/wileychi/genmed/clinical/ [Accessed November 19, 2012].

108. Edelstein ML, Abedi MR, Wixon J, Edelstein RM (2004) Gene therapy clinical trials worldwide 1989–2004—an overview. *The Journal of Gene Medicine* 6:597–602.

109. Bett AJ, Haddara W, Prevec L, Graham FL (1994) An efficient and flexible system for construction of adenovirus vectors with insertions or deletions in early regions 1 and 3. *PNAS* 91:8802–8806.

110. Graham F, Prevec L (1995) Methods for construction of adenovirus vectors. *Molecular Biotechnology* 3:207–220.

111. Hardy S, Kitamura M, Harris-Stansil T, Dai Y, Phipps ML (1997) Construction of adenovirus vectors through Cre-lox recombination. *J Virol* 71:1842–1849.

112. Ng P et al. (1999) A high-efficiency Cre/loxP-based system for construction of adenoviral vectors. *Hum Gene Ther* 10:2667–72.

113. Ng P, Parks RJ, Cummings DT, Evelegh CM, Graham FL (2000) An enhanced system for construction of adenoviral vectors by the two-plasmid rescue method. *Hum Gene Ther* 11:693–9.

114. Ng P, Parks RJ, Graham FL (2002) Preparation of helper-dependent adenoviral vectors. *Methods Mol Med* 69:371–88.

115. Simon RH et al. (1993) Adenovirus-mediated transfer of the CFTR gene to lung of nonhuman primates: toxicity study. *Hum Gene Ther* 4:771–780.

116. Yang Y et al. (1994) Cellular immunity to viral antigens limits E1-deleted adenoviruses for gene therapy. *Proc Natl Acad Sci U S A* 91:4407–4411.

117. Morral N, O'Neal W, Zhou H, Langston C, Beaudet A (1997) Immune responses to reporter proteins and high viral dose limit duration of expression with adenoviral vectors: comparison of E2a wild type and E2a deleted vectors. *Hum Gene Ther* 8:1275–1286.

118. Yang Y, Wilson JM (1995) Clearance of adenovirus-infected hepatocytes by MHC class I-restricted CD4+ CTLs in vivo. *The Journal of Immunology* 155:2564–2570.

119. Yang Y, Su Q, Wilson JM (1996) Role of viral antigens in destructive cellular immune responses to adenovirus vector-transduced cells in mouse lungs. *Journal of virology* 70:7209–7212.

120. Raper SE et al. (2003) Fatal systemic inflammatory response syndrome in a ornithine transcarbamylase deficient patient following adenoviral gene transfer. *Mol Genet Metab* 80:148–58.

121. Schiedner G et al. (1998) Genomic DNA transfer with a high-capacity adenovirus vector results in improved in vivo gene expression and decreased toxicity. *Nat Genet* 18:180–183.

122. Chen H-H et al. (1997) Persistence in muscle of an adenoviral vector that lacks all viral genes. *Proc Natl Acad Sci U S A* 94:1645–1650.

123. Morsy MA et al. (1998) An adenoviral vector deleted for all viral coding sequences results in enhanced safety and extended expression of a leptin transgene. *Proc Natl Acad Sci U S A* 95:7866–7871.

124. Morral N et al. (1998) High doses of a helper-dependent adenoviral vector yield supraphysiological levels of alpha1-antitrypsin with negligible toxicity. *Hum Gene Ther* 9:2709–2716.

125. Morral N et al. (1999) Administration of helper-dependent adenoviral vectors and sequential delivery of different vector serotype for long-term liver-directed gene transfer in baboons. *Proc Natl Acad Sci U S A* 96:12816–12821.

126. Davison AJ, Benko M, Harrach B (2003) Genetic content and evolution of adenoviruses. *J Gen Virol* 84:2895–908.

127. Hearing P, Samulski RJ, Wishart WL, Shenk T (1987) Identification of a repeated sequence element required for efficient encapsidation of the adenovirus type 5 chromosome. *J Virol* 61:2555–8.

128. Mitani K, Graham FL, Caskey CT, Kochanek S (1995) Rescue, propagation, and partial purification of a helper virus-dependent adenovirus vector. *Proc Natl Acad Sci U S A* 92:3854–3858.

129. Kim HW, Svendsen CN (2011) Gene Editing in Stem Cells Hits the Target. *Cell Stem Cell* 9:93–94.

130. Kochanek S et al. (1996) A new adenoviral vector: Replacement of all viral coding sequences with 28 kb of DNA independently expressing both full-length dystrophin and beta-galactosidase. *PNAS* 93:5731–5736.

131. Parks RJ, Graham FL (1997) A helper-dependent system for adenovirus vector production helps define a lower limit for efficient DNA packaging. *Journal of virology* 71:3293–3298.

132. Parks RJ, Bramson JL, Wan Y, Addison CL, Graham FL (1999) Effects of stuffer DNA on transgene expression from helper-dependent adenovirus vectors. *J Virol* 73:8027–8034.

133. Sandig V et al. (2000) Optimization of the helper-dependent adenovirus system for production and potency in vivo. *Proc Natl Acad Sci U S A* 97:1002–1007.

134. Sternberg N, Hamilton D (1981) Bacteriophage P1 site-specific recombination: I. Recombination between loxP sites. *Journal of Molecular Biology* 150:467–486.

135. Parks RJ et al. (1996) A helper-dependent adenovirus vector system: removal of helper virus by Cre-mediated excision of the viral packaging signal. *Proc Natl Acad Sci U S A* 93:13565–70.

136. Chen L, Anton M, Graham FL (1996) Production and characterization of human 293 cell lines expressing the site-specific recombinase Cre. *Somat Cell Mol Genet* 22:477–488.

137. Andrews BJ, Proteau GA, Beatty LG, Sadowski PD (1985) The FLP recombinase of the 2 micron circle DNA of yeast: interaction with its target sequences. *Cell* 40:795.

138. Ng P, Beauchamp C, Evelegh C, Parks R, Graham FL (2001) Development of a FLP/frt system for generating helper-dependent adenoviral vectors. *Mol Ther* 3:809–815.

139. Buchholz F, Angrand PO, Stewart AF (1998) Improved properties of FLP recombinase evolved by cycling mutagenesis. *Nature biotechnology* 16:657–662.

140. Umana P et al. (2001) Efficient FLPe recombinase enables scalable production of helper-dependent adenoviral vectors with negligible helper-virus contamination. *Nat Biotechnol* 19:582–5.

141. Fisher KJ, Choi H, Burda J, Chen SJ, Wilson JM (1996) Recombinant adenovirus deleted of all viral genes for gene therapy of cystic fibrosis. *Virology* 217:11–22.

142. Sakhuja K et al. (2003) Optimization of the generation and propagation of gutless adenoviral vectors. *Hum Gene Ther* 14:243–254.

143. Józkowicz A, Dulak J (2005) Helper-dependent adenoviral vectors in experimental gene therapy. *Acta Biochim Pol* 52:589–599.

144. Ng P, Evelegh C, Cummings D, Graham FL (2002) Cre levels limit packaging signal excision efficiency in the Cre/loxP helper-dependent adenoviral vector system. *J Virol* 76:4181–9.

145. Mountain A (2000) Gene therapy: the first decade. *Trends Biotechnol* 18:119–128.

146. Gallaher SD (2007) In vivo delivery and persistence in mouse of an episomal expression cassette by a helper dependent adenovirus -- Epstein-Barr virus hybrid gene therapy vector. Available at: http://search.proquest.com/docview/304872334/abstract/13A2E44847D6A447447/1?accountid=14512 [Accessed November 4, 2012].

147. Tsurumi T, Fujita M, Kudoh A (2005) Latent and lytic Epstein-Barr virus replication strategies. *Rev Med Virol* 15:3–15.

148. Yoo HS et al. (2006) In vivo gene therapy of type I diabetic mellitus using a cationic emulsion containing an Epstein Barr Virus (EBV) based plasmid vector. *Journal of controlled release* 112:139–144.

149. Mei WH, Qian GQ, Zhang XQ, Zhang P, Lu J (2006) Sustained expression of Epstein–Barr virus episomal vector mediated factor VIII in vivo following muscle electroporation. *Haemophilia* 12:271–279.

150. Dorigo O et al. (2004) Development of a Novel Helper-Dependent Adenovirus-Epstein-Barr Virus Hybrid System for the Stable Transformation of Mammalian Cells. *J Virol* 78:6556–6566.

151. Lindner SE, Sugden B (2007) The plasmid replicon of Epstein–Barr virus: Mechanistic insights into efficient, licensed, extrachromosomal replication in human cells. *Plasmid* 58:1–12.

152. Yates JL, Warren N, Sugden B (1985) Stable replication of plasmids derived from Epstein–Barr virus in various mammalian cells. Available at: http://www.nature.com/nature/journal/v313/n6005/abs/313812a0.html [Accessed November 19, 2012].

153. Gallaher SD, Gil JS, Dorigo O, Berk AJ (2009) Robust In Vivo Transduction of a Genetically Stable Epstein-Barr Virus Episome to Hepatocytes in Mice by a Hybrid Viral Vector. *J Virol* 83:3249–3257.

154. Gil JS, Gallaher SD, Berk AJ (2010) Delivery of an EBV episome by a self-circularizing helper-dependent adenovirus: long-term transgene expression in immunocompetent mice. *Gene Ther* 17:1288–1293.

155. Bergelson JM et al. (1997) Isolation of a common receptor for Coxsackie B viruses and adenoviruses 2 and 5. *Science* 275:1320–3.

156. Roelvink PW et al. (1998) The coxsackievirus-adenovirus receptor protein can function as a cellular attachment protein for adenovirus serotypes from subgroups A, C, D, E, and F. *J Virol* 72:7909–15.

157. Meier O, Greber UF (2004) Adenovirus endocytosis. *The Journal of Gene Medicine* 6:S152–S163.

158. Kawabata K, Sakurai F, Koizumi N, Hayakawa T, Mizuguchi H (2006) Adenovirus vector-mediated gene transfer into stem cells. *Mol Pharm* 3:95–103.

159. Segerman A, Mei YF, Wadell G (2000) Adenovirus types 11p and 35p show high binding efficiencies for committed hematopoietic cell lines and are infective to these cell lines. *J Virol* 74:1457–67.

160. Sakurai F, Mizuguchi H, Hayakawa T (2003) Efficient gene transfer into human CD34+ cells by an adenovirus type 35 vector. *Gene Ther* 10:1041–8.

161. Nilsson M et al. (2004) Development of an adenoviral vector system with adenovirus serotype 35 tropism; efficient transient gene transfer into primary malignant hematopoietic cells. *J Gene Med* 6:631–41.

162. Sakurai F, Kawabata K, Yamaguchi T, Hayakawa T, Mizuguchi H (2005) Optimization of adenovirus serotype 35 vectors for efficient transduction in human hematopoietic progenitors: comparison of promoter activities. *Gene Ther* 12:1424–33.

163. Segerman A, Lindman K, Mei YF, Allard A, Wadell G (2006) Adenovirus types 11p and 35 attach to and infect primary lymphocytes and monocytes, but hexon expression in T-cells requires prior activation. *Virology* 349:96–111.

164. Johnstone RW, Loveland BE, McKenzie IF (1993) Identification and quantification of complement regulator CD46 on normal human tissues. *Immunology* 79:341–347.

165. Gaggar A, Shayakhmetov DM, Lieber A (2003) CD46 is a cellular receptor for group B adenoviruses. *Nat Med* 9:1408–12.

166. Anderson BD, Nakamura T, Russell SJ, Peng K-W (2004) High CD46 Receptor Density Determines Preferential Killing of Tumor Cells by Oncolytic Measles Virus. *Cancer Res* 64:4919–4926.

167. Gaggar A, Shayakhmetov DM, Liszewski MK, Atkinson JP, Lieber A (2005) Localization of regions in CD46 that interact with adenovirus. *J Virol* 79:7503–13.

168. Wang H et al. (2007) Identification of CD46 binding sites within the adenovirus serotype 35 fiber knob. *J Virol* 81:12785–92.

169. Krasnykh VN, Mikheeva GV, Douglas JT, Curiel DT (1996) Generation of recombinant adenovirus vectors with modified fibers for altering viral tropism. *J Virol* 70:6839–6846.

170. Wickham TJ et al. (1997) Increased in vitro and in vivo gene transfer by adenovirus vectors containing chimeric fiber proteins. *J Virol* 71:8221–8229.

171. Reynolds PN, Curiel DT (2002) New generation adenoviral vectors improve gene transfer by coxsackie and adenoviral receptor-independent cell entry. *Kidney International* 61:S24–S31.

172. Shayakhmetov DM, Papayannopoulou T, Stamatoyannopoulos G, Lieber A (2000) Efficient gene transfer into human CD34(+) cells by a retargeted adenovirus vector. *J Virol* 74:2567–83.

173. Shayakhmetov DM et al. (2002) A high-capacity, capsid-modified hybrid adenovirus/adeno-associated virus vector for stable transduction of human hematopoietic cells. *J Virol* 76:1135–43.

174. Balamotis MA, Huang K, Mitani K (2004) Efficient delivery and stable gene expression in a hematopoietic cell line using a chimeric serotype 35 fiber pseudotyped helper-dependent adenoviral vector. *Virology* 324:229–237.

Chapter 2

New insights into adenovirus small e1a regulated host cell transcription and H3K18 histone acetylation

INTRODUCTION

Adenoviruses have taught us much about transcriptional regulation and cell cycle control because the cells they commonly infect are end-differentiated non-cycling cells. In order for these cells to be adequate hosts for viral replication, the virus must force the cells into the cell cycle (1). Adenoviruses express the small e1a protein immediately upon infection, which is responsible for initiating cell replication (2). Small e1a interacts with both the transcriptional co-activators p300/CBP and the transcriptional repressor RB-family proteins in order to induce epigenetic reprogramming that results in activation of cell cycle genes and inactivation of genes detrimental to adenoviral replication (3, 4).

Collaborative studies between the Berk and Kurdistani labs have demonstrated that small e1a expression results in a global reduction of H3K18 acetylation (H3K18ac) markers throughout intergenic regions of the genome, but an increase in specific peaks of H3K18ac around promoters of cell cycle genes (5–7). In the original simplified model for these interactions, e1a binds to and inactivates the RB repressor, thereby activating cell cycle genes, and binds to and inactivates the p300/CBP, preventing them from activating their target genes.

The goal of this work was to investigate how the specific interactions between e1a and p300/CBP or e1a and RB-family proteins affect the distribution of the H3K18ac marker throughout the genome. We have found that a simple model can only begin to describe the complex interactions between e1a and it's cellular partners. The e1a interaction with p300/CBP appears to be more important for global hypoacetylation than the interaction with RB-family proteins, but surprisingly, the e1a and RB interaction is required for hyperacetylation and activation of cell cycle promoters.

General Experimental Approach

Cell cycle arrested cells were infected with adenovirus e1a mutants that either cannot interact with p300/CBP (p300- e1a), or cannot interact with RB-family proteins (RB- e1a). The genome wide distribution of the histone marker H3K18ac following infection with wild-type e1a (e1awt), p300- e1a, or RB- e1a, compared to mock infected cells, was determined by chromatin immunoprecipitation with anti-H3K18ac antibody followed by massive parallel sequencing (ChIP-seq). Correlations between H3K18ac and expression levels were established through whole transcriptome sequencing (RNA-seq).

MATERIALS AND METHODS

Cell Culture

IMR90 cells (Human primary lung embryo fibroblasts/ATCC) and 293-Cre expressing cells (human embryonic kidney transformed with Ad5 DNA so that they constitutively express E1A and E1B proteins/ATCC) were grown to 100% confluency at 37°C and 5% CO_2 in Dulbecco's modified Eagles' Medium (DMEM) supplemented with 100U/mL penicillin, 100μg/mL streptomycin, and 10% heat-inactivated fetal bovine serum (hiFBS). Unless otherwise noted in subsequent methods, DMEM refers to DMEM supplemented with penicillin and streptomycin.

Viruses

Psi5* adenovirus vectors, which are Psi5 vectors (8) that have the CMV promoter removed, were used to express wild-type or mutant e1a from the native e1a promoter.

Adenovirus Psi5* vectors were propagated in 293-Cre cells and titered by infectious genome QPCR assay (9). Psi5*e1awt expresses only the small e1a (12S) protein, but not the larger E1A (13S) protein. Psi5*R2G4X expresses a form of e1a that was mutated in the N-terminus and CR1 at residues important for establishing interactions with p300 and CBP proteins: R2G, E59A, V62A, F66A, E68A (10, 11). The e1a mutant with abrogated binding to the RB-family member proteins (Psi5*CR1-3A/Δ-CR2) has three point mutations in CR1 (L43A, L46A, Y47A) (12) and the deletion of amino acids 112-128 in CR2 that contain the LxCxE motif (Δ-CR2) (13). Psi5*R2G4X and Psi5*CR1-3A/Δ-CR2 were constructed by Dr. Gauri Jawdekar (UCLA). The adenovirus dl312 mutant, which has a deletion of most of the E1A region and cannot express either large or small e1a, was used an infection control (14).

Antibodies

For E1A/actin combined western blots, mouse primary monoclonal against E1A (M73; hybridoma supernatant (15)) and mouse primary monoclonal anti-actin (C2; Santa Cruz sc-8432) were diluted at 1:100 and 1:2000, respectively, in LI-COR Odyssey Blocking Buffer. For histone western blots, mouse primary monoclonal anti-H3 (ab10799; Abcam) and rabbit primary polyclonal anti-H3K18ac (814; a gift of Roberto Ferrari (6)) were diluted at 1:2000 and 1:500, respectively, in LI-COR Odyssey Blocking Buffer. LI-COR secondary antibodies labeled with infrared dyes were used for detection. Goat-anti-rabbit labeled with green fluorescent dye (IRDye 800CW; LI-COR) and goat-anti-mouse labeled with red fluorescent dye (IRDye 680LT; LI-COR) were diluted 1:3000 in LI-COR Odyssey Blocking Buffer. Primary antibodies were incubated overnight at 4°C with shaking. Secondary antibodies were protected from light and incubated for one hour at room temperature with shaking.

Western blot

All western blots were performed using Invitrogen-Life Technologies NuPAGE Bis-Tris 4-12% precast gradient gels with 1X NuPAGE MES SDS Running Buffer, and the iBlot 7-minute protein transfer system, according to manufacturer instructions. The LI-COR Odyssey Infrared Imaging System was used for protein detection and quantification. Samples and 10μL of Precision Plus Protein Kaleidoscope standard (Bio-Rad) were loaded for each gel, and electrophoresis was performed for 20 minutes at 100 volts, then at 190 volts until the dye front reached approximately 1cm from the end of the gel.

A razor blade was used to cut out the region of interest between the 75kD and 25kD marker bands for e1a and the loading control actin, and between the 25kD and 10kD bands for histones. Membranes were placed on a horizontal shaker in a western blot box containing enough Odyssey Blocking Buffer (LI-COR) to cover for 60 minutes at room temperature. The blocking buffer was discarded and primary antibodies were diluted as described above in fresh Odyssey Blocking Buffer and added to the appropriate membrane strip for overnight incubation at 4°C with shaking. The primary antibody solutions were then removed and the membranes were washed twice quickly with PBS plus 0.1% Tween-20 (PBST). At this point the membranes were combined in one western blot box and washed twice with Odyssey Blocking Buffer by adding enough blocking buffer to cover the membranes and incubating at room temperature with shaking for 15 minutes.

LI-COR secondary antibodies were diluted in fresh Odyssey Blocking Buffer and added to the washed membrane strips. All secondary antibody steps were performed with precautions to protect the antibodies and membranes from light, which could bleach the fluorescent signal. The membranes were incubated with the secondary antibodies for 1 hour with shaking at room

temperature. The secondary antibodies were removed and the membranes were washed twice quickly with PBST, and twice with enough PBST to cover the membranes with shaking for 15 minutes at room temperature. The membranes were analyzed using the Image Studio 2.1 Imaging Software for the Odyssey CLx Imaging System (LI-COR). The e1a/actin blots were scanned at the 700nm (red) channel and each band was quantified; the e1a signal for each sample was manually normalized to the actin signal in the same lane. The histone blots were duplexed for two-color detection and scanned at both the 700nm (red) and 800nm (green) channels. The histone bands were quantified separately at each channel (700nm for anti-H3, and 800nm for anti-H3K18ac), and the 800nm H3K18ac signal was automatically normalized to the 700nm H3 signal for each sample.

Empirical Titering

IMR90 cells were grown to 100% confluency in 6-well tissue culture plates. Cells counts were performed by first aspirating the media and washing one well with 1X trypsin, then adding 0.5mL fresh trypsin to the well and incubating at 37°C for 5 min. One mL of DMEM plus 10% hiFBS was added to the well and a single-cell suspension was created by repeated pipetting with a 1000μL pipettor. The cell suspension was diluted 1:1 with 2X trypan blue and was counted using a hemocytometer. The appropriate volume of each virus for a Multiplicity Of Infection (MOI) of 100, 200, or 400 was mixed with 500μL of DMEM (without FBS). Media was aspirated from each well and the diluted virus was added gently to the monolayer; 500μL of DMEM was added to a single well for mock infection. The plates were incubated at 37°C for 1 hour with periodic rocking to keep the monolayer from drying out, then 2mL of DMEM with 10% hiFBS was added back to each well.

After 24 hours post-infection (p.i.) the viral medium was aspirated and the cells were washed twice with 1mL 1X PBS (Gibco), then 0.5mL of 1X PBS with protease inhibitor (Roche Complete Mini EDTA-free Protease Inhibitor) was added to each well. The cells were then harvested by scraping, transferred to a 1.5mL microfuge tube, and pelleted by centrifugation at 2000 x g for 2 minutes. Cell pellets were resuspended in 200µL RIPA buffer (50mM Tris-HCl pH 7.4, 150mM NaCl, 2mM EDTA, 1% NP-40, 0.1% SDS) with 1X protease inhibitor and incubated on ice for 20 minutes to lyse the cells. The cell lysates were then sonicated using a Bioruptor (Diagenode) for 10 minutes with 30 second ON/OFF pulses to shear the chromatin. Protein concentration was determined by Qubit fluorometric quantification (Invitrogen/Life Technologies) according to the manufacturer instructions. Working stocks of lysates were prepared at 1mg/mL in RIPA buffer with 25% 6X sample preparation buffer (0.375M Tris pH 6.8, 12% SDS, 60% glycerol, 0.6M DTT, 0.06% bromophenol blue), then denatured at 95-100°C for 10 minutes. Ten micrograms of each sample were analyzed by western blot.

Chromatin Immunoprecipitation

Infection and cross-linking

Chromatin immunoprecipitation for ChIP-seq analysis was performed by infecting confluent 15-cm plates of IMR90 cells that had been growth arrested by contact inhibition for 2 days. Four 15-cm plates were infected with Psi5*e1awt, Psi5*R2G4X, and Psi5*CR1-3A/Δ-CR2 at MOI 100, 400, and 1000, respectively, for 1 hour in serum-free DMEM. Three 15-cm plates were mock infected for 1 hour with serum-free DMEM, then DMEM with 2% hiFBS was added back to all plates. Cells were cross-linked 24 hours post infection by 1% final concentration of formaldehyde for 30 minutes at 37°C. Formaldehyde cross-linking was quenched for 30 minutes

at room temperature by direct addition of glycine at a 0.14M final concentration. Each plate was washed twice with 15mL ice cold 1X phosphate buffered saline (PBS), then cross-linked cells were harvested by scraping in 3mL 1X PBS plus 1X protease inhibitor (Complete Protease Inhibitor Cocktail, Roche; PBS+PI). Cells were centrifuged at 500 x g at 4°C for 5 minutes, then resuspended in 1X PBS+PI at a density of 2 x 10^7 cells/mL in 1 mL aliquots. Aliquots were stored at -80°C for future sonication.

Sonication of chromatin

Cell pellets (2 x 10^7 cells) were thawed on ice then resuspended in 450μL lysis buffer with 1X protease inhibitor and incubated on ice for 10 minutes. Lysates were sonicated using a Misonix S-4000 cup-horn sonicator at an amplitude of 85Hz for 3x10 minute cycles with pulses of 30 seconds ON/40 seconds OFF. A 20μL aliquot of each lysate was set aside for western blot analysis of e1a expression and H3K18ac levels (Fig. 2.4), and 10μL of each sonicated lysate was removed to check the size of the sheared chromatin (Fig. 2.1). Each 10μL sample was diluted with 140μL of lysis buffer without protease inhibitors and incubated overnight at 65°C to reverse the cross-links. RNA was digested by adding 1μL 10mg/mL RNase A to each sample and incubating at 37°C for 30 minutes, followed by Proteinase K digestion at 0.4mg/mL final concentration for 2 hours at 56°C. DNA was isolated by QIAgen PCR Purification columns according to the manufacturer instructions. Chromatin fragments were eluted in 30μL QIAgen EB and 25μL were loaded onto a 1% agarose/1X TBE gel. As shown in Figure 2.1, the majority of chromatin fragments were in the desired 100-300bp range.

Chromatin Immunoprecipitation (ChIP)

Buffers

Lysis Buffer
1% SDS
50mM Tris-HCl pH 8
20mM EDTA
Fresh Protease Inhibitor

10X ChIP Dilution Buffer
16.7mM Tris-HCl pH 8
0.1% SDS
1.1% Triton X-100
1.2mM EDTA
167mM NaCl

Wash Buffer A
50mM Hepes pH 7.9
0.1% SDS
1% Triton X-100
0.1% deoxycholate
1mM EDTA
140mM NaCl

Wash Buffer B
50mM Hepes pH 7.9
0.1% SDS
1% Triton X-100
0.1% deoxycholate
1mM EDTA
500mM NaCl

LiCl Buffer
20mM Tris-HCl pH 8
0.5% NP-40
0.5% deoxycholate
1mM EDTA
250mM LiCl

TE Buffer
50mM Tris-HCl pH 8
1mM EDTA

Elution Buffer
50mM Tris-HCl pH 8
1mM EDTA
1% SDS

Day 1

The sonicated lysates were cleared by centrifugation at 4000 RPM at 4°C for 10 minutes and transferred to new microfuge tubes; 10μL of the soluble chromatin was stored at -80°C as the ChIP input sample. For each ChIP, 100μL of soluble chromatin (from approximately 5 x10 ^{6} cells) was diluted with 900μL 10X ChIP Dilution Buffer with freshly added protease inhibitors. Four ChIPs (400μL of soluble chromatin) were performed for each of the infection conditions (e1awt, p300- e1a, and RB- e1a), and three ChIPs (300μL of soluble chromatin) were performed for the mock infection. For each ChIP, 30μL of Protein A Dynabeads (Invitrogen) were pre-washed in 10X ChIP Dilution Buffer plus protease inhibitors then added to the diluted chromatin as a pre-clearing step for 1 hour at 4°C. The beads were removed and 4μL (2μg) of rabbit anti-H3K18ac antibody (see above) were added for each ChIP to the pre-cleared lysates and incubated on a rotator overnight at 4°C.

Day 2

For each ChIP, 60μL of pre-washed Protein A Dynabeads were added to the chromatin/antibody solution and incubated on a rotator at 4°C for 2 hours. The beads were collected and the supernatant was removed and retained. The beads were then washed twice with 500μL per ChIP of each of the following buffers (see above for buffer components), in order: Wash Buffer A, Wash Buffer B, LiCl buffer, and TE Buffer. After the final wash, the beads were collected and the chromatin was eluted in 100μL Elution Buffer per ChIP at 65°C for 10 minutes. The 10μL input chromatin aliquot set aside previously was diluted in 140μL of Elution Buffer. All samples, immunoprecipitated chromatin and input chromatin, were incubated at 65°C overnight to reverse the cross-links.

Day 3

The immunoprecipitated chromatin samples were separated into 150μL aliquots in microfuge tubes for isolation of DNA. Each 150μL ChIP and input aliquot were treated with 1μL of 10mg/mL RNase A for 30 minutes at 37°C, then with Proteinase K at a 0.4mg/mL final concentration for 2 hours at 56°C. Each aliquot was extracted with 1 volume of Ultrapure Phenol:Chloroform:Isoamyl alcohol. The aqueous layer from each tube was supplemented with 1μL 20mg/mL glycogen (Roche) prior to ethanol precipitation with 15μL (0.11 volumes) 3M sodium acetate and 375μL (2.5 volumes) 100% ice-cold ethanol. Chromatin pellets were washed with 400μL 70% ice-cold ethanol and air-dried. The pellets for each ChIP sample (mock, e1awt, p300- e1a, and RB- e1a) were combined in 12μL of 10mM Tris-Cl, pH 8.5, and each input sample was resuspended in 20μL of 10mM Tris-Cl, pH 8.5. The concentration of double

stranded DNA was measured for each sample using the Qubit dsDNA HS Buffer system (Invitrogen) according to manufacturer instructions.

ChIP-qPCR and Library qPCR

Equal amounts of chromatin were used as templates in qPCR reactions with Roche 1X FastStart Universal SYBR Green Master (with Rox normalization) and 0.24μM final concentration of each primer. Quantitative PCR was performed on an Applied Biosystems 7500 Real Time PCR machine in duplicate. H3K18ac ChIP fold enrichment over input was calculated for each primer set using the $2^{-\Delta\Delta C}{}_T$ method (16).

The immunoprecipitated chromatin was checked for specific loci enrichment over input by ChIP-qPCR with the following primers:

CCNE2-F 5'-CCTTCGCTGCCTCTATGAAT-3'
CCNE2-R 5'-ATCTTTGTTCCCGGAGCTGT-3'
COL6A3-F 5'-CACTTCTGAGCAGCCAACTG-3'
COL6A3-R 5'-AAGGGTGATCCCACAGAATGC-3'

The following primers, in addition to the COL6A3 primers above, were used to check enrichment over input for specific loci in the libraries generated for sequencing:

CCNE2_F600 5'-GGGTCCACTCTACCGGGCCT-3'
CCNE2_R692 5'-CGCGGAGAAGGAGCCCCTGA-3'

Library Preparation

The Ovation Ultralow Dedicated Read (DR) Multiplex System (NuGEN, Part No. 0330) was used to create sequencing libraries from immunoprecipitated and input chromatin according to the manufacturer instructions, with some modifications. DNA fragmentation and purification were performed as described above for ChIP, and only 0.8ng of fragmented immunoprecipitated

chromatin or input chromatin in 10μL of 10mM Tris-Cl, pH 8.5 was used as the starting material for each sample. See Table 2-1 for dedicated read adapters used for each library. The concentrations of the amplified and purified libraries were determined by Qubit dsDNA HS Buffer system (Invitrogen) according to manufacturer instructions, and 4μL of each library were loaded per lane into a 1% agarose/1X TBS gel. The sizes of each library were concentrated between 200-400bp, with an average size of approximately 300bp (Fig. 2.2). All eight libraries were combined in equal mass ratios at 1.5ng/μL final concentration in 10mM Tris-Cl, pH 8.5 plus 0.1% Tween-20 for multiplex sequencing using the Illumina HiSeq 2000 sequencing instrument in duplicate lanes.

Table 2.1. Dedicated Read barcodes used for libraries

LIGATION ADAPTOR MIX	**BARCODE SEQUENCE**	**SAMPLE NAME**
L2DR-BC1	AAGGGA	Mock input
L2DR-BC2	CCTTCA	e1awt input
L2DR-BC3	GGACCC	RB- e1a input
L2DR-BC4	TTCAGC	p300- e1a input
L2DR-BC5	AAGACG	mock ChIP
L2DR-BC6	CCTCGG	e1awt ChIP
L2DR-BC7	GGATGT	RB- e1a ChIP
L2DR-BC8	TTCGCT	p300- e1a ChIP

ChIP-seq Analysis

Primary sequencing analysis was performed by Dr. Roberto Ferrari (UCLA). The sequenced reads where mapped to the human genome (hg19) (17) using Bowtie software and analyzed as described by Ferrari et al. (2012). Briefly, peaks of enrichment were defined for 50-bp windows across the human genome, comparing ChIP and input normalized read counts. The input sample was used to estimate the expected counts in a window, and the average value for all windows was assigned to any windows with zero counts. The ChIP enrichment for each window was determined by using Poisson distribution to calculate *P*-values (*P*-val). A cut-off *P*-val of $< 10^{-4}$ was used to determine significant windows. The total number of peaks and total kb coverage of the genome for mock, e1awt, p300- e1a and RB- e1a H3K18ac peaks are reported in Table 2.2.

To determine regions that were significantly different between two ChIP samples, such as mock and e1awt, the same analysis was performed as above, with mock ChIP counts in place of the input sample ChIP counts. This algorithm produced files used for downstream analysis: BED (.bed) files contained the coordinates of significant windows of enrichment; Wiggle (.wig) files of 50bp fixed chromosome tiles with normalized read counts for significant windows (a tag value of zero was used for windows that were not significant; GR files of normalized raw input and ChIP samples were created for visualization on a genome browser. In addition, tiling profiles of promoter regions for the hg19 annotated human promoters were generated for 50 bp windows spanning 5 kb on either side of the transcription start sites (TSSs). Significant windows were reported as the number of reads, and non-significant windows were reported as zero.

Clustering by expression and H3K18ac downstream of the TSS

For this analysis, RPKM (Reads Per Kilobase per Million mapped reads) of two RNA-seq experiments performed by Dawei Gou were determined (18). The RPKM values for the average of two experiments for each mRNA transcript identification number (NM number) were used to calculate the ratio over mock for the dl312, e1awt, p300- e1a, and RB- e1a. A gene list was created that met the following criteria: (1) Genes were not activated or repressed by dl312, meaning that dl312 over mock did not change by >2 fold up or down, indicating that observed changes in expression were due to e1a and not just the infection process. (2) The genes also had to be either activated or repressed by e1awt by 2-fold over mock, that is they had to change up or down by greater than or equal to 2-fold. (3) The average RPKM value was greater than 0.5 for e1awt in activated genes, or greater than 0.5 in mock for genes repressed by e1awt. The conservative cutoff of RPKM > 0.5 was used in order to only observe the more highly expressed genes, and avoid skewed ratios resulting from dividing by very small numbers.

A list of genes (2X_e1awt) meeting these criteria was used for generating clustering by both the expression and the H3K18ac levels. The expression values for mock, e1awt, p300- e1a and RB- e1a were calculated by taking the log2 of the average RPKM value for each gene. The H3K18ac levels used for clustering were calculated by taking the log2 of the maximum (MAX) -logP for the fifty 50bp tiles downstream of the TSS. The MAX value was the highest -logP in any of the 50 tiles from +1 to +2500bp. The MAX downstream peak was determined for mock, e1awt, p300- and RB- for each gene in the 2x_e1awt list.

The significant reads of the original data were calculated so that any *P*-values less than $1x10^{-16}$ were considered infinitely significant, and therefore were given a cutoff value of 16 for the -logP. The log2 of the MAX peak -logP was calculated for the purpose of heat map

generation. The log2 values for expression and MAX H3K18ac downstream peaks were clustered using the Cluster 3 program (19) to generate 16 clusters, with a default of 100 runs. Clusters generated were only considered if the program found only 1 possible solution. The patterns of clusters generated by the program were not necessarily biologically significant, so further clustering was performed manually. First, the gene list was separated according to whether the genes were activated or repressed by e1awt. The clusters were then grouped by similarity of the profile and the gene ontology that was returned by the DAVID gene ontology program (20, 21).

Clustering by MAX H3K18ac upstream and downstream of all TSS by e1a over mock ratio

The maximum upstream and downstream H3K18ac -logPvals from ChIP-seq were determined for every transcript ID (~36,700) as described previously for the 2-fold induced/repressed genes. The analysis was then limited to only those transcript IDs that had at least one significant peak (-logP >= 4) in any of the datasets (mock, e1awt, p300- e1a, RB- e1a) in either the upstream or the downstream max peak value. This narrowed the list to approximately 18,300 transcript IDs. Next the ratio of H3K18ac over mock was calculated for each, after first substituting the value 0.05 for any transcript ID with a max peak value of zero. This was done to avoid dividing by zero when calculating the ratios. The max peak value for e1awt upstream of the TSS was divided by the max peak value for mock upstream, and the e1awt downstream max peak value was divided by the mock downstream max peak value. This was repeated for each transcript ID for both the p300- e1a and the RB- e1a mutants. The log2 of each ratio was calculated for the purposes of heatmap visualization. The H3K18 hypoacetylation and hyperacetylation patterns were determined by k-means clustering using the Cluster 3 program

(12 clusters, 100 runs, solution found 1 time) for the ratios of infected over mock in both the upstream and downstream of the TSS peaks for e1awt, p300- e1a, and RB- e1a. Several clusters with similar patterns were combined, for a total of 8 clusters (k1-k8). The log2 of the ratio of the average RPKM values for e1a divided by mock, from RNA-seq expression described above, were used to expression generate box plots for each cluster.

RESULTS

Empirical titering of adenoviral stocks

Empirical titering was performed in order to determine the appropriate MOI to infect IMR90 cells to get equivalent levels of e1a expressed by e1awt and the p300- and RB- mutant e1a viruses. IMR90 cells were infected at MOIs of 100, 200, and 400, and then assayed for e1a expression by western blot. Figure 2.3 demonstrates that increasing MOIs did not correspond to linear increases in e1a expression for e1awt and RB- e1a. The relative normalized e1a levels were equivalent for e1awt at an MOI of 100 and p300- e1a at MOI of 400. However, even at an MOI of 400 the RB- e1a was only expressed at about 10% of the level of e1awt. An MOI of 1000 was used for future experiments with the RB- e1a mutant. These results may indicate that the mutant e1a proteins may be expressed at lower levels or were less stable that the wild-type e1a protein.

Validation of infections and library preparation for ChIP-seq by western blot and qPCR

Infection and western blot

Two-day growth arrested IMR90 cells at passage 7 were either mock infected or infected at the MOIs determined by empirical titering of the viral stocks: e1awt at an MOI of 100, p300- e1a at an MOI of 400, and RB- e1a at an MOI of 1000. Twenty-four hours post infection (p.i.) cells were cross-linked and harvested for ChIP-seq analysis. After sonication, 20μL of each sample lysate was used for western blot analysis and quantification (Fig. 2.4). The p300- e1a and RB- e1a were 50% and 25%, respectively, of e1awt protein levels at 24 hours post infection. Even at an MOI 10x higher than e1awt, the RB- e1a mutant still only showed a fraction of the level of e1a protein by western blot. However, we did see that the expected H3K18 hypoacetylation for e1awt, and RB- e1a reduced H3K18ac to about 50% of the level in mock, indicating that even the reduced level of RB- e1a was able to affect a change in the global pattern of H3K18 acetylation. The p300- e1a did not show global decrease in H3K18ac, rather it increased to 1.4x that of mock. Based on these observations, the remaining lysates were used for chromatin immunoprecipitation with anti-H3K18ac antibody.

ChIP-qPCR

Primers were designed for qPCR to analyze enrichment of H3K18ac in genomic areas of interest. The intergenic region between the *COPS8* and *COL6A3* genes was previously reported to be enriched for H3K18ac in mock infected IMR90 cells, as well as the promoter region upstream of the *CCNE2* cell cycle gene in e1a-expressing IMR90 cells (6). ChIP-qPCR results (Fig. 2.5A) showed that the mock chromatin immunoprecipitation was greatly enriched at the *COL6A3* locus with over 36-fold enrichment over input, while p300- e1a was enriched about

twice as much (14-fold enrichment) as either e1awt or RB- e1a (7-fold enrichment). The enrichment at the CCNE2 locus was lower overall, but e1awt and p300- e1a were both enriched to a greater extent (about 7-fold enrichment) than either mock or RB- e1a. These results indicate that the chromatin immunoprecipitations with the anti-H3K18ac antibody were successfully enriched for regions known to have H3K18 acetylation.

Library generation and qPCR

Libraries were generated using the NuGEN Ovation Ultralow Dedicated Read (DR) Multiplex System for sequencing from each H3K18ac ChIP and from their respective input chromatin. Analysis of the amplified libraries by qPCR (Fig. 2.5B) corroborated the trends from the ChIP-qPCR, with ~14-fold enrichment at the *COL63A* locus for mock and p300- e1a, and 8-fold to 10-fold enrichment at *CCNE2* for p300- e1a and e1awt, respectively. These results, along with the expected 200-400bp size of the libraries by agarose gel (Fig. 2.2), validated the library generation. All of the barcoded ChIP and input libraries were combined for multiplex Next-Generation Sequencing (NGS) on an Illumina HiSeq 2000 sequencing instrument.

Small e1a interaction with the p300/CBP proteins is required for global hypoacetylation seen by western blot and ChIP-seq

In order to investigate whether the e1a interaction with p300/CBP or with RB-family proteins were important for the global redistribution of H3K18ac upon expression of e1a, growth arrested IMR90 cells were infected with adenovirus mutants expressing e1awt, an e1a mutant unable to bind p300/CBP (p300- e1a), an e1a mutant unable to bind RB-family proteins (RB- e1a), or were mock infected. Comparison of the cell lysates by western blot showed an

approximately 50% decrease in the H3K18ac levels for e1awt and RB- e1a infection compared to mock, while the H3K18ac for the p300- e1a resembled mock infected levels (Fig. 2.4).

H3K18ac ChIP-seq was used to determine the total number of H3K18ac marker peaks across the whole human genome. The total number of H3K18ac peaks by ChIP-seq for e1awt (62,447) and RB- e1a (52, 985) were reduced to 43% and 37%, respectively, of the number of peaks in mock infected cells (144,803), while the p300- e1a (121,440) only showed a slight decrease to 84% of mock. This recapitulates the global hypoacetylation observed for e1awt and RB- e1a by western blot, but the slight increase for H3K18ac by p300- e1a seen by western blot was not reflected in either the total peak number or genome coverage (Table 2.2).

Figure 2.6 demonstrates that e1awt and RB- e1a had dramatically lower H3K18ac peak densities than mock infected, but RB- e1a had a higher peak density than e1awt. The p300- e1a had a lower peak density than mock, but was not as low as either e1awt or RB- e1a, indicating the e1a interaction with p300/CBP is required for the global decrease in H3K18ac.

Global hypoacetylation by e1a in intergenic regions

We wanted to determine the distribution of the significant peaks of H3K18ac across different regions of the genome. GREAT, the Genomic Regions Enrichment of Annotations Tool (22), was used to examine peaks with respect to TSS (Fig. 2.7A) and a version of CEAS, Cis-regulatory Element Annotation System (23, 24), was used to divide the whole genome into three annotation categories: promoters (TSS ± 3kb), introns, and intergenic regions (Fig. 2.7B). Intergenic regions were defined as regions >3kb from TSSs and >3kb from the final exon of annotated GenBank (25) transcript reference sequences (refseq).

By both the GREAT and CEAS analysis we observed that both e1awt and RB- e1a had higher percentages of H3K18ac peaks within promoter regions, for GREAT (TSS ±5kb) and CEAS (TSS ±3kb), than mock or p300- e1a, and lower percentages of peaks in intergenic regions. The relative percentages of H3K18ac in introns were about the same for all conditions. This indicates that neither the promoter regions nor intronic regions were responsible for global H3K18ac decreases, but it was rather the hypoacetylation of intergenic regions that likely cause these global changes.

A heatmap was constructed for the approximately 14,000 total intergenic regions of the genome, normalized for size (Fig. 2.7C). Each intergenic region was divided into 40 bins, regardless of size, and the average counts of H3K18ac for each bin were calculated. The intergenic regions were then sorted by the total sum of all bins in mock. The intergenic region heatmap demonstrated that both e1awt and the RB- e1a induced extensive hypoacetylation in intergenic regions, while the p300- e1a intergenic heatmap was much like mock infected for the highly acetylated regions. These results indicate that the global hypoacetylation observed upon e1a expression was due to the interaction with p300/CBP. Note, however, that there were peaks of H3K18ac following infection with adenovirus mutants that express wt e1a, p300- e1a, and RB- e1a that were not present in the intergenic regions in mock.

p300- e1a does not affect total levels of H3K18ac, but does result in the redistribution of H3K18ac peaks

In order to determine if the H3K18ac peaks after infection were also present after mock-infection, or were new peaks resulting from infection, we analyzed the number of peaks from the e1awt, p300- e1a and RB- e1a expressing viruses that overlapped mock-infection peaks. The

significant H3K18ac peaks overlapping by ≥1base pair (bp) in mock or e1a infected cells are presented as Venn diagrams (Fig. 2.8). Upon e1awt expression, 76.6% (110,908) of mock H3K18ac peaks were removed, while 45.7% (28,552) of the total H3K18ac peaks present after e1awt expression were new peaks (Fig. 2.8A). The RB- e1a mutant, which like e1awt can still interact with p300/CBP, resulted in 78.9% (114.118) of mock H3K18ac peaks being removed and replaced with 42.1% (22,300) new peaks (Fig. 2.8C). This indicates that the e1a interaction with p300/CBP is likely to be responsible for the observed H3K18 global hypoacetylation 24 hours post infection with e1a expressing viruses.

For p300- e1a, 63.5% of mock H3K18ac peaks were removed upon e1a expression, while 56.5% of the total H3K18ac peaks present after p300- e1a expression were new peaks (Fig. 2.8B). Interestingly, although the total number of H3K18ac peaks was not greatly changed upon p300- e1a expression, over half of the peaks were redistributed compared to mock.

The Venn diagrams (Fig. 2.8) demonstrate that although most of the peaks were removed, some peaks were retained upon infection (overlapping region), and some new peaks were added. The Venn diagrams represent e1a peaks that overlap mock peaks by at least one base pair, but the "new" peaks outside of the overlapping regions may not necessarily represent distinct regions that were specifically acetylated in e1a expressing cells. Peaks that may be shifted slightly in the same region of the genome would be counted as new peaks. We wanted to determine how many peaks were added to distinct regions of the genome solely as a result of the e1a expression. Lists of "specific peaks" that were separated at least 1000 bp from regions containing peaks in mock-infected cells were generated for e1awt, p300- e1a and RB- e1a (Fig. 2.9A). Note that these were called "p300- specific" or “RB- specific peaks,” but they may actually be some of the same peaks specific for e1awt. We found that there were about 5,000 specific peaks for both e1awt and RB-

e1a, representing about 9% of the total peaks for each. The p300- e1a had over 20,000 specific peaks, corresponding to 17% of the total peaks.

The distributions of the specific peaks were determined for promoters, introns, and intergenic regions. About half (48%) of the specific p300- e1a peaks were in intergenic regions, which correspond to over 10,000 new intergenic peaks (Fig. 2.9C). This data, along with the intergenic region heatmap in Figure 2.7C, strongly indicates that while the total H3K18ac levels were not affected by the p300- e1a mutant, in the absence of an interaction with p300, the e1a/RB complex redistributes the peaks of H3K18ac within the intergenic regions. The RB- e1a induced a similar number of total specific peaks to e1awt-induced specific peaks (Fig. 2.9B), but Figure 2.9D indicates that RB-e1a had many more specific peaks in promoter regions (TSS ±3kb). This finding is investigated in further detail in a subsequent section.

H3K18ac at Promoters does not account for global hypoacetylation levels

Initial findings recapitulated the global H3K18ac decrease observed for cells expressing e1awt in previous studies (5, 7), and determined that the e1a interaction with p300/CBP appears to be more important for global hypoacetylation than the interaction with RB-family proteins. We next wanted to investigate how the e1a interactions with p300/CBP versus RB-family proteins affect H3K18ac in promoter regions. To this end, the -logP values for H3K18ac in 50 bp windows for 5 kb upstream and downstream from the TSS of each transcript ID were calculated and presented as a heatmap (Fig. 2.10). In genes with significant H3K13ac in all four categories, the upstream peaks in all e1a-expressing categories were reduced compared to mock, while the downstream peaks were less reduced, especially for RB-e1a. The remaining clusters with significant peaks, which had lower starting levels of H3K18ac in mock, were mostly

reduced upstream and downstream for e1awt and p300- e1a compared to mock. RB- e1a however caused an increase in downstream H3K18ac in most of these clusters and less reduction, or even some increase, in upstream peaks. These results indicate that the H3K18ac levels at the TSS were not primarily responsible for the global hypoacetylation observed for cells expressing RB- e1a.

H3K18ac hyperacetylation at TSS +1 to +2500 bp corresponding to activation of cell-cycle genes is dependent on the e1a-pRB interaction

We next wanted to investigate how the e1a interactions with p300/CBP or RB-family members affect expression, and whether changes in expression were correlated with H3K18ac levels at transcription start sites (TSS).

A heat map was generated by k-means clustering of the log2 of the RPKM expression for genes activated or repressed at least 2-fold by e1awt over mock, and the log2 of the MAX peak within 2.5kb downstream from the TSS (Fig. 2.11A). The left panel of Figure 2.11A shows the log2 of the RPKM expression data for mock, e1awt, p300- e1a, and RB- e1a; the right panel shows the log2 of the MAX downstream peak of H3K18ac genes in the same order from top to bottom.

The genes with expression activated by at least 2-fold by e1awt were characterized into 5 clusters (act_1 – act_5), and the 2-fold repressed by e1awt genes were placed into a single cluster (rep_1). The DNA replication and cell cycle related genes fell mainly into the first two clusters. Cluster act_1 genes (377 transcript IDs) were activated by e1awt and p300- e1a, but not RB- e1a, and the H3K18ac levels reflected the same pattern of low in mock, hyperacetylated by e1awt and p300- e1a, and low in RB- e1a. This cluster was characterized by a gene ontology analysis of -

logPval > 30 for cell cycle and DNA replication genes (Fig. 2.11B). These were extremely significant values, indicating that the overwhelming majority of genes in this cluster were related to cell cycle and DNA replication.

Among the most highly expressed genes in the first activated cluster were genes related to DNA replication, such as eight different mini-chromosome maintenance genes (*MCM*), the *GINS* family of genes involved in initiation of DNA replication, and six different DNA polymerase subunits, in addition to *PCNA* and other cofactors. Figure 2.12 shows representative Integrated Genome Browser (26) views of H3K18ac and pRB for *MCM3* (Fig. 2.12A), *MCM7* (Fig. 2.12B), and *PCNA* (Fig. 2.12C). There was no peak of H3K18ac downstream of the TSS for *MCM3*, but e1awt introduces a large, very significant peak downstream. The p300- e1a induced significant, but smaller, peaks downstream of the TSS in addition to inducing another small peak ~1.5 kb upstream of the TSS. H3K18ac peaks induced by the RB- e1a mutant were much smaller than the peaks induced by e1awt. Significant peaks of H3K18ac were induced by e1awt and p300- e1a for *MCM7,* but not RB- e1a. *PCNA* has two possible TSSs, but RNA-seq data showed that only the downstream TSS was used in these fibroblasts expressing e1awt and p300- e1a. H3K18ac near the active *PCNA* TSS was interesting in that there was a large peak of H3K18ac upstream of this TSS in mock-infected cells, but then there was a shift of the peak to downstream of the TSS induced by e1awt and p300- e1a, but not by RB- e1a. Figure 2.12A also includes the nearby intergenic region downstream of *MCM3*, which had a significant peak of H3K18ac in mock-infected cells that was substantially reduced by expression of e1awt and RB- e1a, both of which bind p300/CBP, but not p300- e1a, which does not. The intergenic region did not have any peaks of RB1 in mock-infected cells. In mock-infected cells, there were large peaks

of RB1 coinciding with the TSS of these genes, between the peaks of H3K18ac upstream and downstream of the TSS.

Cluster act_1 is particularly significant in that it was clear that the e1a interaction with RB-family proteins was required, not only to increase expression of these cell cycle genes induced by e1a, but that the interaction with RB-family proteins also was integral to the hyperacetylation induced just downstream of the TSSs of these genes. Cluster act_1 was the only activated cluster in which the expression pattern reflected the H3K18ac pattern. It was surprising that the e1a interaction with RB, but not p300/CBP, was required for hyperacetylation near the TSS of act_1 cluster genes because it is p300/CBP that is responsible for acetylating H3K18 (7). These results raise the question: Why would the interaction with RB-family proteins be required for hyperacetylation in the promoter regions of these genes?

Cluster act_2 (426 transcript IDs), while also categorized by a gene ontology including DNA metabolic process and DNA repair, had much less significant -logP values (< 5) for these categories (Fig. 2.11C). This cluster also contained genes related to mitochondria and ATP binding. Within cluster act_2 was a subset represented by various chaperone protein genes in which expression started out high, and was increased still further at least 2-fold by e1awt. As a whole, cluster act_2 also required the e1a interaction with RB to activate expression maximally, but expression levels induced by RB- e1a were higher than in cluster act_1.

Cluster act_2 was also represented by initiation of DNA replication genes, including some DNA polymerase subunits (*POLH, POLE3*) and accessory proteins such as *RFC4* and *PCNA*. In addition, genes such as *CDC25A* were represented, which were required for progression from the G1 to S-phase of the cell cycle. Cluster act_2 also was represented by the solute carrier family 25 mitochondrial membrane transport proteins (*SLC25*), which are

responsible for the transport of metabolites for a number of processes including intramitochondrial DNA synthesis (27).

Noticeably, the H3K18ac patterns in this cluster were not reflected by changes in expression, and were not affected by expression of e1awt or either of the e1a mutants, suggesting that an increase in acetylation downstream of the TSS is important only for the act_1 cluster. However, cluster act_2 started out with high H3K18ac levels in mock-infected cells, so perhaps there were increases in H3K18ac in this cluster that were not captured within the limitations of a -logPval cutoff of 16. The genes in this cluster could be hyperacetylated above mock, but the changes might not be observed with this method of analysis

In summary, clusters act_1 and act_2 were the main clusters of genes associated with DNA replication and cell cycling, and both required the e1a interaction with RB to activate expression maximally, but only the act_1 cluster showed expression levels corresponding to changes in H3K18 acetylation. The act_2 cluster genes were highly acetylated downstream of the TSS in mock and all e1a expressing conditions, and the lack of e1a interaction with RB proteins did not affect expression as strongly as in cluster act_1.

Role of e1a-p300 interaction in protection from apoptosis post infection

The act_3 cluster (164 transcript IDs) was interesting in that these genes required the interaction of e1a with p300 for e1a-activation of expression, but H3K18ac in the promoter region was not greatly affected by loss of the e1a interaction with either p300/CBP or the RB-family proteins. Envelope genes for mitochondrial transport and cell adhesion were represented in this cluster (Fig. 2.11D). Some of the *SLC25* mitochondrial transport genes also fall into this category, along with other mitochondrial genes such as the *TIMM8A* inner membrane

translocase, and the intermembrane space *SUOX* sulfite oxidase gene. This cluster also contained *AMIGO1* and *AMIGO3*, adhesion molecules with Ig-like domains, as well as the intercellular adhesion molecule *ICAM1*, which was the most highly expressed gene in this cluster.

Interestingly, *ICAM1*, which was represented in both the adhesion and viral replication gene ontology categories, acts as a cellular adhesion molecule and as a binding site for another virus also responsible for infecting respiratory epithelial cells, the rhinovirus (28). It has been reported that the interaction of e1a with p300 and NFκB can recruit the transcriptional machinery to the promoter of *ICAM1* to up-regulate transcription in response to inflammation stimuli (29), and that up-regulation of NFκB dependent *ICAM1* expression plays an important role in cell attachment and survival in response to cellular stress (Chen et al., 2011). Recent work also has demonstrated that over expression of *AMIGO* family members resulted in increased resistance to apoptosis in dendritic cells (30). This suggests that the e1a interaction with p300/CBP plays a possible role in protecting the infected cell from the inflammatory response and subsequent apoptosis. This is further supported by the chemokine and Toll-like receptor domain containing genes in this cluster.

Induction of RNA processing genes is not dependent on e1a interaction with either p300/CBP or RB-family proteins

The act-4 cluster (703 transcript IDs) was characterized by an increase in expression in response to e1a, independent of the e1a-interaction with either p300/CBP or RB-family proteins. However, the p300- e1a mutant appears to have activated to a slightly lower level than e1awt or the RB- mutant. The H3K18ac levels do not appear to change significantly between mock and e1awt or p300- e1a-expressing cells, but do appear to be slightly elevated by the RB- mutant e1a.

Gene ontology analysis of this cluster was strongly correlated with genes related to RNA processing (Fig. 2.11E), including several members of the *NOP*-family of nucleolar protein homologs responsible for processing pre-18S rRNA, and members of the *EXOSC*-family of 3' to 5' exoribonucleases. Mitochondrial ribosomal proteins, including *MRPL12*, *MRPL28*, and others, were also represented in this cluster. These results indicate that neither e1a interactions with p300/CBP, nor RB-family proteins were important their induction by e1a. The up-regulation of these genes is clearly important for viral replication, as the virus needs to not only activate the DNA replication machinery, but must also prepare the host cell to make sufficient amounts of the structural viral proteins. These genes were for the most part already expressed at high level in mock-infected cells, but were induced to higher levels upon infection. Since neither mutant resulted in reduced levels of activation, the results suggest that the e1a interacts with some other host cell protein, or proteins, to activate these genes.

When e1a cannot displace RB-family proteins from the E2F family of transcription factors, genes encoding zinc-finger transcription factors are induced

In contrast to the act_4 cluster, the act_5 cluster of genes (498 transcript IDs) were expressed at extremely low levels in mock-infected cells (RPKM values < 0.5, indicated by blue bars in the heat map Fig. 2.11A). Upon infection, e1awt and p300- e1a induced these genes so that they express transcripts with RPKM values of ~ 1 (black bars in heat map). The RB- mutant e1a appears to induce these genes somewhat less effectively. The levels of H3K18ac for these genes were generally low in both mock and infected cells expressing e1awt or either of the mutants. Gene ontology analysis of this cluster indicated regulation of transcription as the prominent category, although at 2.5 the -log(P-val) for this was not extremely significant (Fig.

2.11F). When the analysis was expanded to include protein domains as well as gene ontology, the -log(P-val) for zinc-finger domains were very significant. This cluster included over 50 uncharacterized zinc-finger proteins, in addition to known zinc-binding proteins such as TRAF-interacting protein (*TRAIP*).

The interaction of e1a with p300/CBP contributes to repression

The final cluster contains genes were repressed at least 2-fold from mock upon e1awt expression. The general trend for expression of this cluster of genes was that they were highly expressed in mock-infected cells and infected cells expressing p300- e1a, but were repressed at least 2-fold by both e1awt and RB- e1a. The H3K18ac levels in mock were high, and were reduced by e1awt and RB- e1a but not eliminated. H3K18ac levels in cells expressing p300- e1a were more similar to mock, but were somewhat reduced. Gene ontology analysis of this cluster showed that genes responsible for regulation of the cell cycle were repressed, as well as genes responsible for differentiated fibroblast functions (Fig. 2.11G). The growth arrest specific genes *GAS1*/*GAS7*, which block entry into S-phase, and the tumor suppressor-like genes *CAV1* and *INHBA* were all represented in this repressed cluster. Fibroblast function genes such as *PLAT*, *SERPINE1*, and *CD44* were also repressed by e1awt and RB- e1a, but not p300- e1a. This indicates that the e1a interaction with p300/CBP likely inactivates or sequesters p300/CBP, preventing H3K18ac at the TSS and subsequently repressing these genes.

The interaction of e1a with RB is required for hypoacetylation and repression at the TSSs of many non-cell cycle genes

An average profile of the -logP values for H3K18ac around the TSS for all genes (Fig. 2.13), generated using Sitepro (31), shows that the e1a-interaction with RB was required for maximal general H3K18ac hypoacetylattion near TSSs, as was also evident in Fig. 2.10. Without the e1a interaction with RB, the global H3K18ac downstream of the TSS appears more like that observed in mock-infected cells. The e1a-interaction with RB was apparently required for hyperacetylation at cell cycle gene's TSS and hypoacetylation of other genes. We observed a distinctive downstream pattern for H3K18ac at the TSS of some of the 2x e1awt activated genes that was different from what we observed for all TSSs. These results led us to investigate if there was a correlation between these different patterns of H3K18ac for different gene classes.

A heatmap was generated from k-means clustering of the log2 of the ratio of e1a/mock for the maximal peaks upstream and downstream of the TSS and is shown in the left panel of Figure 2.14A. In left heatmap left panel for H3K18ac, a red band (1 = 2-fold increase, 2 ≥ 4-fold increase) indicates hyperacetylation compared to mock, and a green band (-1 = 2-fold decrease, -2 ≥ 4-fold decrease) indicates hypoacetylation compared to mock, while a black band indicates no change from the mock peak. The center panel displays the fold change in expression (log2 of the ratio of e1a RPKM /mock RPKM) for the clusters generated by the H3K18ac patterns; red and green represent 2-fold activation and repression, respectively. The right panel displays the log2 of the MAX of RB1 peak near the TSS in mock-infected IMR90 cells (data published by Ferrari et al., 2012); red bands indicate a -logP value of ≥4. DAVID gene ontology analysis was performed for each cluster (Fig. 2.14B).

The first cluster, k1 (1252 transcript IDs), was characterized by a peak shift upon infection, as seen in the Integrated Genome Brower (IGB) plot of PCNA (Fig. 2.12C). There was a large peak of H3K18ac upstream of the TSS in mock-infected cells, but upon expression of e1awt, or p300- e1a, the peak was removed from the upstream position and replaced with a peak of H3K18ac downstream of the TSS. These genes were generally activated compared to mock, with higher levels of RB1 corresponding to higher expression. Interestingly, it appears that the RB- e1a could not activate expression in the genes with the highest levels of RB1, but was able to increasingly active genes as the relative level of RB1 decreased. Conversely, the genes with the highest levels of RB1 were activated the most strongly by both e1awt and p300- e1a. This indicates that this cluster of genes follow the traditional model of RB repressing E2Fs at the promoters, and expression of e1a capable of displacing RB (e1awt and p300- e1a) results in their activation. RNA processing, DNA replication, and translation genes were represented in the gene ontology of this cluster.

Cluster k2 (943 transcript IDs) had the characteristic pattern of having no H3K18ac peaks either upstream or downstream of the TSS in mock and the addition of a new peak, or peaks, of H3K18ac following expression of e1awt and/or p300- e1a and RB- e1a. The new peaks were most commonly downstream of the TSS, but some genes had new peaks both upstream and downstream. Notably, the RB- e1a mutant seemed to be responsible for more upstream peaks than the e1awt or the p300- e1a, and these differences would not have been observed in the expression and H3K18ac clustering done previously, since that clustering only analyzed downstream maximum H3K18ac peaks. These genes were strongly activated by e1awt and p300- e1a, and somewhat less so by RB- e1a. Again higher RB1 levels appear to correlate with

lack of activation by the e1a incapably of binding RB-family proteins. Gene ontology of this cluster showed cell cycle and DNA replication genes with a high degree of significance.

Cluster k3 had an interesting pattern of H3K18ac; e1awt induced little change, while p300- e1a caused hypoacetylation, and RB-e1a caused hyperacetylation and activation of expression. For clusters k4 and k5, the interaction of e1a with RB was required for hypoacetylation, either upstream or downstream, but not for upstream hyperacetylation. Expression in clusters k3-k5 was specifically activated by RB- e1a, and by e1awt to a lesser extent, independent of RB1 levels. Each of these clusters had gene ontology terms related to mitochondrion and zinc-finger proteins.

The total H3K18ac levels for RB- e1a in clusters k3, k4, and k5 indicate that the e1a interaction with RB was required for hypoacetylation downstream of the TSS at a large number of zinc-finger related genes. The interaction of e1a with RB results in the hypoacetylation of these clusters, but the absence of the interaction with RB causes these genes to *not* become hypoacetylated, resulting in increased expression by RB- e1a. These three clusters combined represent 8,859 out of 18,322 of the transcript IDs used in this analysis; this indicates that these genes were likely responsible for the higher average H3K18ac profile around the TSS for the RB- e1a mutant (Fig. 2.13).

Cluster k6, in contrast to most of the other clusters, was hypoacetylated predominately upstream of the TSS by expression of e1awt or the e1a mutants and was little changed for H3K18ac downstream. Interestingly, expression levels appeared to correlate with RB1 levels for e1awt and both mutants, but not H3K18ac. Genes with RB1 near the TSS were mainly activated, while genes without RB1 were somewhat repressed. Cytoskeletal organization and protein/vesicle transport were the predominant gene ontology terms in this cluster.

Cluster k7, represented by signal transduction and cellular biosynthetic processes, and cluster 8, represented by chromatin assembly genes, were both hypoacetylated downstream of the TSS by e1awt and both mutants, with the difference between the clusters being that cluster k7 had little upstream mock H3K18ac to begin with, and cluster k8 had higher upstream H3K18ac before infection. Both of these clusters were mainly repressed, fitting with the traditional model of hypoacetylation downstream of the TSS causing transcriptional repression. Clusters k6-k8 were hypoacetylated at the TSS independently of whether e1a could interact with p300 or RB, indicating that this hypoacetylation was mediated through some other protein interaction.

In summary, although some genes in clusters k1 and k2 followed the traditional model of e1a displacing RB from E2Fs at the promoters of genes to cause hyperacetylation and activation of transcription, most genes did not. The interaction of e1a with RB played a role in the hypoacetylation of H3K18 downstream of the TSSs and the subsequent repression of expression in roughly half of the over 18,000 genes examined in this analysis.

DISCUSSION

The ChIP-seq results presented here recapitulate the global H3K18ac decrease observed for e1awt in previous ChIP-seq studies (6) and observed by western blot and immunofluorescence (5, 7). This work has also provided evidence that the e1a interaction with p300/CBP appears to be more important for global hypoacetylation than the interaction with the RB-family members. When e1a can interact with p300/CBP, but not RB-family members, the global pattern of H3K18ac looks much like the pattern for wild-type e1a. However, when e1a

can only interact with RB in the absence of p300/CBP, the peaks of H3K18ac were not maintained like mock-infection, even though the total numbers of peaks were similar. Rather, over half of the total peaks in the p300- infection were new peaks not overlapping with mock.

This could suggest that e1a possibly retargets p300/CBP to acetylate other genomic loci, allowing histone deacetylases to remove the H3K18ac from the original, mostly intergenic, regions. A recently published study identified SIRT7 as a specific H3K18 deacetylase, and found that its expression was required both for e1a mediated global hypoacetylation and for small e1a to force contact inhibited cells into the cell cycle (32). A contradictory study published around the same time reported that SIRT7 had little or no actual deacetylase activity, but rather played a role in connecting transcriptional machinery with chromatin remodeling complexes (33). The exact mechanism by which e1a causes global hypoacetytion still needs further study, but this work demonstrates that the interaction with p300/CBP is the key to the process.

The truly surprising finding of this work is that the e1a interaction with the histone acetyltransferases primarily responsible for H3K18ac, p300/CBP, is not required for the e1a mediated H3K18 hyperacetylation at the promoters for activation of cell cycle genes. Instead, e1a's interaction with RB-family proteins plays a dual role in both activating cell cycle genes through H3K18 hyperacetylation downstream of the TSS and preventing the activation of a large number of other genes by mediating their hypoacetylation. A tentative hypothesis to tie all these results together could be that e1a's interaction with p300/CBP somehow mobilizes p300/CBP from the intergenic regions to promoters of genes to be activated. When e1a can interact with RB-family proteins and disrupt binding of E2Fs, as is the case for e1awt, p300/CBP can become associated with the liberated E2F activation domains with the consequence of downstream H3K18 hyperacetylation and increased transcription. If E2Fs remain repressed by RB due to e1a

not binding RB (RB- e1a), the mobilized p300/e1a associates with activation domains of other transcription factors, resulting in hyperacetylation and increased expression of other groups of genes.

CONCLUSION

We have begun to understand the formerly elusive role of p300/CBP in small e1a induction of the cell cycle, but this work has raised as many questions as it has answered. To fully unravel the role of the interactions of e1a with p300/CBP and RB-family proteins we must next determine the genome wide distribution of all of the players upon expression of e1awt, p300- e1a, and RB- e1a.

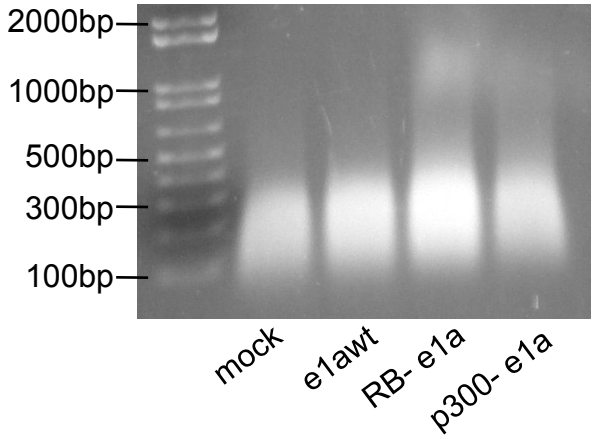

Figure 2.1. Sonicated chromatin. Cross-links were reversed in an aliquot of cross-linked chromatin. The DNA was purified and analyzed on a 1% agarose/TBE gel to check fragment size.

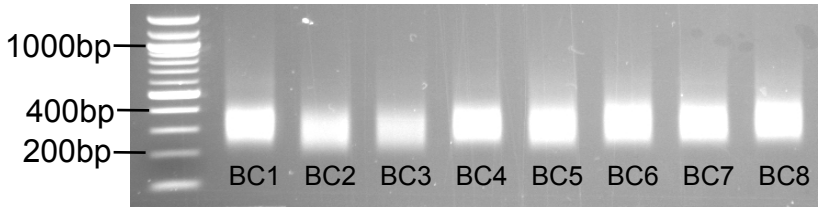

Figure 2.2. ChIP-seq barcoded libraries. Immunoprecipitated and input chromatin fragments were used in the Ovation Ultralow Dedicated Read (DR) Multiplex System (NuGEN) to create libraries for Illumina sequencing. Barcodes 1-4 (BC1-BC4) were from mock, e1awt, RB- e1a, and p300- e1a input, respectively, and BC5-BC8 were immunoprecipitated chromatin in the same order.

Table 2.2. Comparison of genome wide H3K18 acetylation peak number and coverage area in mock, e1awt, p300- e1a, and RB- e1a expressing cells.

	Number of peaks	Ratio of e1a/mock	Peaks coverage (kb)	Ratio of e1a/mock
mock	144,803		32,800	
e1awt	62,447	0.43	11,454	0.35
p300- e1a	121,440	0.84	24,358	0.74
RB- e1a	52,985	0.37	11,586	0.35

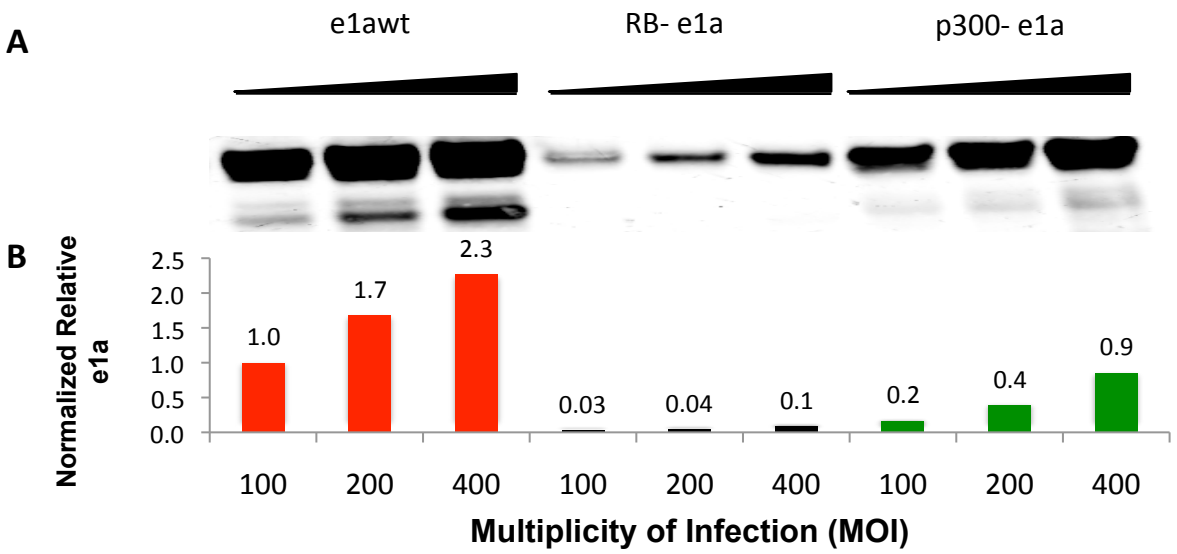

Figure 2.3. Empirical titering of Psi5*e1a viruses. IMR90 cells were infected with each virus at a Multiplicity of Infection (MOI) of 100, 200, or 400, and the e1a levels were measured by LI-COR quantitative western blot. (A) Western blot for e1awt, RB-e1a, and p300- e1a. (B) Quantification of e1a levels: e1a was normalized to actin loading control and the relative amounts of e1a were compared to e1awt at an MOI of 100.

A

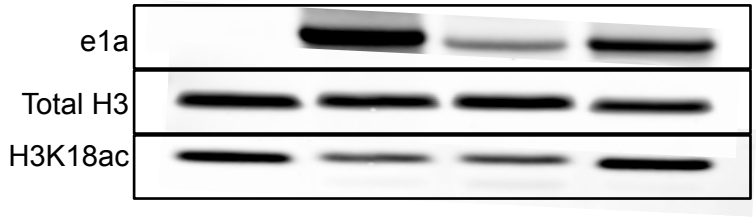

B

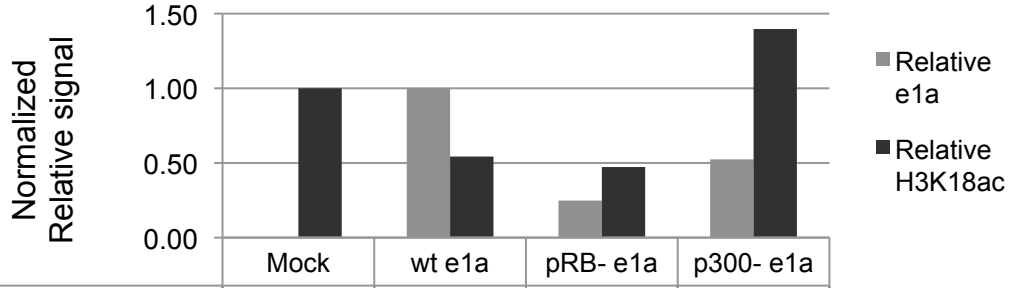

	Mock	wt e1a	pRB- e1a	p300- e1a
Relative e1a	0.00	1.00	0.25	0.52
Relative H3K18ac	1.00	0.54	0.47	1.40
MOI	0	100	1000	400

Figure 2.4. Western blot analysis of lysates used for ChIP-seq. The lysates were from infections at the indicated MOIs (A) LI-COR quantitative western blot for e1a, H3K18ac, and total H3. (B) Quantification of e1a: e1a was normalized to actin loading control and the relative amounts of e1a were compared to e1awt. Quantification of H3K18ac: H3K18ac was normalized to total H3 and the relative amounts of H3K18ac for e1awt, RB- e1a, and p300- e1a were compared to mock.

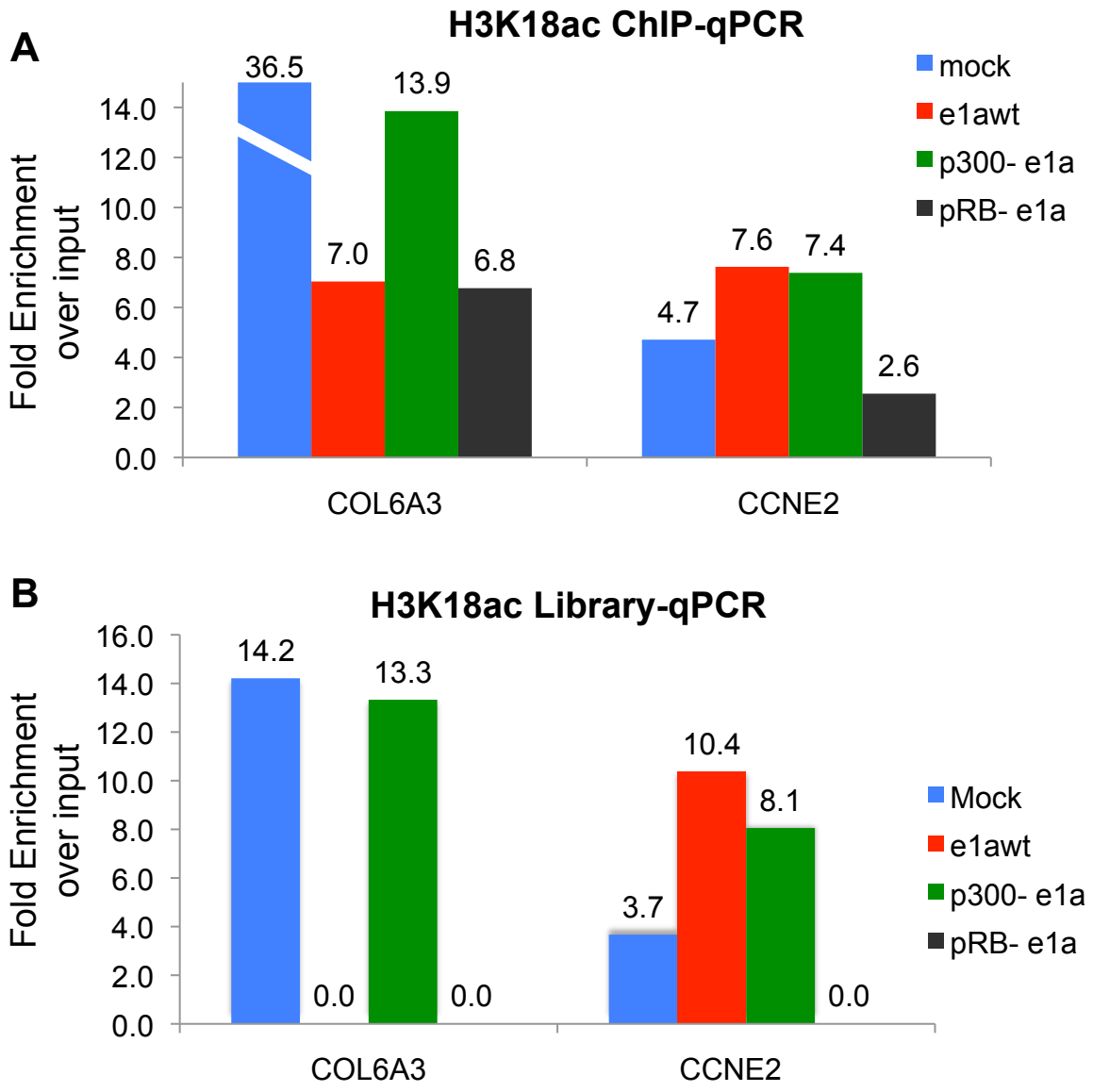

Figure 2.5. Enrichment of H3K18ac ChIP over input. Fold enrichment over input was calculated by the ΔΔCt method qPCR of equal masses of template. (A) qPCR of immunoprecipitated chromatin compared to input chromatin. (B) qPCR of ChIP barcoded libraries compared to input libraries.

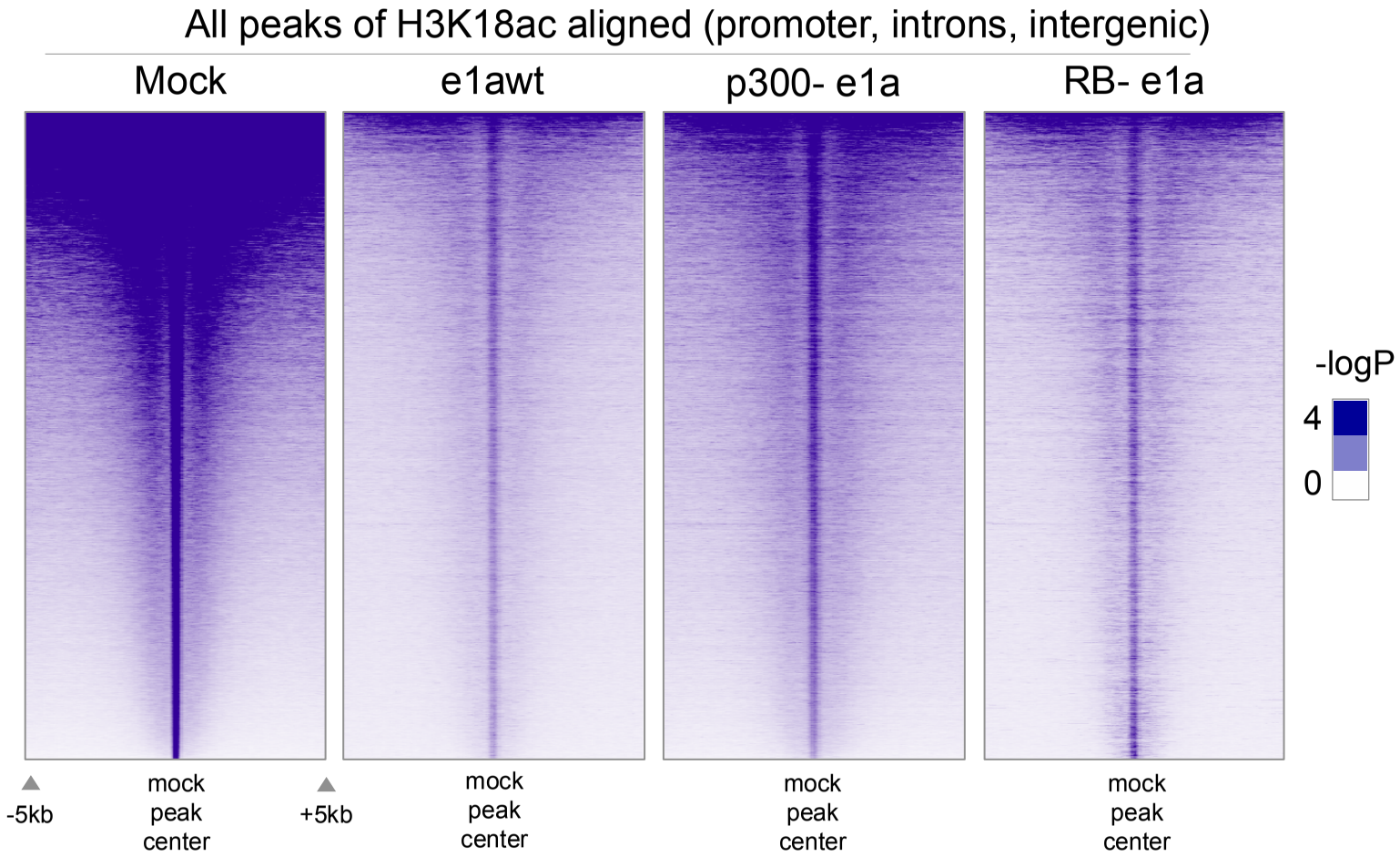

Figure 2.6. Analysis of H3K18ac peak density compared to mock. The -log of the *P*value (-logP) for each peak of H3K18ac in mock infected cells was calculated. Each peak was then aligned at its center. Then the -logP for all H3K18ac peaks within 5kb of the centered peak were determined in each direction from the center peak. The sum of the total -logP values ± 5Kb from the centered peak in 50bp windows were used to sort the mock peaks from highest density to lowest density of peaks. The process was repeated for e1awt and each of the mutants. Dark blue regions represent windows with significant peaks with P-values less than $1x10^{-4}$.

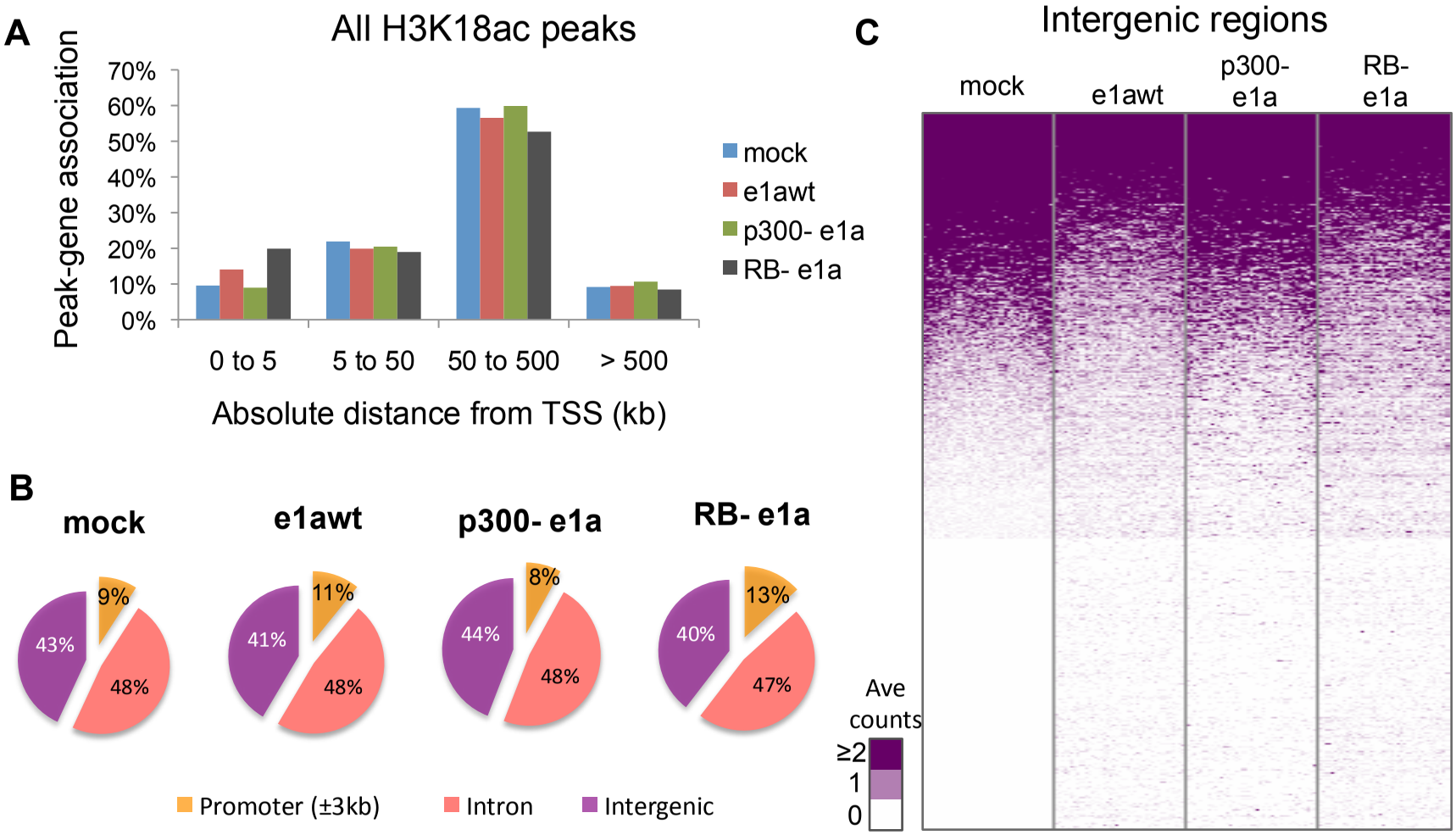

Figure 2.7. Distribution of H3K18ac peaks across the genome. (A) Distribution of significant peaks of H3K18ac relative to TSS. (B) Overview of peak distribution relative to gene structures represented as pie charts. (C) Heatmap of all intergenic regions normalized for size. Each intergenic region was divided into 40 bins, regardless of size, and the average counts of H3K18ac for each bin were calculated. The sums of the average counts per bin for each intergenic region in mock were used for ranking from highest to lowest H3K18ac.

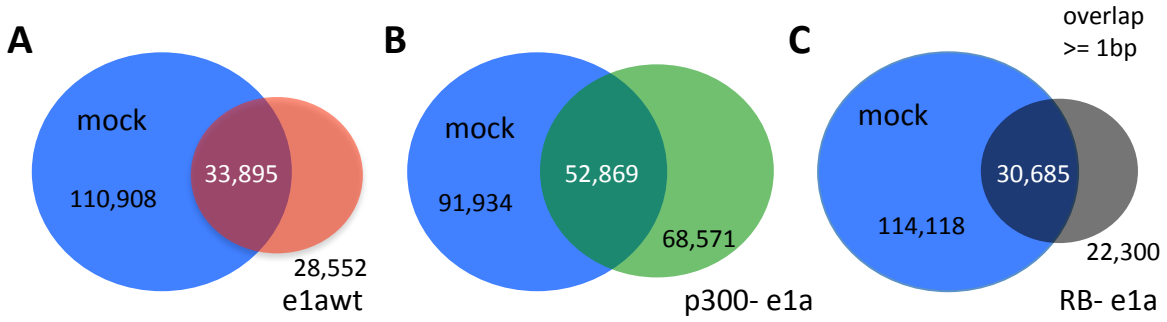

Figure 2.8. Venn diagrams of significant H3K18ac peaks overlapping by ≥1bp in mock or e1a infected cells. (A) Mock vs. e1awt: 76.6% of mock H3K18ac peaks were removed upon expression of e1awt, while 45.7% of the total H3K18ac peaks present after e1awt expression were new peaks. (B) Mock vs. p300- e1a: 63.5% of mock H3K18ac peaks were removed upon expression of p300- e1a, while 56.5% of the total H3K18ac peaks present after p300- e1a expression were new peaks. (C) Mock vs. RB- e1a: 78.9% of mock H3K18ac peaks were removed upon expression of RB- e1a, while 42.1% of the total H3K18ac peaks present after RB- e1a expression were new peaks.

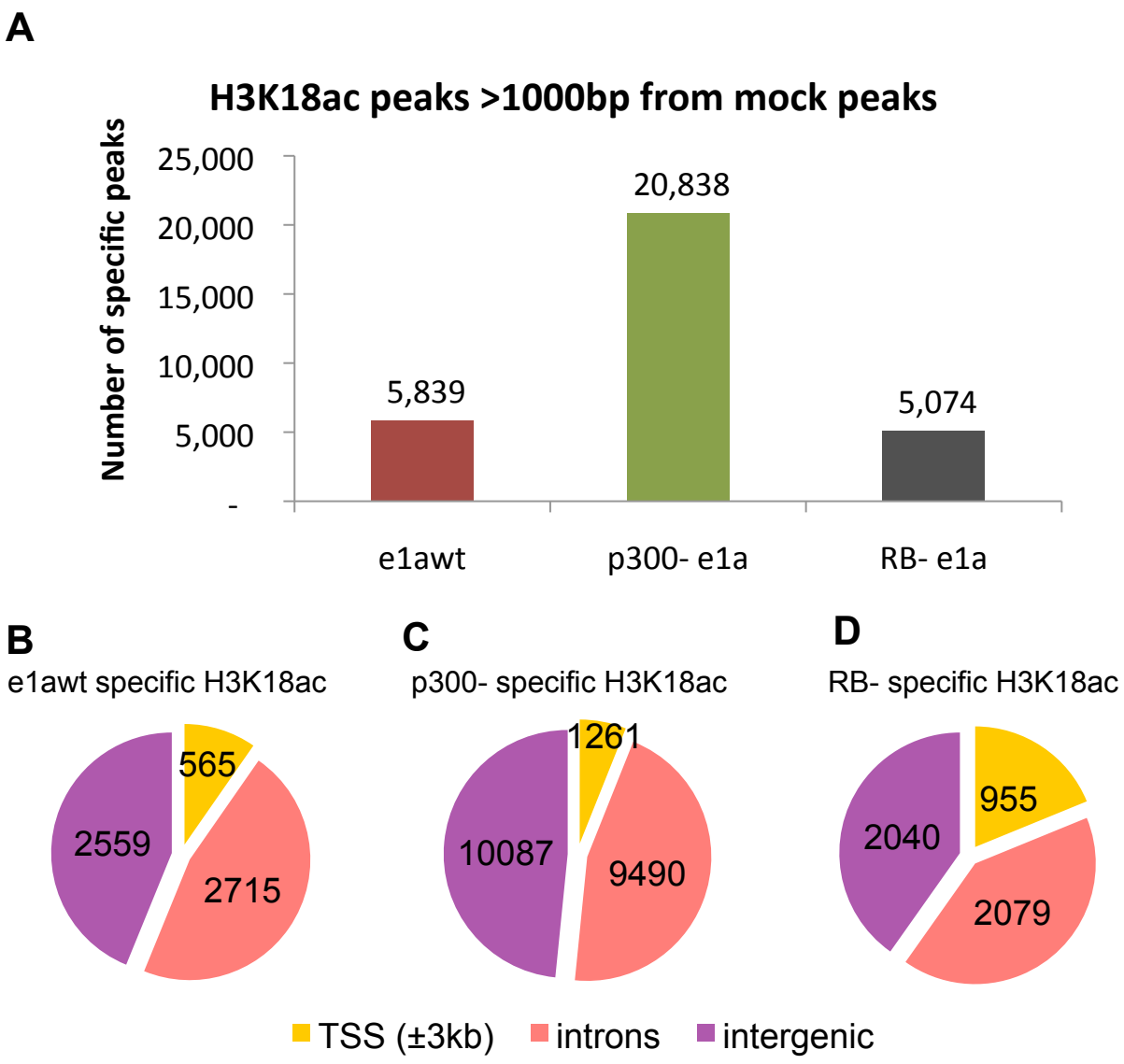

Figure 2.9. Specific Peaks of H3K18ac upon e1a expression. (A) Total number of specific peaks for e1awt, p300- e1a and RB- e1a that were separated from any mock peak by at least 1000bp. (B-D) Distribution of specific peaks within annotated genomic regions.

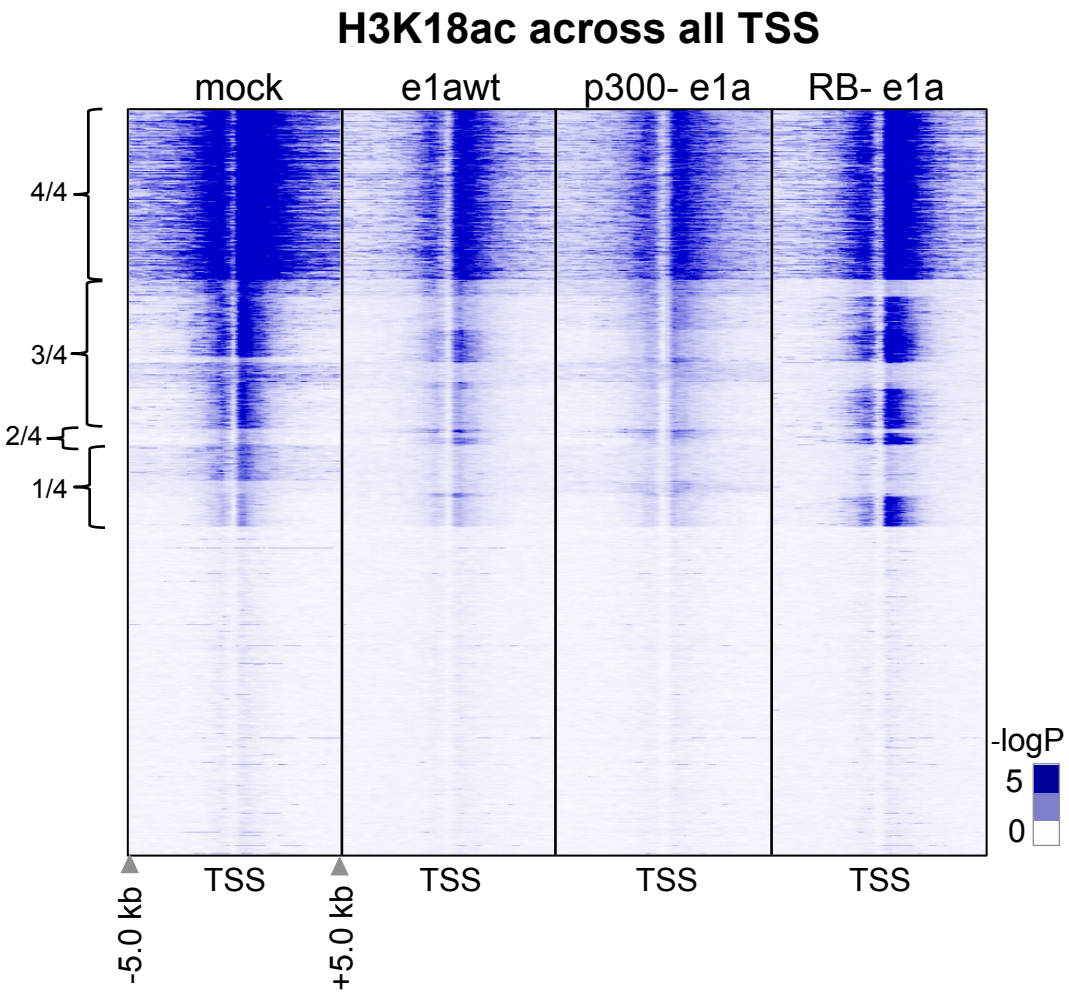

Figure 2.10. H3K18ac across the TSS of all genes. The -logP values for 50 bp windows 5 kb upstream and downstream of the TSS of all transcripts were determined. The transcripts were then clustered by the pattern of significant H3K18ac in mock, e1awt, p300- e1a and RB- e1a. At the top of the figure are transcripts with significant levels of H3K18ac in all four categories. The following clusters have significant H3K18ac in 3 out of the 4 possible categories, then combinations of 2 out of 4 categories, then those that only have significant H3K18ac in a single category. The bottom of the figure represents transcripts without significant H3K18ac in the indicated region.

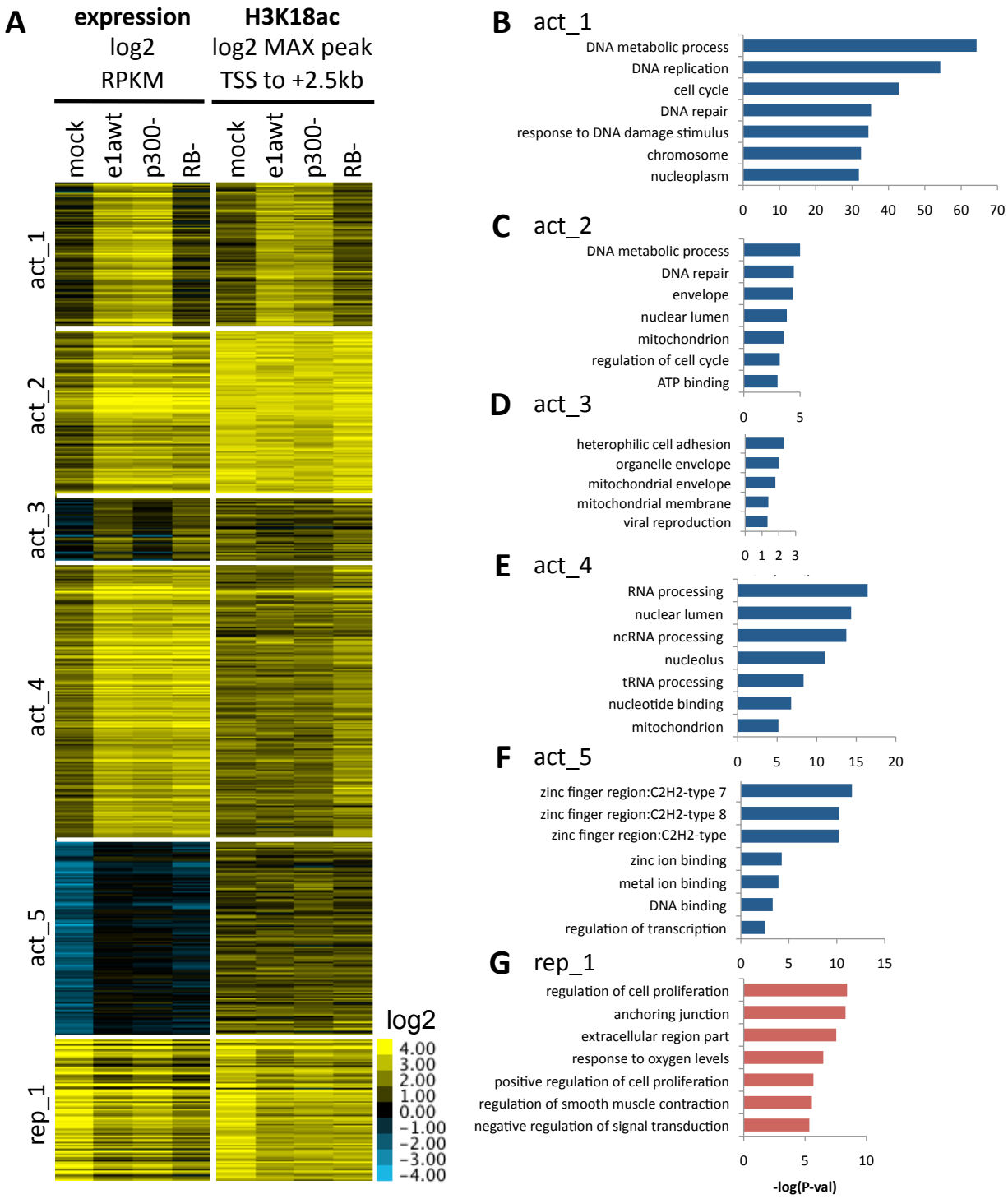

Figure 2.11. Clustering by expression and H3K18ac. (A) k-means clustering by the log2 of the RPKM expression values and log2 of MAX downstream -logP for mock, e1awt, p300- e1a, and RB- e1a. In the left (expression) panel: yellow bars represent ≥ 2-fold gene activation, blue bars represent ≥ 2-fold gene repression. In the right (H3K18ac) panel: Bright yellow bars (log2 ≥ 2) represent significant windows of H3K18ac. (B-G) Gene ontology terms for each cluster.

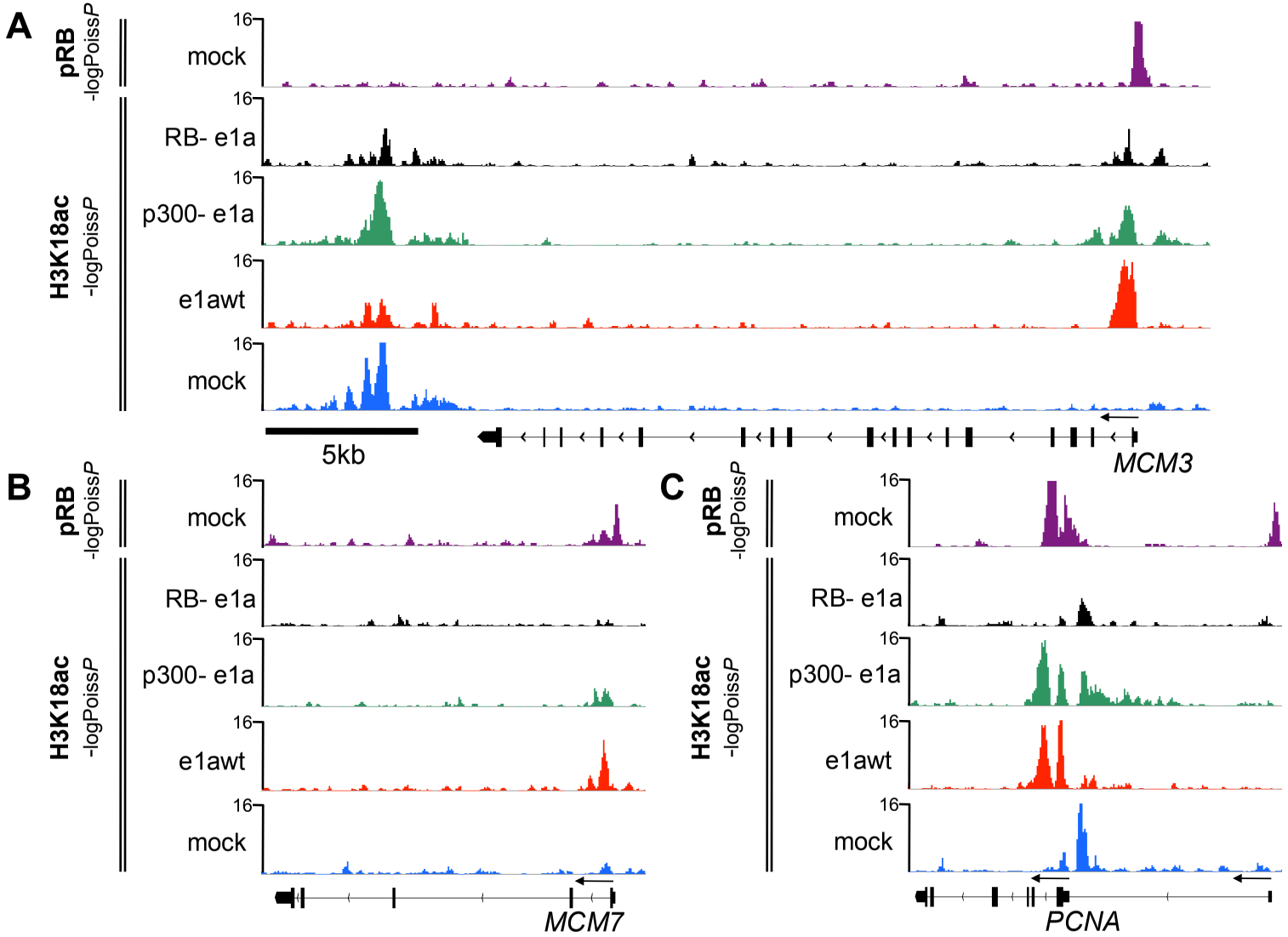

Figure 2.12. Patterns of H3K18ac and pRB of representative genes from activated cluster act_1. Black arrows represent TSS, the scale is the same for each gene. Blue peaks are H3K18ac from mock, red peaks are H3K18ac from e1awt, green peaks are H3K18ac from p300- e1a, black peaks are H3K18ac from RB- e1a, and purple peaks are RB1 from mock. (A) *MCM3.* (B) *MCM7.* (C) *PCNA.*

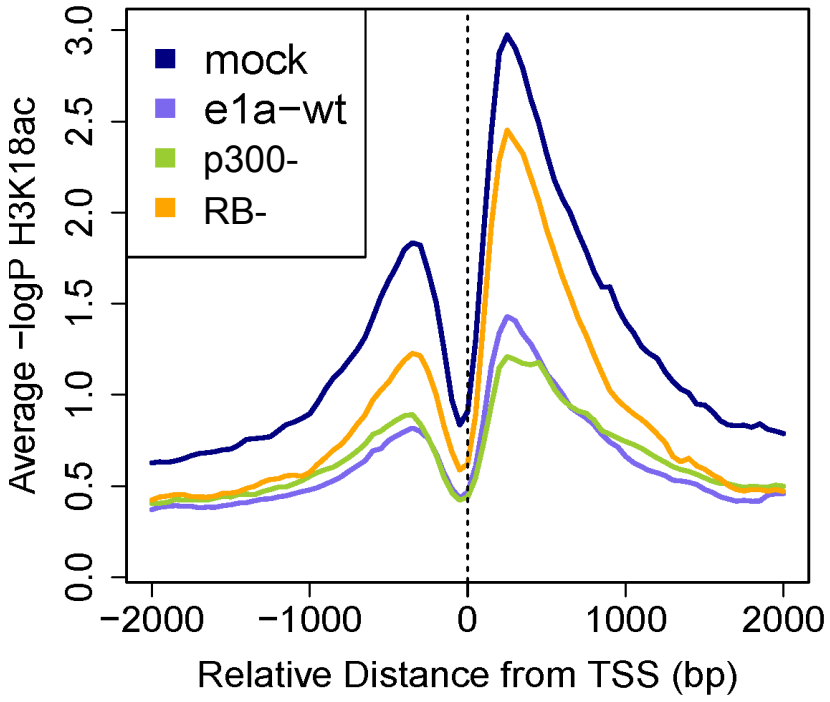

Figure 2.13. Average profiles of H3K18ac around all TSS. Sitepro was used to profile levels of H3K18ac for defined genomic intervals of 2kb around the TSS of all peaks.

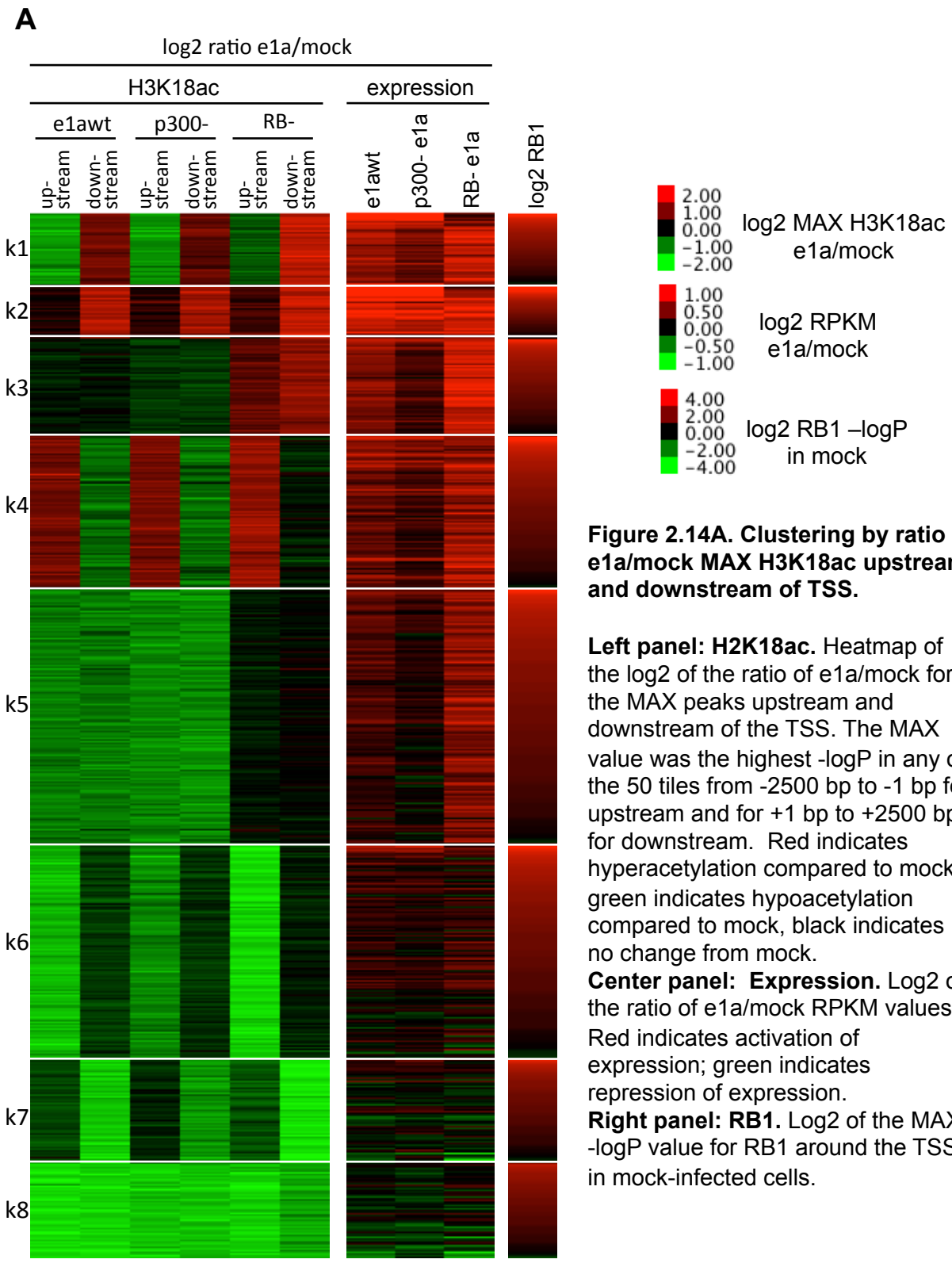

Figure 2.14A. Clustering by ratio of e1a/mock MAX H3K18ac upstream and downstream of TSS.

Left panel: H2K18ac. Heatmap of the log2 of the ratio of e1a/mock for the MAX peaks upstream and downstream of the TSS. The MAX value was the highest -logP in any of the 50 tiles from -2500 bp to -1 bp for upstream and for +1 bp to +2500 bp for downstream. Red indicates hyperacetylation compared to mock, green indicates hypoacetylation compared to mock, black indicates no change from mock.
Center panel: Expression. Log2 of the ratio of e1a/mock RPKM values. Red indicates activation of expression; green indicates repression of expression.
Right panel: RB1. Log2 of the MAX -logP value for RB1 around the TSS in mock-infected cells.

B

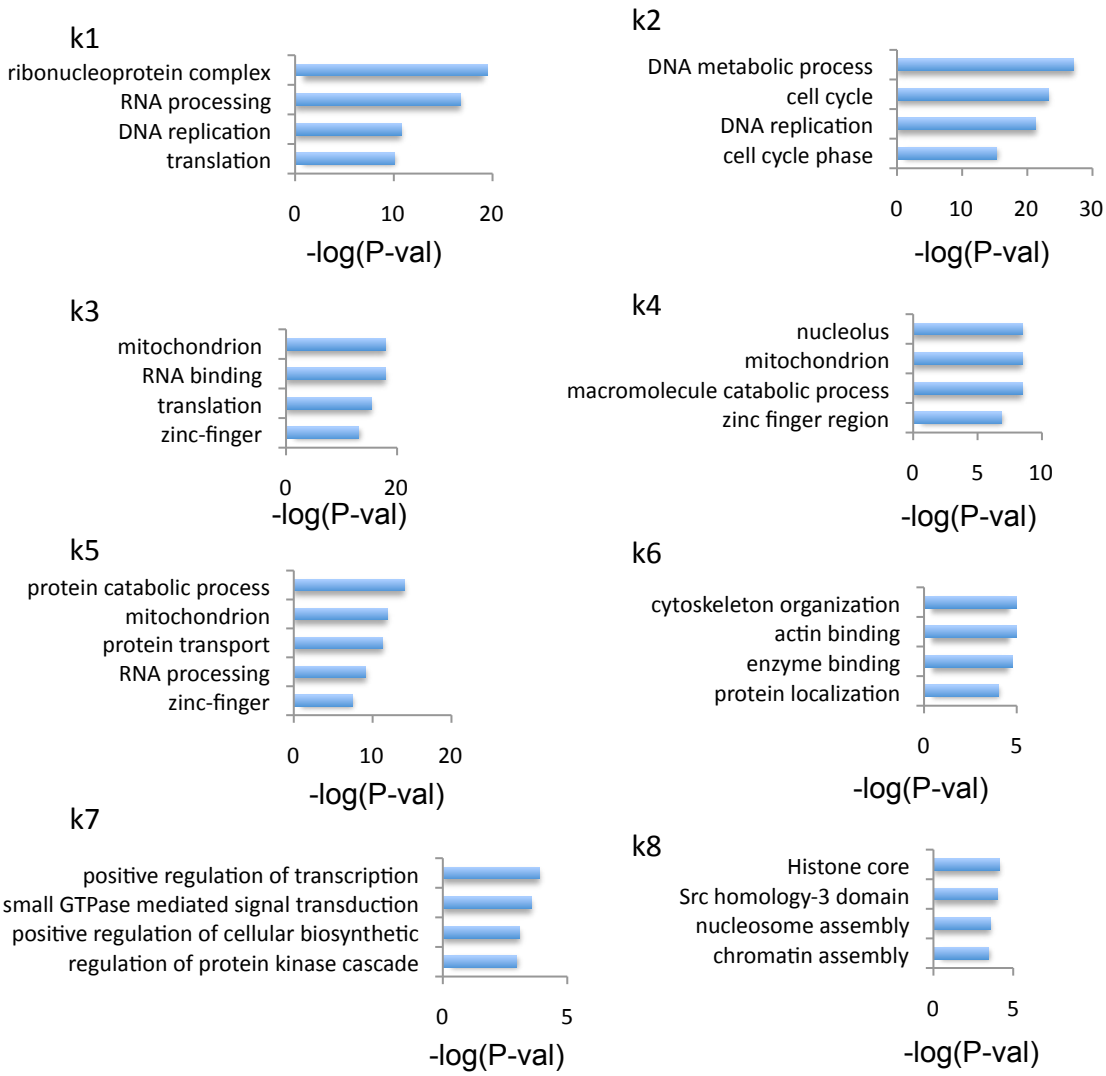

Figure 2.14B. Gene ontology for ratio of e1a/mock MAX H3K18ac upstream and downstream clusters. Genes from clusters in figure 2.14 were used for GO analysis. Bars represent -log10 of the P-value for the selected GO terms.

REFERENCES:

1. Berk AJ (2007) in *Fields Virology*, eds Knipe DM, Howley PM (Lippincott Williams & Wilkins).Fifth.

2. Montell C, Courtois G, Eng C, Berk A (1984) Complete transformation by adenovirus 2 requires both E1A proteins. *Cell* 36:951–961.

3. Howe JA, Mymryk JS, Egan C, Branton PE, Bayley ST (1990) Retinoblastoma growth suppressor and a 300-kDa protein appear to regulate cellular DNA synthesis. *Proc Natl Acad Sci U S A* 87:5883–5887.

4. Ghosh MK, Harter ML (2003) A Viral Mechanism for Remodeling Chromatin Structure in G0 Cells. *Molecular Cell* 12:255–260.

5. Ferrari R et al. (2008) Epigenetic reprogramming by adenovirus e1a. *Science* 321:1086–1088.

6. Ferrari R et al. (2012) Reorganization of the Host Epigenome by a Viral Oncogene. *Genome Res*. Available at: http://genome.cshlp.org/content/early/2012/05/20/gr.132308.111 [Accessed June 6, 2012].

7. Horwitz GA et al. (2008) Adenovirus small e1a alters global patterns of histone modification. *Science* 321:1084–1085.

8. Hardy S, Kitamura M, Harris-Stansil T, Dai Y, Phipps ML (1997) Construction of adenovirus vectors through Cre-lox recombination. *J Virol* 71:1842–1849.

9. Gallaher SD, Gil JS, Dorigo O, Berk AJ (2009) Robust In Vivo Transduction of a Genetically Stable Epstein-Barr Virus Episome to Hepatocytes in Mice by a Hybrid Viral Vector. *J Virol* 83:3249–3257.

10. Wang HG, Moran E, Yaciuk P (1995) E1A promotes association between p300 and pRB in multimeric complexes required for normal biological activity. *J Virol* 69:7917–7924.

11. Ferreon JC, Martinez-Yamout MA, Dyson HJ, Wright PE (2009) Structural basis for subversion of cellular control mechanisms by the adenoviral E1A oncoprotein. *Proc Natl Acad Sci U S A* 106:13260–13265.

12. Liu X, Marmorstein R (2007) Structure of the retinoblastoma protein bound to adenovirus E1A reveals the molecular basis for viral oncoprotein inactivation of a tumor suppressor. *Genes Dev* 21:2711–2716.

13. Lee JO, Russo AA, Pavletich NP (1998) Structure of the retinoblastoma tumour-suppressor pocket domain bound to a peptide from HPV E7. *Nature* 391:859–865.

14. Jones N, Shenk T (1979) An adenovirus type 5 early gene function regulates expression of other early viral genes. *Proc Natl Acad Sci U S A* 76:3665–9.

15. Harlow E, Franza BR, Schley C (1985) Monoclonal antibodies specific for adenovirus early region 1A proteins: extensive heterogeneity in early region 1A products. *Journal of virology* 55:533–546.

16. Livak KJ, Schmittgen TD (2001) Analysis of relative gene expression data using real-time quantitative PCR and the 2(-Delta Delta C(T)) Method. *Methods* 25:402–408.

17. Karolchik D (2004) The UCSC Table Browser data retrieval tool. *Nucleic Acids Research* 32:493D–496.

18. Mortazavi A, Williams BA, McCue K, Schaeffer L, Wold B (2008) Mapping and quantifying mammalian transcriptomes by RNA-Seq. *Nature Methods* 5:621–628.

19. Hoon MJL de, Imoto S, Nolan J, Miyano S (2004) Open source clustering software. *Bioinformatics* 20:1453–1454.

20. Huang DW, Sherman BT, Lempicki RA (2009) Bioinformatics enrichment tools: paths toward the comprehensive functional analysis of large gene lists. *Nucleic Acids Res* 37:1–13.

21. Huang DW, Sherman BT, Lempicki RA (2009) Systematic and integrative analysis of large gene lists using DAVID bioinformatics resources. *Nature Protocols* 4:44–57.

22. McLean CY et al. (2010) GREAT improves functional interpretation of cis-regulatory regions. *Nat Biotechnol* 28:495–501.

23. Ji X, Li W, Song J, Wei L, Liu XS (2006) CEAS: cis-regulatory element annotation system. *Nucleic Acids Research* 34:W551–W554.

24. Shin H, Liu T, Manrai AK, Liu XS (2009) CEAS: cis-regulatory element annotation system. *Bioinformatics* 25:2605–2606.

25. Benson DA, Karsch-Mizrachi I, Lipman DJ, Ostell J, Sayers EW (2011) GenBank. *Nucleic Acids Res* 39:D32–37.

26. Nicol JW, Helt GA, Blanchard SG, Raja A, Loraine AE (2009) The Integrated Genome Browser: free software for distribution and exploration of genome-scale datasets. *Bioinformatics* 25:2730–2731.

27. Palmieri F (2004) The mitochondrial transporter family (SLC25): physiological and pathological implications. *Pfl*[illegible]*gers Archiv European Journal of Physiology* 447:689–709.

28. Greve JM et al. (1989) The major human rhinovirus receptor is ICAM-1. *Cell* 56:839–847.

29. Morimoto K et al. (2009) Adenovirus E1A regulates lung epithelial ICAM-1 expression by interacting with transcriptional regulators at its promoter. *Am J Physiol Lung Cell Mol Physiol* 296:L361–L371.

30. Chen Y, Hor HH, Tang BL (2012) AMIGO is expressed in multiple brain cell types and may regulate dendritic growth and neuronal survival. *Journal of Cellular Physiology* 227:2217–2229.

31. Liu T et al. (2011) Cistrome: an integrative platform for transcriptional regulation studies. *Genome Biology* 12:R83.

32. Barber MF et al. (2012) SIRT7 links H3K18 deacetylation to maintenance of oncogenic transformation. *Nature* 487:114–118.

33. Tsai Y-C, Greco TM, Boonmee A, Miteva Y, Cristea IM (2012) Functional proteomics establishes the interaction of SIRT7 with chromatin remodeling complexes and expands its role in regulation of RNA polymerase I transcription. *Mol Cell Proteomics* 11:60–76.

Chapter 3

Inherent challenges in preparing a Helper Dependent Adenovirus gene therapy vector targeted to hematopoietic cells without helper contamination

INTRODUCTION

Adenoviruses are not only useful tools for understanding cellular processes, but also have wider clinical implications as effective vectors for delivery of therapeutic DNA. Helper Dependent Adenoviruses (HDAd) that have been deleted of all viral coding regions have been demonstrated to efficiently deliver transgenic DNA without significant toxicity, immunogenic effects, or risk of insertional mutagenesis. Although HDAd vectors can deliver high levels of expression, a major drawback of traditional HDAd vectors is that expression is rapidly diminished, as the non-integrating vector DNA is lost during cell division.

The Berk lab has developed a hybrid HDAd vector that uses components of Epstein-Barr virus (HDAd/EBV) to maintain a circularized extra-chromosomal, or episomal, vector by initiating its replication and segregation into daughter cells. In this system, the linear adenoviral genome is circularized by concomitant delivery of Cre recombinase. The HDAd/EBV vector has been shown to efficiently deliver and persist in expressing transgenic DNA in tissue culture and in hepatocytes *in vivo* (1–3). However, hepatocytes are not an optimal model system for demonstrating maintenance in dividing cells due to their low basal level of replication (4). Hematopoietic stems cells (HSC), however, are a rapidly dividing cell population that differentiate into a number of different cell types that manifest diseases (5), making them an excellent target for the HDAd/EBV vector.

The commonly used adenovirus serotype 5 (Ad5) only poorly infects HSC due to the scarcity of the coxsackievirus-adenovirus receptor (CAR) (6). Adenovirus serotype 35 (Ad35), however, can efficiently infect HSCs via the membrane cofactor protein CD46 receptor (7). In this chapter I will discuss the construction and validation of an adenovirus "helper virus" for

targeting the HDAd/EBV hybrid system targeted to HSCs by a chimeric Ad5/35 fiber. This helper virus must necessarily use the FLPe/FRT recombinase system for limiting helper virus contamination, since Cre/loxP is essential for the circularization of the HDAd/EBV episome.

This chapter also discusses the challenges associated with developing an adenovirus replication permissive cell line (HEK293) with adequate levels of FLPe expression to limit helper virus contamination in the HDAd/EBV vector stock. Initial attempts to increase FLPe expression through gene amplification (8, 9) where ultimately unsuccessful. We hypothesized that this could be due to subtle deleterious effects of FLPe that selected against its expression, and that an inducible system may prove more effective.

Several systems were considered, and it was decided that a temperature sensitive Sindbis virus replicase based system could give both tightly controlled and highly expressed transient levels of FLPe recombinase (10). Sindbis viruses are enveloped, positive single stranded RNA viruses that have been established as a system for high expression of heterologous protein in both transient and temperature regulated systems (11–15). Sindbis uses an RNA dependent RNA replicase to both replicate its genome (replicon) and create high copy numbers of message RNA for its structural proteins from a subgenomic promoter. A layered DNA-RNA system described by Boorsma et al. established stable expression from of the Sindbis replicon from an RSV promoter via integration of a mammalian expression plasmid (13). The replicase carried two key mutations that reduced the cytopathicity of the replicase (16) and caused it to be temperature sensitive so that it would only be active at permissive temperatures below 35°C (15).

We demonstrate here that expression from a Sindbis virus based replicon, either from a layered DNA/RNA system or from a Sindbis virus vector, is not supported in the adenovirus replication permissive cell line HEK293.

MATERIALS AND METHODS

Cell Culture

Human embryonic kidney HEK293 (293; Microbix Biosystems), 293T (ATCC), 293Cre4 (ATCC) and 293FLPe cells (Gift of Dr. Pedro Lowenstein, Cedars-Sinai) were grown in high-glucose Dulbecco's Modified Eagle Medium (DMEM) supplemented with 100U/mL penicillin, 100μg/mL streptomycin, and 10% heat inactivated fetal bovine serum (FBS). 293Cre4 cells were maintained under hygromycin selection at 200μg/mL, and 293FLPe cells were maintained under puromycin selection at 1.5μg/mL.

M07e cells (a gift of Dr. Hal Broxmeyer, Indiana University School of Medicine) were cultured in RPMI-1640 (Gibco/Life Technologies) supplemented with 20% FBS, 100U/mL penicillin/streptomycin, 100ng/mL Recombinant Human GM-CSF (Granulocyte Macrophage Colony Stimulating Factor, BioVision), 50μM beta-mercaptoethanol, and 250ng/mL amphotericin B. Baby hamster kidney (BHK) cells (Gift of Dr. Odisse Azizgolshani, UCLA) were maintained in Eagle Minimal Essential Media (EMEM) with 10% FBS.

Adenovirus propagation, titration, and DNA isolation

Adenoviruses were propagated in 293 cells in DMEM with 2% FBS as previously described (17, 18) and isolated by CsCl banding when purified stocks were required (19, 20). Helper-dependent adenoviral vectors were propagated as previously described (21–23). Adenoviral stocks were titered by infectious genome assay (24).

Adenoviral DNA was isolated from purified virus after dialysis in 20mM Tris, pH 8 and concentration using an Amicon Ultra-4 Concentrator (Millipore) according to manufacturer instructions. Concentrated stocks were brought to a 1x final concentration of PBS in 200μL, and

adenoviral DNA was isolated according to the QIAgen DNeasy protocol for animal blood and cultured cells.

Ad5/35.FRT recombinant adenovirus production

An Ad5/35.FRT recombinant adenovirus vector was created in 293 cells by *in vivo* recombination of cotransfected virion DNA (17). Ad5/35 (25) was digested with *Pme*I restriction endonuclease (New England BioLabs) and Ad.FRT (FL helper) (23) was digested with *Spe*I restriction endonuclease (New England BioLabs) overnight. After heat inactivation, equal masses of each digest were co-transfected into 60% confluent 293Cre4 cells by Effectene (QIAgen) according to the manufacturer instructions.

In order to check the efficiency of each digest, and confirm that no virus could be propagated from the digested DNA, each digest was transfected alone into 293Cre4 cells. Uncut viral DNA from each parental virus was transfected separately into 293Cre4 cells as controls. Recombinant viruses were harvested and clones were isolated for screening by $TCID_{50}$ limiting dilution.

$TCID_{50}$ Limiting dilution assay

Replicate serial 10x dilutions of the virus containing lysate were added to flat-bottomed 96-well plates seeded with $1x10^4$ cells per well in DMEM plus 2% FBS. After 10 days, wells exhibiting cytopathic effects (CPE) were scored for each dilution. Six wells with CPE from the dilution determined to have likely originated from a single virus were harvested by repeated pipetting, lysed by 3X freeze/thaw cycles, and stored at -80°C.

Recombinant virus screening

Recombinant viral clone lysates were diluted in DNase-free water for use as PCR templates. Purified DNA from the Ad5/35 and Ad.FRT parental viruses were used as controls at $1x10^5$ copies per reaction. In addition, pFG-140, which contains the entire sequence of wild-type Ad5, was used for comparison. PCR was performed using FastStart Universal SYBR Green MasterMix (with Rox normalization). Three 100-fold dilutions were made for each clone lysate and 5μL of the final dilution was used for each reaction, along with 1X SYBR green mix, and 0.2μM of each primer. PCR reactions were incubated at 95°C for 10 minutes to disassemble virion particles, then 40 cycles of 95°C for 30sec, 60°C for 30sec, 72°C for 2min; ending with a 10min hold at 72°C.

Ad5/35 screening primers

Ad35FiberRW	AGCAAAGCCTTTATGCCAAG
Ad35FiberLW	GGCATAGGCAACATTGGAAG

Psi packaging signal screening primers

Psi1	GGCGGGTGACGTAGTAGTGT
Psi2	TGCTTCCATCAAACGAGTTG
Psi3	AATTTTCGCGCGGTTTTAG
Psi4	CTTACTCGGTTACGCCCAAA

Functional FRT PCR Assay

Ad5/35.FRT and the parental virus Ad.FRT were infected into 293 cells or 293 cells expressing FLPe recombinase (293FLPe) at a multiplicity of infection (MOI) of 10 for 24 hours. Total DNA was then isolated according to the QIAgen DNeasy protocol for animal blood and cultured cells and assayed via PCR with primers Psi1/Psi2 as described above.

FLPe Amplification by Methotrexate treatment

293 cells were transfected with the pCAGGS.FLPe.EDH construct by Effectene (QIAgen) according to the manufacturer instructions, followed by hygromycin selection at 200μg/mL to select for stable clones. Stable clones were cultured in DMEM minus glycine supplemented with 10% FBS during methotrexate (MTX) amplification and were maintained under hygromycin selection. Methotrexate was added to the media at 100nM, 200nM, 400nM, 800nM, or 1600nM in step-wise increments. Some transfected 293 cells underwent Arabinofuranosyl Cytidine (AraC) treatment at 1000μM prior to hygromycin and MTX selection. For each step increase in MTX, some cells from each clonal population were maintained at each concentration for comparison.

FLPe Amplification by initiation region containing plasmids

The initiation region and matrix attachment region containing plasmid pSFVdhfr (Gift of Dr. Noriaki Shimizu, Hiroshima University) was cotransfected with pCAGGS-FLPe by Effectene (500ng each) according to the manufacturer protocol. Blasticidin treatment at 2.5μg/mL in DMEM + 10% FBS was used to isolate stable IR-FLPe clones.

FLPe Luciferase Reporter Assay

A luciferase reporter assay was used to measure FLPe recombinase activity (Fig. 3.6A). The luciferase reporter construct has FRT sites flanking a stop codon between the promoter and the luciferase gene. In the absence of FLPe recombinase, the stop codon is in-frame and prevents translation of the luciferase open reading frame. In the presence of FLPe the stop codon is recombined out of the reporter construct, allowing for luciferase expression. With sufficient

copies of the reporter construct in the cell, this process is linear in that increasing FLPe activity will result in higher levels of luciferase expression and subsequent bioluminescence upon addition of the luciferin substrate.

In this assay an E1 deleted (first generation) adenovirus carrying a firefly luciferase reporter construct (Ad.AC.lucif, gift of Dr. P. Lowenstein) was infected into FLPe expressing 293 cells at an MOI of 50. Exactly 24 hours later, all cells were harvested for luciferase assay. For the luciferase assay, cells are lysed at -80°C for 15 minutes in 200μL 1X Passive Lysis Buffer (Promega). The lysates were centrifuged for 30 seconds at 14,000 RPM in a table-top microcentrifuge to pellet cell debris. The supernatant was diluted 1:100 in 1% FBS, and 5μL of diluted lysate was combined with 100μL room temperature luciferase reagent (Promega) immediately prior to the measurement of the bioluminescence by Monolight 2010 luminometer (BD Biosciences) for 5 seconds.

***FLPe* copy number qPCR**

Total DNA was isolated from 293 cells, 293FLPe cells, MXT treated 293FLPe.EDH clones, and IR-FLPe clones according to the QIAgen DNeasy protocol for animal blood and cultured cells. qPCR was performed using FastStart Universal SYBR Green MasterMix (with Rox normalization) on 5μL of total cellular DNA for each reaction, along with 1X SYBR green mix, and 0.2μM of each primer. PCR reactions were incubated at 95°C for 10 minutes, then 40 cycles of 95°C for 30sec, 60°C for 30sec, 72°C for 2min; ending with a 10min hold at 72°C.

FLPe Primers

FLPeF2	GCGCCTTATCCAATCTTTGC
FLPeR2	GTTAGGCCCTTCATTGACAGAAA

Sindbis plasmid manipulation

Mutations were introduced into the Sindbis non-structural replicase genes with the primers below using the QuikChange II XL Site-Directed Mutagenesis Kit (Agilent). The replicase was made temperature sensitive by introducing a point mutation of A for G at nucleotide position 6226 in the nsp4 gene (G159E) (13, 15) and non-cytopathic by introducing a point mutation of T for C at nucleotide position 3855 in nsp2 of the nsp123 polyprotein gene (P726S) (16) of pSin-ΔCP-lucif. The point mutations also abolished a *Bsm*FI cut site in nsp4 and a *Bst*NI cut site in nsp2, resulting in a distinct restriction digest pattern for screening clones for the mutations. Clones positive for both mutations were sequenced to confirm the desired mutations were present, and a small region containing each mutation was cloned back into the parental plasmid to create pSin-ts/ncp-lucif.

The Rous sarcoma virus (RSV) promoter sequence was synthesized by GeneArt Gene Synthesis Service (Invitrogen/Life Technologies) and was inserted in place of the SP6 in vitro transcription promoter to create pRSV-Sin-lucif. The plasmid backbone was replaced with a version of pcDNA3 with a puromycin acetyltransferase selectable marker to create pPuroRSV-Sin-lucif. The FLPe.EDH cassette previously used for FLPe amplification in 293 cells replaced the luciferase gene driven by the subgenomic promoter in pPuroRSV-Sin-lucif to create the pSin-FLPe.EDH plasmid.

A temperature sensitive enhanced yellow fluorescent protein expressing replicon plasmid (pSINVtsEYFP) was constructed by replacing luciferase with EYFP following the subgenomic promoter in pSin-ts/ncp-lucif. The Sindbis plasmids pSin-ΔCP-lucif, pSINV-EYFP, and the defective helper lacking a packaging signal (DHBB) were supplied by Dr. Odisse Azizgolshani (UCLA). All DNA transfections were performed with Effectene (QIAgen) according to the

manufacturer instructions.

Mutagenesis primers	
c3855t	CTGAATTGCCTTAACTCAGGAGGCACCCTCG
c3855t_antisense	CGAGGGTGCCTCCTGAGTTAAGGCAATTCAG
g6226a	GGATATGGTAGACGAGACAGTCGCCTGCC
g6226a_antisense	GGCAGGCGACTGTCTCGTCTACCATATCC

Sequencing primers	
SINnsp4seqFW	AGTAGCGTACCGGCGAACTA
SINnsp4seqRV	TTGAATGTCGCTGAGTCCAG
SINnsp2seqFW	TTGAAGCTCCCCGTAAGAGA
SINnsp2seqRV	CCGTGTACGGCTGTTGTCTA

In vitro transcription and electroporation of Sindbis replicons

Replicon plasmids with SP6 promoters for *in vitro* transcription (IVT) were digested completely with *Sac*I to remove the plasmid backbone. The digested DNA was purified with RNase-free reagents by phenol:chloroform extraction and ethanol precipitation. Transcripts were prepared from 1μg template according to the mMessage mMachine kit (Ambion), with the addition of 1μL per reaction additional 20mM GTP and 2 hour incubation as suggested for long transcripts (Sindbis replicon was approximately 9.5kb). IVT transcripts were analyzed by agarose gel electrophoresis and the concentration was determined by NanoDrop spectrophotometer reading (Thermo Scientific).

Actively growing BHK or 293 cells were trypsinized and harvested and then washed with ice-cold RNase-free phosphate buffered saline (PBS) three times before being resuspended at a density of $1x10^7$ cells/mL in Opti-MEM (Gibco; Life Technologies). Electroporations were performed in chilled 0.4cm cuvettes containing 20μg RNA per $5x10^6$ cells in a 0.5mL total volume. Each cuvette was pulsed twice at 1.5kV, 25μFD, with resistance (Ω) set to ∞ on a BioRad Gene Pulser II electroporation apparatus with Capacitance Extender Plus and Pulse Controller Plus modules. After electroporation, cells were allowed to recover for 10 minutes at

room temperature then were diluted 20-fold in EMEM (BHK) or DMEM (293) plus 10% serum and plated.

Sindbis vector propagation

Sindbis vectors (SINV) were propagated by co-transfecting replicon (replicase and gene of interest from subgenomic promoter) RNA with the DH-BB defective helper RNA into BHK cells by electroporation. DH-BB provides the structural proteins and *cis*-acting elements for replication, but lacks a packaging signal (26). SINV particles bud out into the media and were harvested by collecting the supernatant every 24 hours (27, 28). It was observed that SINV vectors produced from temperature sensitive replicons (SINV-tsEYFP) resulted in several orders of magnitude lower Yellow Transducing Units (YTU) than those produced with wild-type replicons (SINV-EYFP) at 48 hours, but higher concentration stocks could be obtained by harvesting viral supernatant 8 days post transfection.

Lentivirus Production

Lentiviruses expressing the laminin receptor (LAMR) *RPSA* gene were produced by cloning the *RPSA* cDNA into the Lenti-X pLVX-puro expression vector (Clontech). The expression vector was co-transfected into 293T cells with pΔVPR helper (29), and pVSV-G for pseudotyping (30), by calcium phosphate transfection as described (31). 293 cells were transduced with the Lenti-LAMR virus and selected for by puromycin selection at 1.5μg/mL to generate 293LR cells.

Laminin Receptor RT-qPCR

Total RNA was harvested from BHK, 293, and 293LR cells using the RNeasy Total RNA purification kit (QIAgen) according to the manufacturer instructions. cDNA was prepared by SuperScript III First-Strand Synthesis System for RT-PCR (Invitrogen) using the supplied oligo$(dT)_{20}$ primers. RT-qPCR was performed on 2μL of cDNA per reaction using FastStart Universal SYBR Green MasterMix (with Rox normalization) with gene specific primers for human, mouse, or syrian hamster LAMR/*RPSA* as described previously.

Human primers
hRPSA-f GGAATTTCAGGGTGAATGGA
hRPSA-r CAGACCAGTCTGCAACCTCA

Mouse primers
mRPSA-f CCTGGGACCTTCACTAACCA
mRPSA-r GGGATCGGTCACCACTAGAA

Syrian hamster primers
shRPSA-f GGGCCATCGTTGCTATTGAG
shRPSA-r TCGCTGCCCAGTGTTCCT

Maps for all plasmids used are in the Appendix to this chapter.

RESULTS

Construction of Recombinant Ad5/35.FRT helper virus

The aim of this project was to create a helper adenovirus with FRT sites flanking the packaging signal, and a chimeric Ad5/35 fiber protein for conferring tropism to hematopoietic stems cells (HSC). This helper was assayed for the ability of the Ad5/35 chimeric fiber to infect CD34+ HSC-like cells compared to Ad5. In order to propagate high quality Helper Dependent Adenovirus (HDAd) vector preparations the Ad5/35.FRT helper must also be adequately

restricted in 293FLPe cells.

The Ad5/35.FRT helper was created by cloning the left end of the Ad.FRT virus, which has FRT sites flanking the packaging signal (21), with the right end of the Ad5/35 virus containing the Ad5/35 chimeric fiber knob (25). In this strategy we used *in vivo* recombination to combine large overlapping fragments of the two viruses (17). This took advantage of the cell's intrinsic ability to perform homologous recombination (32), as well as the fact that the two viruses are both Ad5 viruses and the genome between the packaging site and the fiber gene should be identical.

Viral DNA was harvested from each virus and cut by restriction endonuclease digestion to generate the desired fragments. The left end fragment with the FRT flanked packaging signal was generated by digesting the Ad.FRT viral DNA with *Spe*I. And the right end fragment was generated by digestion of the Ad5/35 viral DNA with *Pme*I. The theory behind this strategy was that *in vivo* recombination would occur between the homologous regions between the two fragments, and only a whole recombined intact genome would give rise to progeny viruses. Figure 3.1A is a schematic diagram of the recombinant vector cloning strategy.

Several precautions were used to ensure that the only virus to replicate would be the recombined virus. The Ad.FRT viral DNA has two *Spe*I sites near each other, increasing the probability that the parent genome would be digested at least once to an appropriately sized fragment, and that there would be little to none of the intact parent DNA left after digestion. After heat inactivation of the restriction endonucleases, equal masses of both digests were transfected into 294Cre4 cells. 293Cre4 cells provide the complementing E1A and E1B that the E1-deleted helpers need to replicate, in addition to expressing Cre recombinase. The Cre recombinase should recombine out the packaging signal from any Ad5/35 parental viral DNA,

preventing non-recombinants from being packaged. Only intact recombined DNA with both the FRT flanked packaging signal and the Ad5/35 fiber should have resulted in viral production (Fig. 3.1B).

PCR screening of recombinant clones

Recombinant viruses were harvested and clones were isolated by limiting dilution and PCR screening for the Ad5/35 fiber knob sequence and the FRT-flanked packaging signal. Primers were designed to recognize sequence internal to the Ad35 fiber sequence. All of the screened clones and the Ad5/35 parent virus had the desired Ad35 fiber sequence band, while the Ad.FRT parent and wild-type Ad5 controls did not (Fig. 3.2A).

Four primers were designed, two within the packaging signal and two flanking the packaging signal. The loxP flanked packaging signal could be determined from the FRT flanked packaging signal because the Ad5/35 loxP flanked signal was constructed to be in the reverse orientation to minimize potential recombination in 293 cells (25), whereas the FRT-flanked packaging signal of the Ad.FRT virus is in the same orientation as wild-type Ad5.

As shown Figure 3.2B, different combinations of primer pairs would give rise to bands depending on the orientation of the packaging signal (Psi or Ψ). Primer pairs Psi1/Psi4 and Psi2/Psi3 would give bands for the native orientation of the packaging signal, while Psi1/Psi3 and Psi2/Psi4 would give bands for the reverse orientation packaging signal. Clones F6 and F8 only had bands for the native orientation primer pairs signifying the FRT flanked packaging signal, and did not have bands for the other two primer pairs (Fig. 3.2C). Control results are shown for the Ad.FRT and Ad5/35 parental viral DNA, as well as wild type Ad5 DNA.

One of the clones validated by PCR was re-purified by limiting dilution to ensure a pure

population. Viral DNA was then isolated from a CsCl gradient ultra-centrifuged stock for sequencing to confirm the chimeric Ad5/35 fiber and the FRT flanked packaging signal. This virus, designated as JP-1 or Ad5/35.FRT was next used for functional analysis assays.

Functional Analysis of Ad5/35.FRT

The first thing we wanted to test was whether Ad5/35.FRT had increased transduction efficiency into CD34+ HSC like M07e cells. M07e cells were infected at a multiplicity of infection (MOI) of 50, and the total number of infectious genomes in the nuclei after 24-hours were quantified via qPCR (24). Ad5/35.FRT had a 3-fold increased transduction efficiency of M07e cells when compared to Ad5 (Ad.FRT) (Fig. 3.3).

The functional activity of the FRT sites was confirmed by an FLPe excision assay. The Psi1/Psi2 primers described previously for clone screening were used to assay whether the FRT sites were intact and could be used to excise the packaging signal by FLPe recombinase. In the absence of FLPe, the Psi1/Psi2 primers resulted in a 475bp band that spanned both FRT sites and the packaging signal (Fig. 3.4A). Upon recombination by FLPe, the packaging signal and one of the FRT sites are eliminated, resulting in a 270bp PCR band (Fig. 3.4B). Ad5/35.FRT and the parental virus Ad.FRT were infected into 293 cells or 293 cells expressing FLPe recombinase (293FLPe) at an MOI of 10 for 24 hours. Total DNA was then isolated and assayed via PCR. In the presence of FLPe, the FRT sites are recombined resulting in the 270bp PCR product for both the Ad5/35.FRT cloned virus and the parental virus (Fig. 3.4C).

Propagation of a Helper-Dependent Adenovirus vector with A5/35.FRT

The validated virus was then used in a propagation experiment to test its use as a helper

virus for generating HDAd vectors. Ad5/35FRT and HDAd.Cre (1) were infected alone or co-infected at an MOI of 5 into 293FLPe cells. After 48 hours cells were harvested and assayed for total vector and helper infectious genomes by qPCR (24) (Fig. 3.5). Blue and yellow bars represent the total number of viral genomes that were introduced upon infection with the vector and helper, respectively, as determined by the titers and MOI. The red bars represent the number of infectious HDAd viral particles that were propagated for the infection, and the green bars represent the number of helper viral particles that were produced. These results indicate that while the helper was able to propagate HDAd vector particles, the helper itself was not restricted from being packaged in the 293FLPe cells. Although PCR results gave evidence that the FRT sites were functional for recombining out the packaging signal, significant amounts of the helper were still packaged. HDAd systems employing the Cre/loxP recombinase system have demonstrated that the level of recombinase expression can be a limiting factor in the efficiency of the excision of the packaging signal (33). Increasing expression of FLPe in 293 cells during HDAd propagations could possibly result in reduced contaminating helper virus in HDAd vector stocks. The remainder of this chapter discusses the challenges of developing a 293 cell line expressing high levels of FLPe.

FLPe Gene Amplification

Two main strategies were employed to increase expression of FLPe by gene copy amplification. In the first method, the EDH cassette was exchanged for an internal ribosome entry sequence (IRES) allowing expression of puromycin acetyltransferase after the *FLPe* gene. Expression of the bicistronic cassette was driven by the CAGGS promoter, which is a CMV early enhancer/chicken beta-actin promoter (34). The EDH cassette contains an

encephalomyocarditis virus (**E**MCV) IRES for expression of a dihydrofolate reductase (***D****HFR*) gene fused to the selectable marker gene hygromycin B phosphotransferase (***H****ph*), followed by an SV40 intron and polyA signal (8).

This construct (pCAGGS-FLPe.EDH) was transfected into 293 cells and stable clones were selected by growth in hygromycin selection media. DHFR, which is essential for purine synthesis and plays a vital role in cell proliferation and growth (35), can be inactivated in a stoichiometric manner by the chemotherapy drug methotrexate (MTX) (36, 37). High copies of the *dhfr* gene can be achieved through step-wise increases in MXT treatment in mammalian cells (38, 39), and placing the *dhfr* gene within the expression cassette for FLP should result in amplification of the FLP gene along with the dhfr gene. It has also been shown that first treating mammalian cells with another chemotherapy agent, Arabinofuranosyl Cytidine (AraC), or other treatments that cause DNA breaks, results in increased frequency of gene amplification (39, 40).

Clones treated with increasing concentrations of MTX, both with and without additional AraC treatment were assayed for FLPe activity by luciferase reporter assay (Fig. 3.6A). Selected representative assays are shown in Figure 3.6B. These results show that increasing resistance to MTX did not correspond with increasing FLP activity measured by luciferase assay. In addition, we saw no improvement over the original 293FLP cells (23).

We next wanted to try a different gene amplification strategy described by Shimizu et al. in which a plasmid containing a mammalian replication initiation region (IR) and matrix attachment region (MAR) is cotransfected with DNA of interest, resulting in amplification of both sequences through an initiation of a process inducing extrachromosomal double minutes (DMs) and homogeneously staining regions (HSRs) (9). The pCAGGS-FLPe plasmid was co-transfected with the IR containing plasmid pSFVdhfr. Blasticidin resistance conferred by the IR

plasmid was used for selection of stable clones. Stable clones were assayed for FLPe activity by luciferase assay.

In addition, IR-FLP clones and MTX amplified clones were assayed for *FLPe* gene copy number in relation to the FLPe activity. We found that *FLPe* gene copy number does not correlate with increased FLPe recombinase activity (Fig. 3.7). Noticeably, the established 293FLP cell line averaged less that one copy per cell but had the highest FLPe activity. The MTX amplified clones had 2-3 copies per cell, while the IR amplified clones ranged from 2-5 copies per cell without significant increases in activity.

We hypothesized that at high levels of expression, the FLPe is somehow detrimental to the 293 cells and is subsequently selected against. We decided that an inducible system for expressing potentially toxic proteins may be required to express adequate levels of FLPe in 293 cells.

Sindbis layered DNA-RNA expression system for FLPe RNA amplification

A Sindbis virus replicon based layered DNA-RNA system for temperature sensitive expression of FLPe was modeled on the system developed by Boorsma et al. (Fig. 3.8) (13). A plasmid system for expression of a temperature sensitive Sindbis replicon from a mammalian promoter was constructed by serial manipulations of the plasmid pSin-ΔCP-lucif. The plasmid pSin-ΔCP-lucif contained a Sindbis virus genome that uses the SP6 promoter for *in vitro* transcription (IVT) of the replicon, including the 3' non-translated region and polyA tail. The plasmid encoded the non-structural proteins 1-4 (nsp1234) that make up the RNA-dependent RNA replicase and the endogenous subgenomic promoter (SGP) driving the expression of luciferase in place of the viral structural genes. It was decided to construct and optimize the

system using the luciferase reporter gene in place of FLPe in preliminary experiments for ease in detection.

PCR mutagenesis was used to introduce the C3855T mutation into nsp2 for reduced cytopathicity and the G6226A mutation in nsp4 for temperature sensitivity. Both mutations disrupted specific restriction sites to give distinct patterns upon digest (Fig. 3.9). Clones with the appropriate restriction digest patterns for both mutations were confirmed by sequencing. Fragments from the plasmids containing the desired mutations were cloned back into the original parental plasmids in order to limit the introduction of extraneous mutations from the PCR mutagenesis.

Expression from Sindbis RNA replicon is temperature sensitive

Sindbis replicons were made by IVT from the parental plasmid pSin-ΔCP-lucif (REP-lucif) and the temperature sensitive plasmid expressing luciferase pSin-ts/ncp-lucif (REPts-lucif). The replicon IVT RNAs, or water for mock, were transfected into BHK or 293 cells by electroporation. The transfected cells were split into two plates and incubated for 18 hours at either the non-permissive temperature of 37°C or the permissive temperature of 32°C. The cells were then harvested for luciferase assay.

The luciferase results, when plotted on a log scale (Fig. 3.10), show that at the non-permissive temperature in 293 cells (dark red) the luciferase activity was at the same level as mock for the temperature sensitive mutant. At the permissive temperature in 293 cells (dark blue), the temperature sensitive mutant had about 10-fold lower luciferase activity than the non-mutated replicon, but this level is still ~60-fold higher than at the non-permissive temperature (dark red). These results indicate that the mutation does indeed result in a temperature

regulatable expression from the Sindbis replicon. However, these levels are significantly reduced (by more than 2 logs), from what is observed in the BHK cells at the permissive temperature (light blue bars). These differenced could be due to the different electroporation transfection efficiencies of the RNA into the BHK and 293 cells, or it could be an issue of the functionality of the replicon in 293 cells.

Sindbis replicon can be expressed from a mammalian promoter

The SP6 promoter for IVT was replaced with an RSV promoter for mammalian expression. The plasmid with the RSV promoter driving expression of the temperature sensitive Sindbis replicon was used for a transient DNA transfection to test that the RSV promoter was active in mammalian cells. A time course assay was performed by transfecting multiple plates of with the pPuroRSV-Sin-lucif plasmid and incubating at either the permissive (32°C) or non-permissive (37°C) temperature and harvesting one plate per day for luciferase assay. At the permissive temperature the luciferase expression peaked 3 days post transfection and very little luciferase activity was observed at the non-permissive temperature for any of the time points (Fig. 3.11). These results indicate that the RSV promoter is indeed active and results in temperature-regulated expression of the gene of interest.

Insufficient nuclear export of replicon may limit expression from Sindbis replicon

The key components of the layered DNA-RNA Sindbis system, temperature regulated expression and expression from a mammalian promoter, were validated by transient assays. We next wanted to establish proof of principle for using this system for the generation of stable cell lines by selecting 293 stable clones expressing luciferase from the Sindbis replicon (293Lucif).

To this end, the plasmid backbone of the expression vector was cloned out and replaced with a backbone for puromycin selection. 293 cells were transfected with the selectable Sindbis replicon expression vector pPuroRSV-Sin-lucif, and stable clones were isolated by puromycin selection. However, when the clones were tested for luciferase activity, no clone expressed higher than background levels of luciferase at the permissive temperature. This result raised the question: why were we not seeing the expected high expression of the protein of interest, even though each of the individual components of the system had been optimized?

It was hypothesized that lack of synchronicity in expression of the Sindbis replicon from the integrated DNA could be to blame for the lack high expression in the population. It is possible that only a fraction of the cells were able to export the large (>9kb) unsliced message out of the nucleus at the same time. All cells would have to have sufficient RNA reach the cytoplasm before the gene of interest could be expressed at high levels from the subgenomic promoter. Research by Boorsma et al. has suggested that these limitations could be overcome by including an SV40 intron in the Sindbis replicon to increase export of the message out of the nucleus through involvement of the slicing machinery. In addition, it was suggested that including secondary selection expressed from an IRES after the gene of interest would ensure that only cells that can get the replicon RNA out of the nucleus would be drug resistant (41). The use of an IRES would allow expression of a drug resistance marker independent of the Sindbis replicase. This strategy was tested by cloning the FLPe.EDH expression cassette, discussed previously for methotrexate amplification, into the Sindbis replicon plasmid behind the sub-genomic promoter. However, no stable clones were observed after transfection of this plasmid into 293 cells and subsequent selection with hygromycin.

Sindbis viral vector for limiting helper contamination in HDAd propagations

At this point in the project, the feasibility of a layered DNA-RNA Sindbis system was questioned. The evidence suggested that the Sindbis replicon was not being exported to the cytoplasm sufficiently enough for our purposes. We still felt that a high burst of FLP expression delivered by a temperature sensitive Sindbis replicon was an attractive idea for controlled expression of FLPe during HDAd vector propagation. We decided to try a strategy employing a Sindbis viral vector (SINV) expressing heterologous FLPe replicon and packaged via defective helper RNA. Sindbis vectors were chosen because of their ability be propagated to high titers, and because they can be easily inactivated by treatment of enveloped virus with solvent/detergent (42).

Propagation of an HDAd vector using a FLPe expressing vector rather than a constitutive cell line would present some specific challenges. It would be a three-virus system in which the helper adenovirus provides the structural proteins needed to propagate the HDAd vector, and the Sindbis virus would provide the FLPe recombinase required to restrict the packaging of the helper adenovirus. A propagation of HDAd stocks would begin with infecting 293 cells with a SINV-FLPe vector and inducing FLPe expression at the permissive temperature of 32°C. The HDAd vector DNA and the helper virus would then be introduced into the FLPe expressing 293 cells, and the temperature elevated to the non-permissive temperature of 37°C for adenovirus replication. Elevation to 37°C would inactivate the Sindbis replicase and allow the adenovirus to take over the cell's resources for replication.

Sindbis infection does not interfere with Adenoviral replication

The first question to investigate the feasibility of the Sindbis virus vector (SINV) system

would be to determine if Sindbis virus infection would affect the replication of the adenovirus. To that end a co-infection experiment was performed in which wild-type Ad5 was infected into 293 cells at an MOI of 20, either alone as a co-infection with wild-type Sindbis virus at an MOI of 5. Mock infection and a Sindbis only infection were used as controls. The morphology of the infected cells are shown in Figure 3.12A-D 48 hours post infection (pi). The MOIs used for each virus were sufficient to induce cytopathic effects (CPE) in individual infection. The adenovirus only and co-infections were harvested and the adenovirus output titers were measured by infectious genome assay (24). The output titer of adenovirus was reduced ~2.5-fold in the co-infection with Sindbis virus (Fig. 3.12E), but this decrease was fairly small given the fact that wild-type Sindbis virus was used in this experiment, and the reduction in adenovirus could be due to the Sindbis replicase inhibiting cellular transcription (43). An actual propagation would be performed with Sindbis vectors mutated in nsp2 as described previously for reduced cytopathicity.

Sindbis virus vectors only poorly infect 293 cells

We needed to determine whether we could get sufficient FLPe recombinase activity from a SINV vector to restrict helper adenoviruses. In order to do this, the vector would need to adequately infect all of the 293 cells, and expression from the replicase would need to be highly amplified upon induction at the permissive temperature. Since assaying for FLPe is multistep process, it was decided to use the temperature sensitive EYFP expressing reporter Sindbis vector SINVts-EYFP for experiments investigating the infectivity of 293 cells by Sindbis vectors.

Equal volumes of SINVts-EYFP supernatant (day 8 sup) were used to infect either 293 cells or BHK cells for one hour at 37°C, then the cells were placed at the permissive temperature

of 32°C for 48 hours to induce expression of EYFP. After 48 hours the cells were imaged by fluorescent microscopy. Figure 3.12 shows that ~100% of the BHK cells expressed EYFP, while only about 1% or less of the 293 cells had a high level of EYFP expression. These results indicate that the 293 cells are refractory to infection by Sindbis. Although the BHK and 293 cells were likely infected with different MOIs based on the cell densities, the differences were not more than 2-fold and would not explain the apparently several logs lower infection efficiency.

Poor infection of 293 cells by Sindbis virus is not due to the receptor

We wanted to determine whether the low level of EYFP expression in 293 cells was caused by lower infectivity due to differences in the Sindbis receptor between 293 cells and BHK cells. The receptor for Sindbis virus, 67-kiloDalton high-affinity laminin receptor (44), is also the receptor for Adeno-Associated Virus (AAV) (45). We hypothesized that since the adenovirus protein e1a is known to repress certain cellular genes, including some cell surface markers (46), the constitutive expression of the adenovirus E1 proteins in 293 cells may be involved in down-regulating the expression of the laminin receptor. The down regulation of the laminin receptor by E1 proteins would possibly protect adenovirus infected cells from subsequent AAV infection. Alternatively, the Sindbis may have a lower affinity for the human laminin receptor than the Syrian hamster laminin receptor present on BHK cells.

A lentivirus vector was created to introduce the Syrian hamster (BHK) laminin receptor (gene name *RPSA*) into 293 cells. The mouse cDNA for the *RPSA* gene, which had 100% amino acid identity to the Syrian hamster laminin (44, 47), was PCR amplified and cloned into a self-inactivating lentivirus expression vector. The VSV-G pseudotyped lentivirus was used to generate stable 293 cells with mouse laminin receptor (293LR).

RT-qPCR was used to determine the expression levels for *RPSA* in 293, 293LR, and BHK cells. Primer sets for human *RPSA* primers measured the endogenous levels in 293 cells and 293LR cells, mouse *RPSA* primers measured the levels of the *RPSA* transgene in 293LR cells, and Syrian hamster *RPSA* primers measured the endogenous levels in BHK cells. All primer sets were normalized to actin expression. 293LR cells express both the endogenous and transgenic *RPSA* at the same levels as 293 and BHK cell, respectively (Fig. 3.14). These results show that the 293LR cells express the structurally identical laminin receptor to that found in BHK cells, in approximately the same abundance, and should therefore be able to be infected by Sindbis virus with the same efficiency. However, upon infection of 293LR cells with the SINV-EYFP (non-temperature sensitive) vector, the productive infection efficiency was not improved over 293 cells (Fig. 3.15).

In conclusion, even with expression of the structurally identical laminin receptor to BHK cells, 293LR cells fail to support Sindbis virus infection, indicating that the interaction with the laminin receptor is not the limiting factor for Sindbis replicase in 293 cells.

DISCUSSION

A recombinant Ad5/35.FRT helper virus was created for use in the HDAd/EBV hybrid gene therapy vector system that efficiently targets HSC-like CD34+ cells. However, this helper failed to be adequately restricted during HDAd vector propagation.

Previous studies have shown that the activity of the recombinase is the limiting factor regarding the ability of the permissive cell line to restrict helper virus contamination in vector propagations (33, 48). Two main factors likely contribute to the high levels of helper

contamination. The first is that the inherent inability of the vector to replicate easily means that the helper rapidly outgrows the vector in a mixed population stock (19, 49–51). Since both the vector and the helper have the Ad5/35 fiber knob, they should both infect 293 cells with the same efficiency, but the competitive advantage of the helper means that even a few cells that were infected with the helper, but not the vector, would rapidly produce large amounts of the helper, while cells infected with both would make smaller amounts of the vector with some helper contamination. Cells only infected with helper dependent vector would be unable to produce any virus.

These factors are compounded by the fact that the Ad5/35 fiber appears to infect 293 cells much less effectively than the wild type Ad5 fiber, possible due to lower densities of the CD46 receptor compared to the CAR receptor on the 293 cell surface (52). This results in fewer numbers of cells that are adequately co-infected with both the helper and the vector. Increasing the relative density of the CD46 receptor on CHO cells has been shown to increase the transduction efficiency of Ad5/35 (53), and could be a possible method to increase the yields of vector from 293FLPe cells.

Secondly, low levels of FLPe expression in the 293FLPe cells may not be sufficient to efficiently excise the packaging signal from the replicating helper virus DNA. It has been demonstrated that increasing levels of Cre recombinase increases the percent excision of the packaging signal (33). And recent work has shown that at low levels FLPe recombinase activity is much less efficient than comparable levels of Cre recombinase, but at high levels FLPe was more efficient than Cre (48). Therefore, increasing levels of expression of the FLPe recombinase in 293 cells may reduce the contaminating helper.

However, after numerous iterations and years of selection we came to the conclusion that

amplification of the *FLPe* gene copy number in 293 cells is not an effective method for increasing total FLPe activity. The MTX/*dhfr* method has been shown to give successful amplification of different genes in varied cell types (36, 54), including the prothrombin gene (*FII*) in 293 cells (8). This suggests that it is the FLPe itself, rather than the methodology, that contributed to the lack of high levels of expression in 293 cells.

This work suggests that high FLPe expression could be detrimental to 293 cells, selecting against expression of FLPe recombinase over a certain threshold level. This hypothesis was supported by the findings of Kondo et al suggesting that the inability to prepare a FLPe expressing adenovirus vector without deletions was due to deleterious effects of FLPe (55). Although specific toxicity has not yet been reported for FLPe recombinase, Cre recombinase has been reported to be toxic to cells (56–58), so deleterious effects from recombinase activity cannot be ruled out. This hypothesis led to the idea of creating an inducible FLPe 293 system based on the Sindbis RNA-dependent RNA-replicase that would only express FLPe recombinase when required for adenoviral HDAd propagation.

Sindbis viruses have a very broad host cell range including insect, avian, and mammalian cell types (59, 60), but are most often used and studied in conjunction with baby hamster kidney (BHK) cells (61). This work has shown that human embryonic kidney HEK293 cells fail to support high levels of transgene expression from either a stably integrated layered DNA-RNA system or from an infection of Sindbis virus vector SINV. We have concluded that poor nuclear export of the large Sindbis replicon may be to be blamed for the former, but the receptor density and source do not seem to affect the latter. This indicates that the bottleneck is at the RNA amplification stage, rather than the infection stage of the Sindbis vector.

A survey of the literature regarding the use of Sindbis expression strategies in 293 cells

was mixed regarding the efficacy. However, upon closer reading it is clear that Sindbis replicons delivered from either a plasmid DNA source (41) or Sindbis vector (62) into 293T cells expressing the SV-40 Large T-antigen show high levels of expression, while plasmids (63) or vectors (16) delivered into the parental 293 cells fail to express at high levels.

Recent work has begun to elucidate the complex role of host factors associating with the Sindbis virus replicase, in particular it has been shown that GTPase-activating protein (SH3 domain) binding protein 1 (G3BP1) and G3BP2 interact with the nsp2, nsp3, and nsp4 proteins of the replicase (64). G3BP1 can unwind RNA/RNA duplexes (65) and probably has a roll in unwinding the subgenomic products of the Sindbis RNA-dependent RNA replicase. The Large T-antigen expressed in 293T cells also acts as a RNA-helicase on double stranded RNA (66), likely enabling the translation of otherwise inactive RNA duplexes. This hypothesis is supported by the finding in the Herweijer paper that the protein levels expressed from a replicon plasmid were equal to a control traditional plasmid, even though the subgenomic mRNA was 30-fold higher from the replicon than the plasmid control (63).

CONCLUSION

In this work we found that a helper adenovirus with a chimeric Ad5/35 fiber and FRT sites flanking the packaging signal for excision by FLPe recombinase was poorly restricted in 293FLPe cells during propagation of a Helper-Dependent Adenovirus (HDAd) vector. In addition, all attempts to increase FLPe expression in 293 cells to limit helper contamination were unsuccessful. There is, however, a possible solution: 293T cells express both the E1 proteins required for adenoviral replication (67) and the Large T-antigen that enhances expression from a

Sindbis replicon (66). Poor transduction in 293 cells by the Ad5/35.FRT virus could be overcome by transducing 293T cells with the Ad35 receptor CD46 (53), and the temperature sensitive Sindbis vector system described here could be used to induce FLPe expression during HDAd vector propagation to limit helper virus contamination.

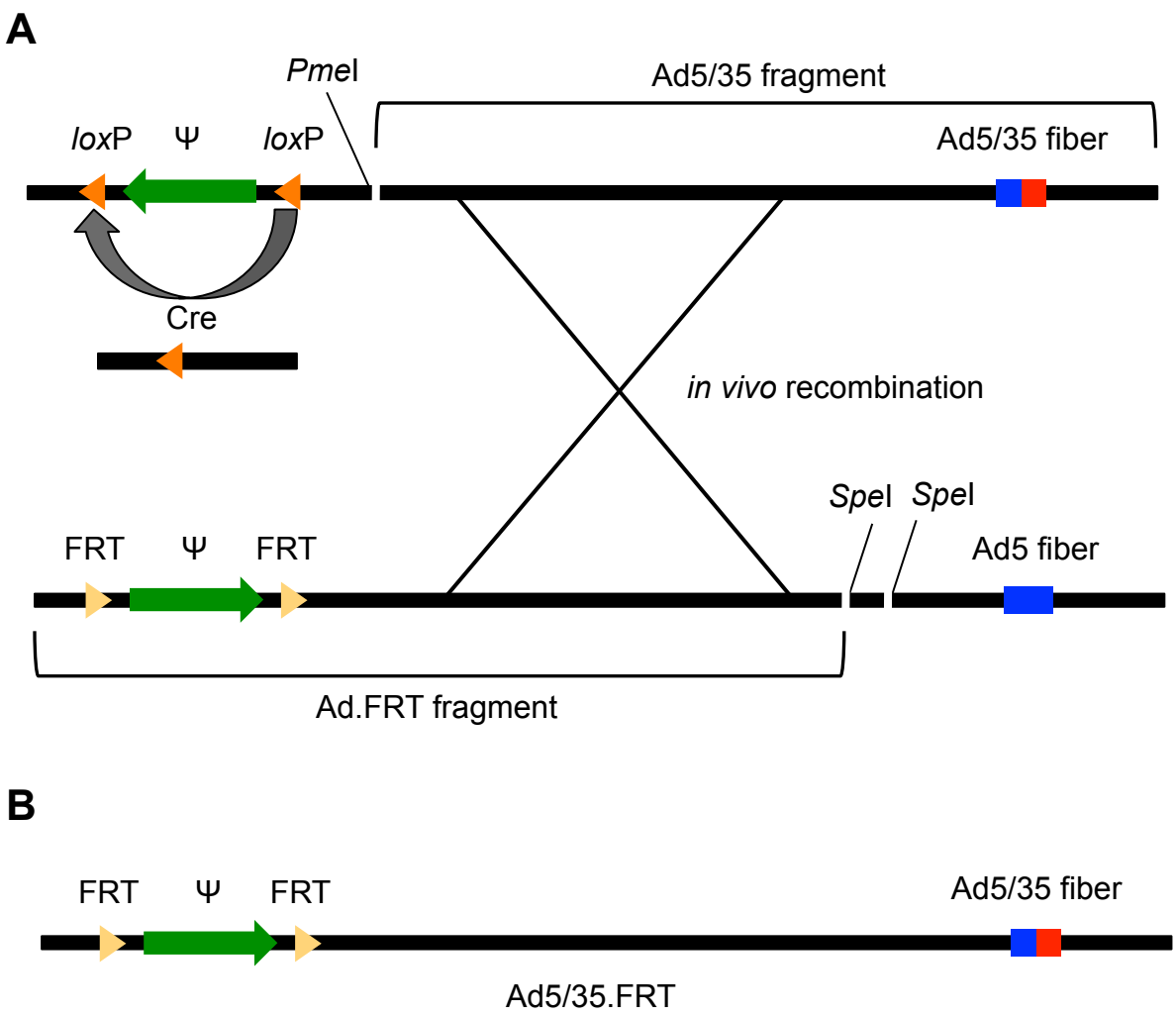

Figure 3.1. Schematic diagram of Ad5/35.FRT recombinant helper virus cloning. Black regions represent homologous sequence, green arrows represent the packaging signal (Ψ), orange and yellow arrows represent *lox*P and FRT sites, blue boxes represent Ad5 fiber sequence, and red boxes represent Ad35 fiber sequence. Diagram is not to scale. A) The Ad5/35 virus genome was digested with *Pme*I to generate a large right end fragment containing the Ad5/35 chimeric fiber gene. The Ad.FRT virus genome was digested with *Spe*I to generate a large left end fragment containing the FRT flanked packaging site. Both digests were co-transfected into 293Cre4 cells were *in vivo* homologous recombination resulted in the generation of an intact genome. B) Schematic of the recombinant helper adenovirus Ad5/35.FRT.

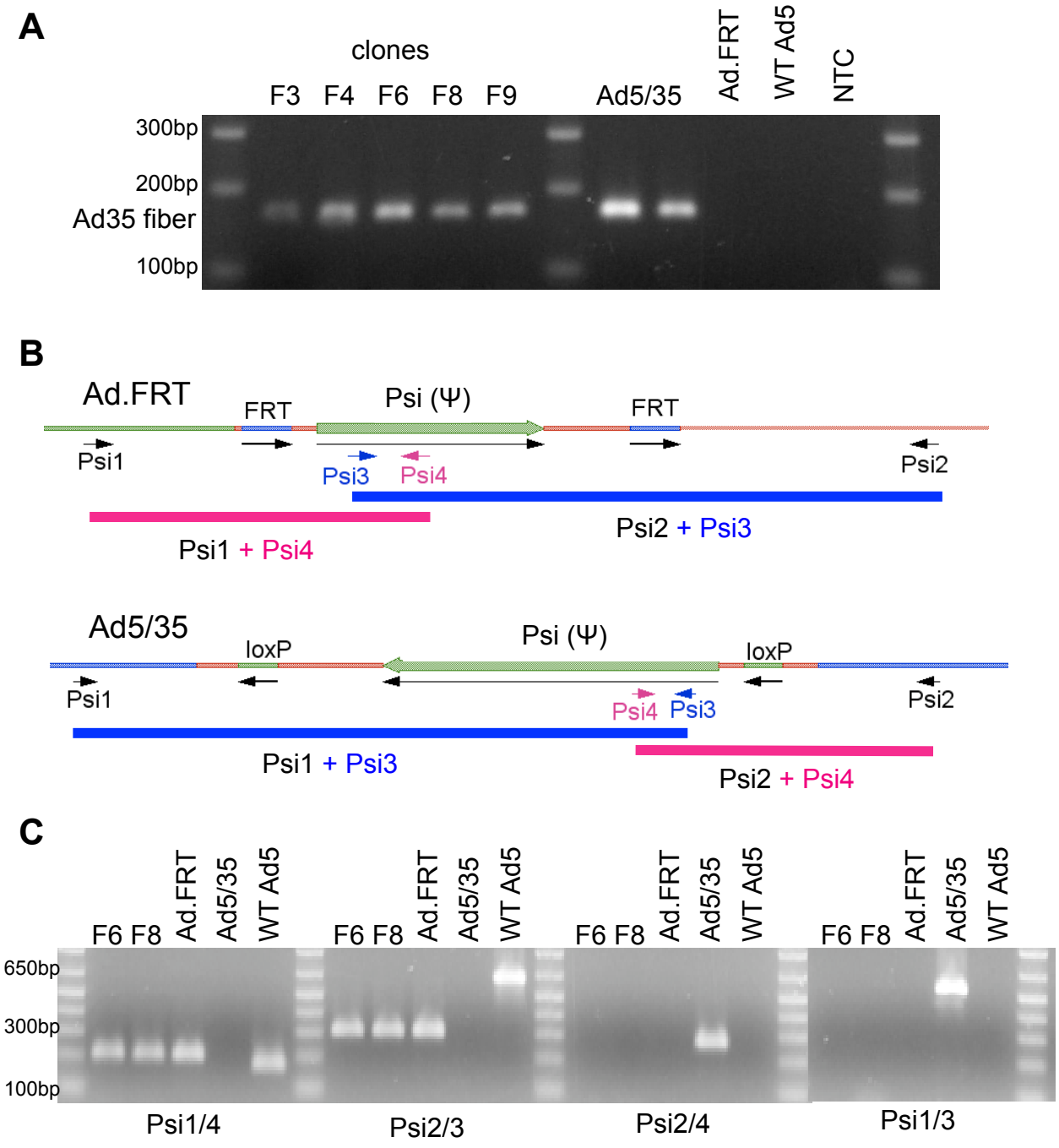

Figure 3.2. Screening putative Ad5/35.FRT clones. DNA from each parental virus, and Ad5 wild-type, were used as controls. A) PCR screen for Ad35 fiber sequence. All clones contained the Ad35 fiber sequence. B) Screening strategy for packaging signal (Ψ) orientation. The Ad.FRT flanked Ψ would give PCR products for primer pairs Psi1/4 and Psi2/3. The Ad5/35 *lox*P flanked Ψ is in the reverse orientation, so primers Psi3 and Psi 4 now read in the opposite direction, giving PCR products for primer pairs Psi1/3 and Psi 2/4. C) Both clones F6 and F8 show bands for the FRT flanked Ψ, but not the *loxP* flanked Ψ.

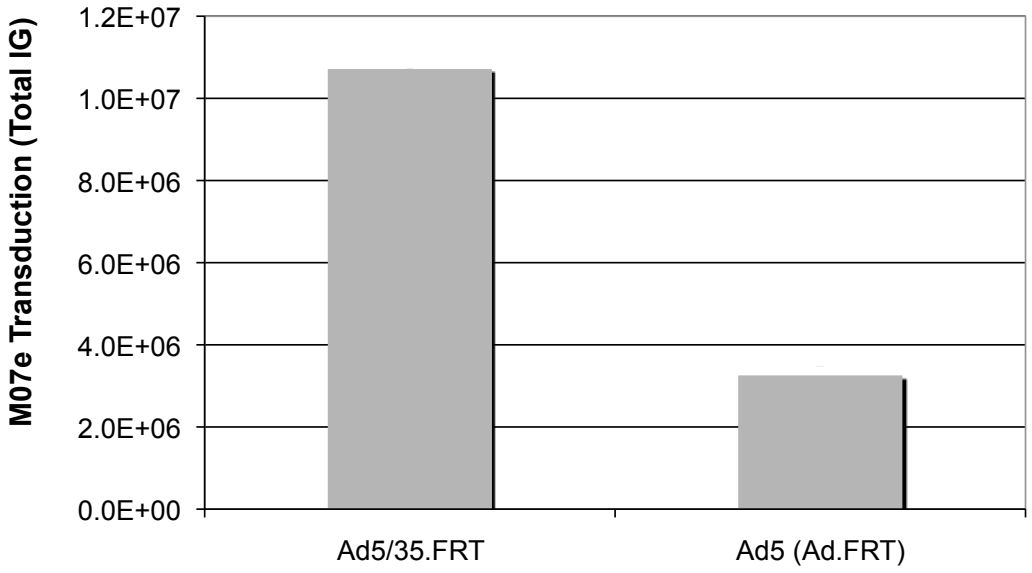

Figure 3.3. Ad5/35.FRT has increased transduction efficiency in HSC-like M07e cells. Ad5/35.FRT has a 3-fold increased transduction efficiency of HSC-like M07e cells when compared to Ad5 (Ad.FRT). $1x10^6$ M07e cells were infected at an MOI=50. The total number of infectious genomes (IG) in the nuclei after 24-hours were quantified via qPCR.

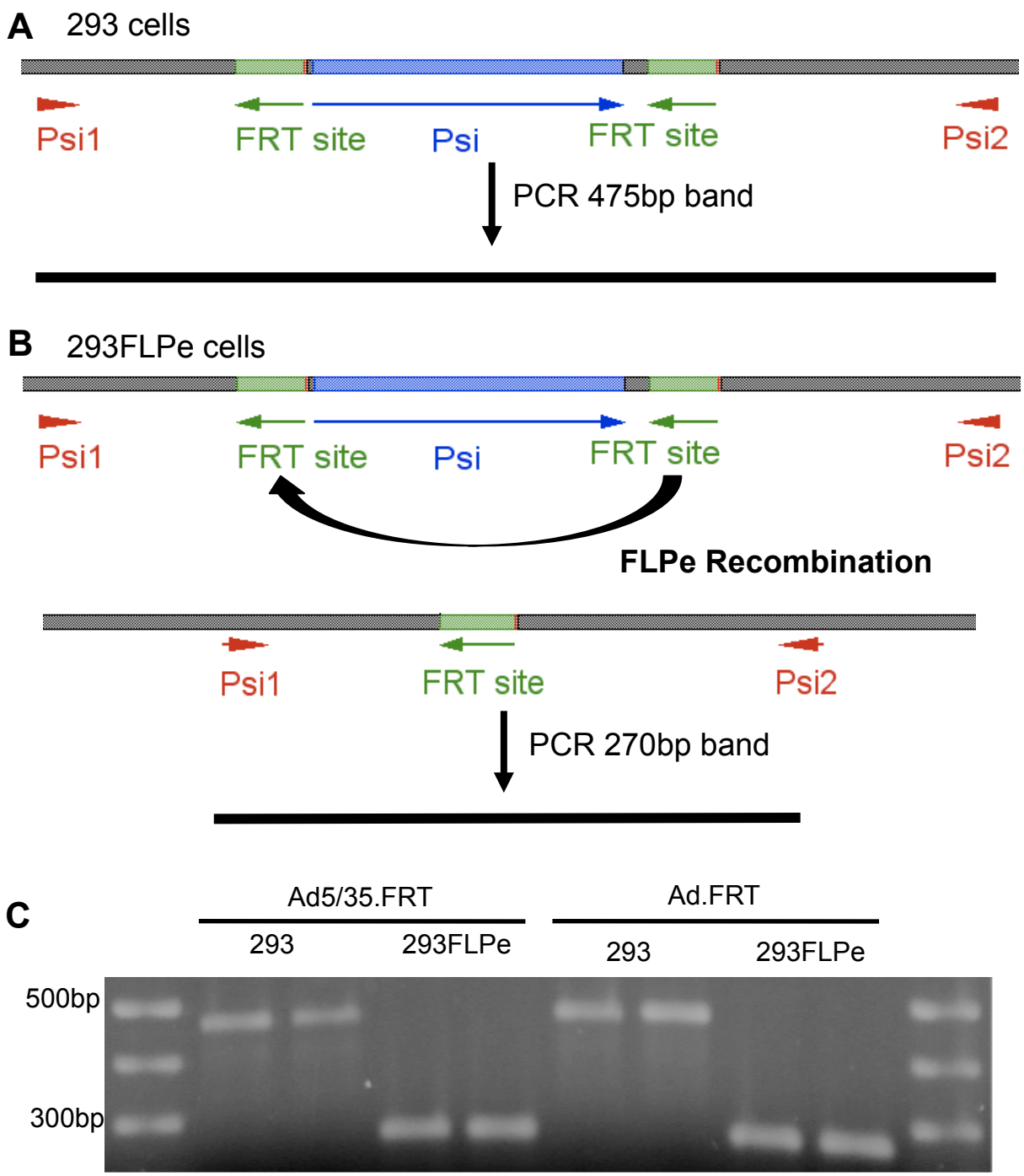

Figure 3.4. Psi is excised by recombination at FRT sites when infected into 293 cells expressing FLPe recombinase. A) Schematic diagram of PCR screening control in 293 cells. B) Schematic diagram of PCR screening for FRT mediated recombination in 293FLPe cells. C) Ad5/35.FRT and the parental virus Ad.FRT were infected in duplicate into 293 cells or 293FLPe cells at an MOI of 10 for 24 hours. Viral DNA was isolated and assayed via PCR.

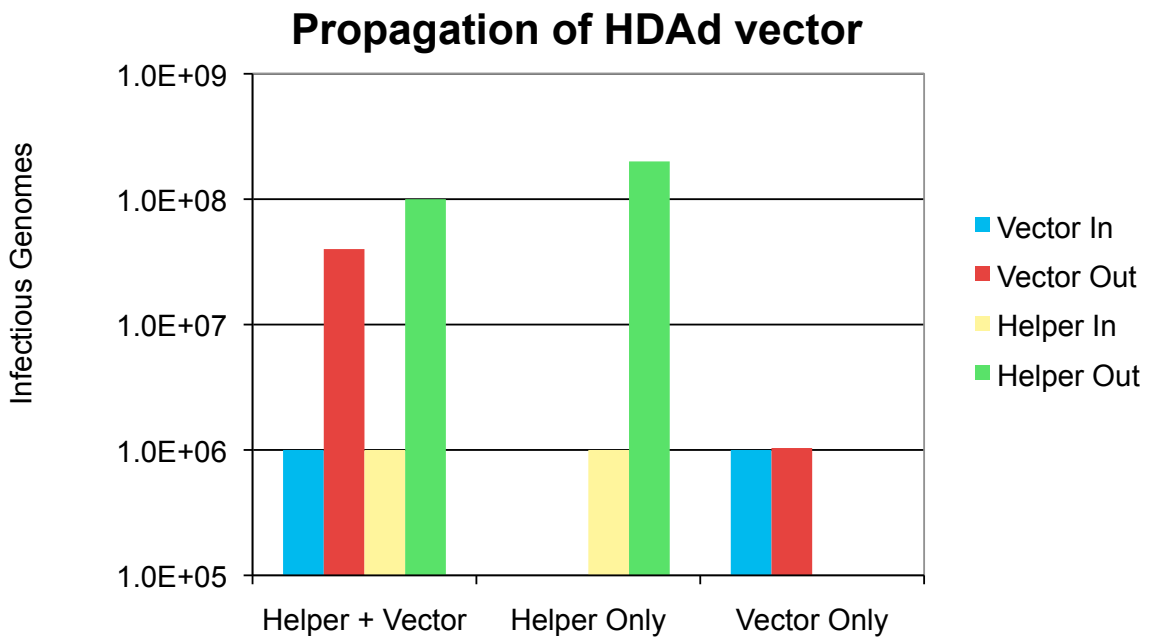

Figure 3.5. Ad5/35.FRT fails to be restricted in 293FLPe cells. Ad5/35.FRT and HDAd.Cre were infected alone or co-infected at MOI=5 into 293FLPe cells. After 48-hours cells were harvested and assayed for total vector and helper infectious genomes (IG) via QPCR. Blue and yellow bars represent the total number of viral genomes that were introduced upon infection with the vector and helper, respectively. Red bars represent the number of infectious HDAd viral particles that were propagated for the infection, and the green bars represent the number of helper viral particles that were produced.

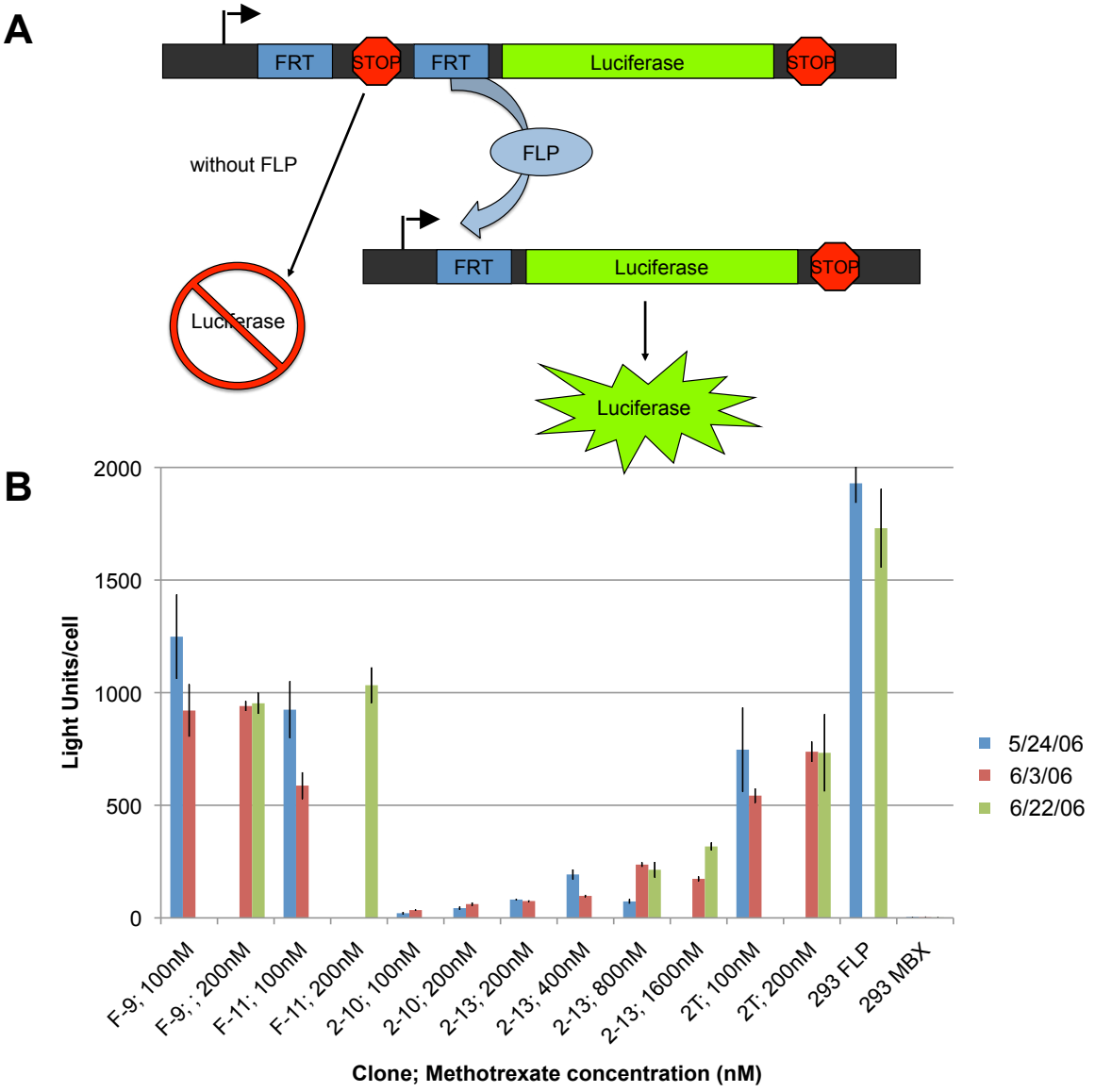

Figure 3.6. FLPe activity luciferase reporter assay. A) Schematic diagram of FLPe luciferase reporter assay. FLPe expressing cells were infected at an MOI of 50 by adenovirus vector Ad.AC.lucif, which delivers an expression cassette with FRT sites flanking a stop codon between the promoter and the firefly luciferase cDNA. In the absence of FLP recombinase expression of luciferase is restricted. In the presence of FLP recombinase the stop codon is removed by FLP-mediated excision, allowing expression of luciferase. Luciferase levels can then be assayed the the addition of luciferin substrate and bioluminescence measuring. B) 293 cells were transfected with a plasmid containing a bicistronic expression cassette with the CAGGS promoter driving FLPe and an EMCV internal ribosome entry sequence for expression of a DHFR-hygromycin B phosphotransferase fusion. Clones were selected for my hygromycin treatment and subjected to increasing concentrations of methotrexate (MTX). Clonal populations were periodically assayed for FLPe expression by luciferase reporter assay.

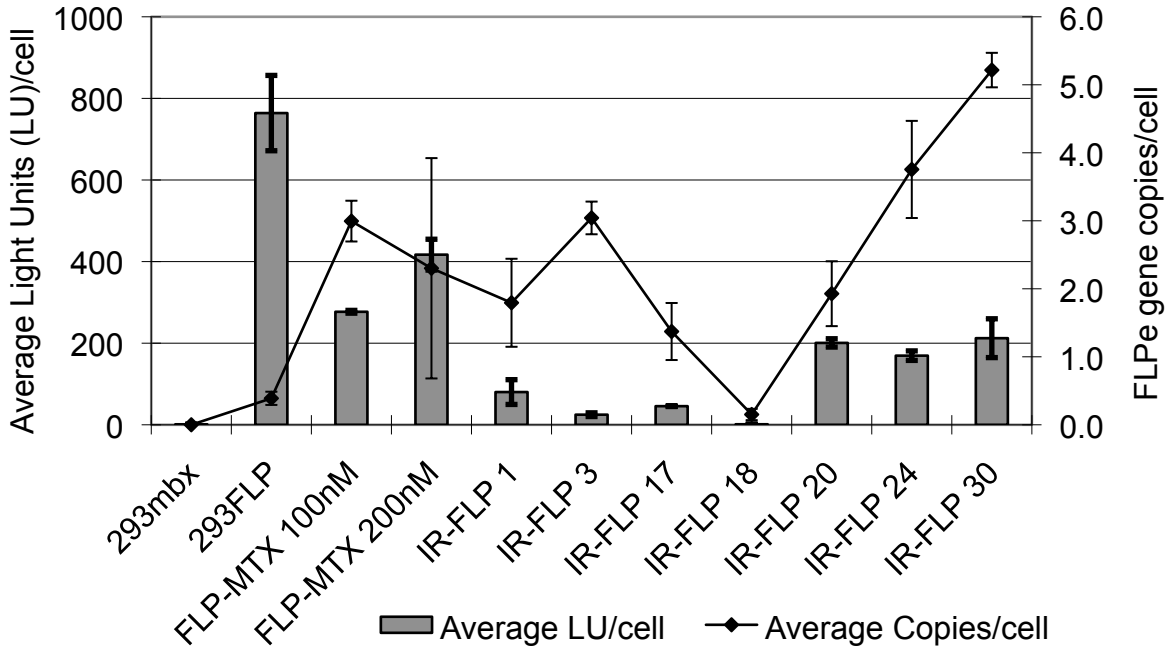

Figure 3.7. Comparison of FLPe activity to gene copy number. Representative clones from the DHFR/methotrexate (FLP-MTX) or initiation region plasmid (IR-FLP) strategies to increase gene copy number were assayed for FLPe activity by luciferase reporter assay. Total genomic DNA was isolated from each clonal population and the FLPe gene copy number was determined by comparison to a housekeeping gene. Gray bars represent the average light units per cell for each clone in the luciferase assay on the left axis. Black diamonds represent the average *FLPe* gene copy number as determined by qPCR on the right axis.

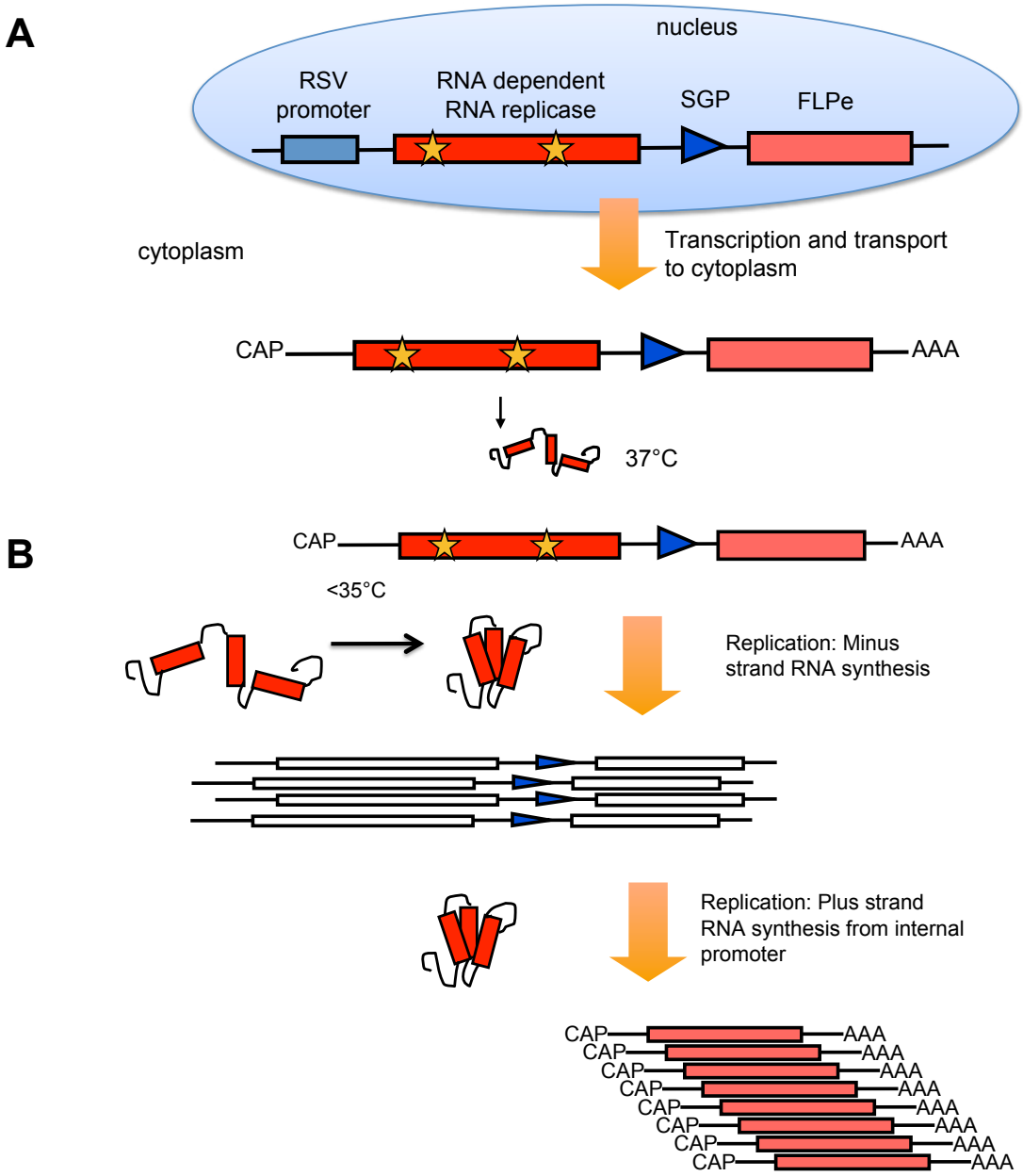

Figure 3.8. RNA amplification from a layered DNA-RNA sindbis replicon system. A) A plasmid containing and RSV promoter driving a non-cytopathic temperature sensitive (mutations represented by yellow stars) RNA-dependent RNA replicase and a FLPe gene under the control of a subgenomic promoter is stably inserted into the host cell chromosome. A plus strand RNA is transcribed by the host machinery and is transported out of the cytoplasm, where the nsp1234 replicase polyprotein is translated, but in active at 37°C. B) Upon transition to the permissive temperature below 35°C, the replicase becomes active and begins minus strand RNA synthesis from the positive strand template. The replicase then recognizes the subgenomic promoter on the minus strand RNA and begins production of high levels of the subgenomic RNA, which in turn lead to high levels of the protein of intersest. Adapted from Boorsma, et al., 2000.

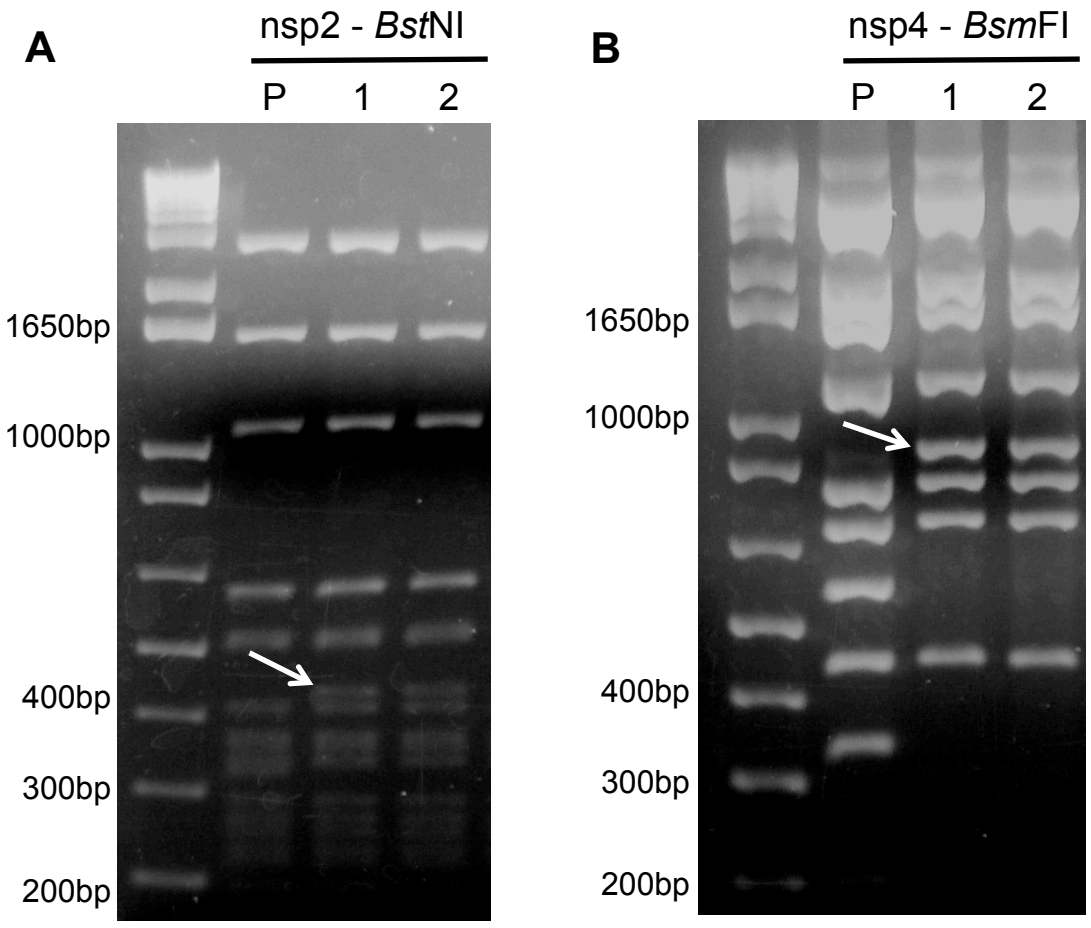

Figure 3.9. Screening for Sindbis replicase mutations. Mutations introduced in the Sindbis replicase for non-cytopathicity and temperature sensitivity disrupted endonuclease recognition sites, resulting in distinct digest patterns. White arrows indicate new bands created by the removal of a cut site in clones 1 and 2; "P" is the digest of the parental plasmid. A) The mutation in nsp2 for non-cytopathicity disrupted an endonuclease recognition site for *Bst*NI. B) Then nsp4 mutation for temperature sensitivity disrupted a recognition site for *Bsm*FI.

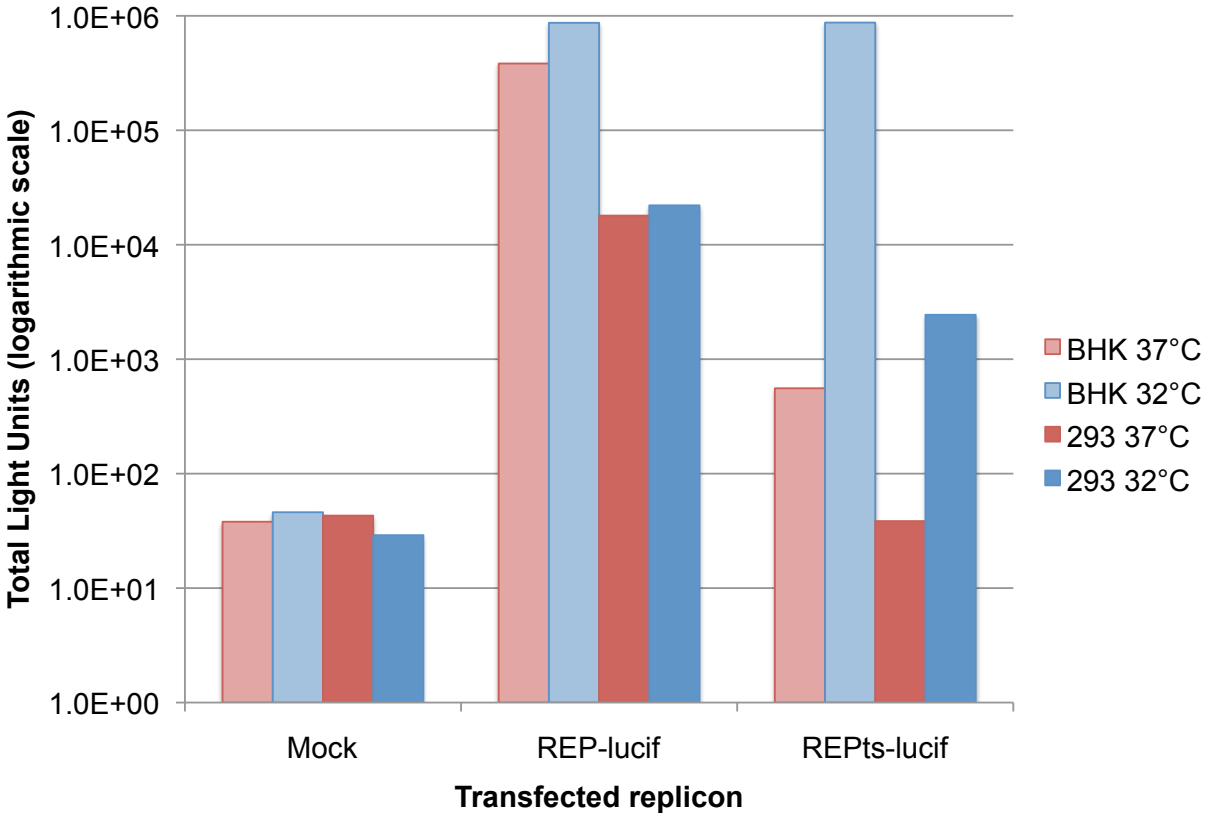

Figure 3.10. Electroporations with Sindbis replicon IVT RNAs. The replicon *in vitro* transcribed (IVT) RNAs, or water for mock, were transfected into BHK or 293 cells by electroporation. The transfected cells were split into two plates and incubated for 18 hours at either the non-permissive temperature of 37°C or the permissive temperature of 32°C. The cells were then harvested for luciferase assay. Light red and light blue are electroporations into BHK cells; dark red and dark blue are electroporations into 293 cells.

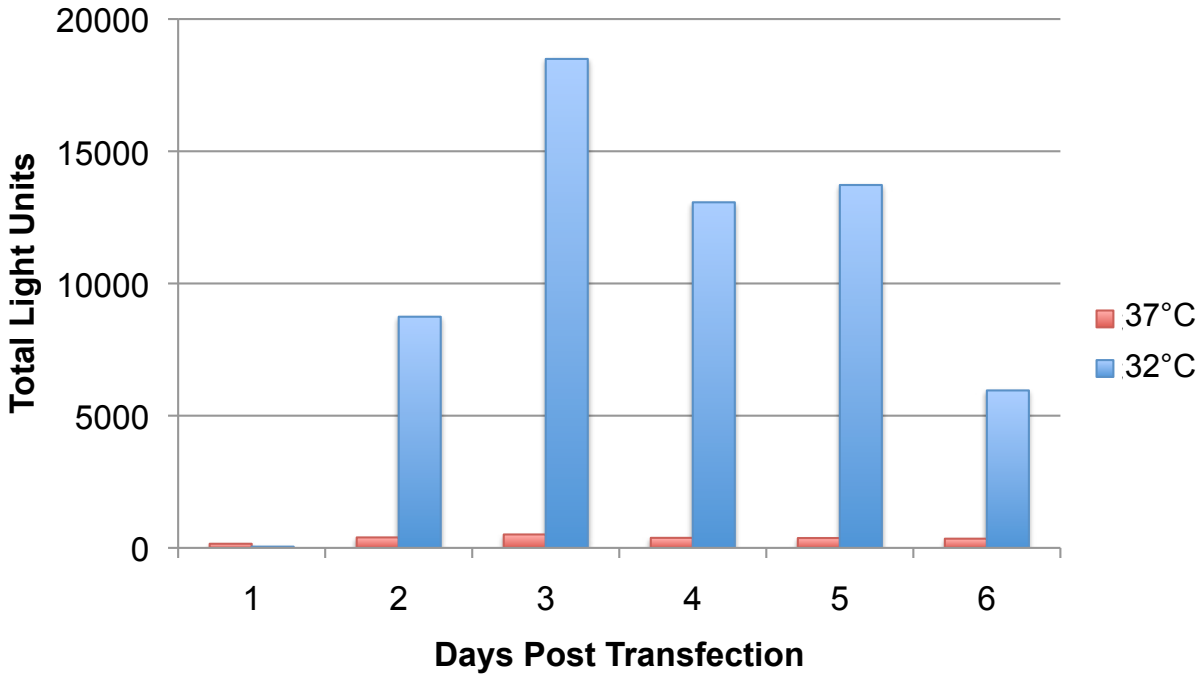

Figure 3.11. Luciferase expression over time from a transient transfection. BHK cells were transiently transfected with the pPuroRSV-Sin-lucif plasmid and incubated at 37°C or 32°C to test the functionality of the synthesized RSV promoter. A time course experiment was performed by harvesting one plate from each temperature every 24 hours and assaying for luciferase activity.

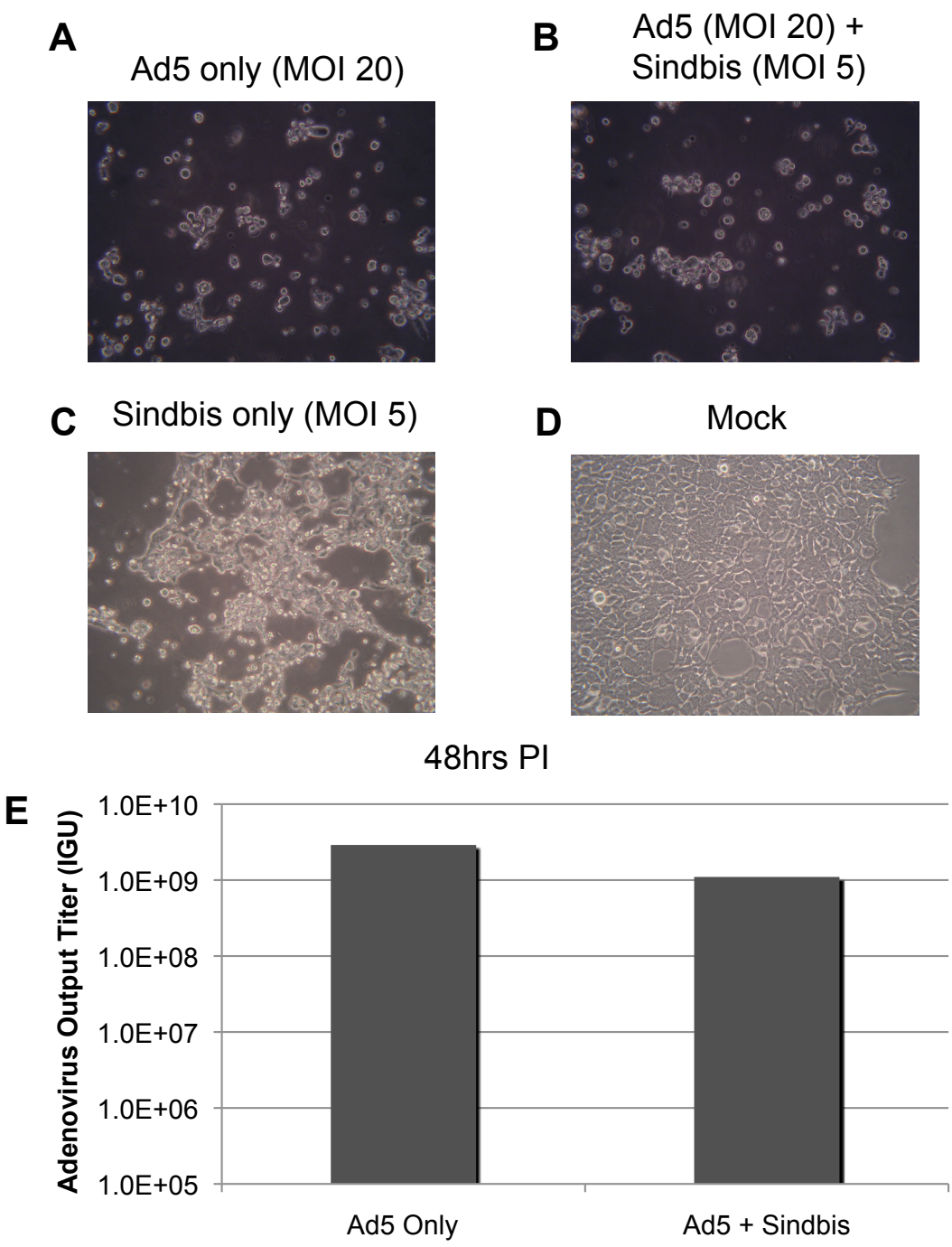

Figure 3.12. Adenovirus/Sindbis virus co-infection. 293 cells were infected with either wild-type Ad5, co-infected with Ad5 and wild-type Sindbis virus, infected with Sindbis alone, or mock infected, and imaged 48 hours post infection (PI) (A-D). E) Ad5 infected and Ad5/Sindbis co-infected cells were then harvested and assayed for viral production by Infectious genome assay. Note the log scale. Co-infection resulted in ~2.5-fold reduction in Ad5 viral production.

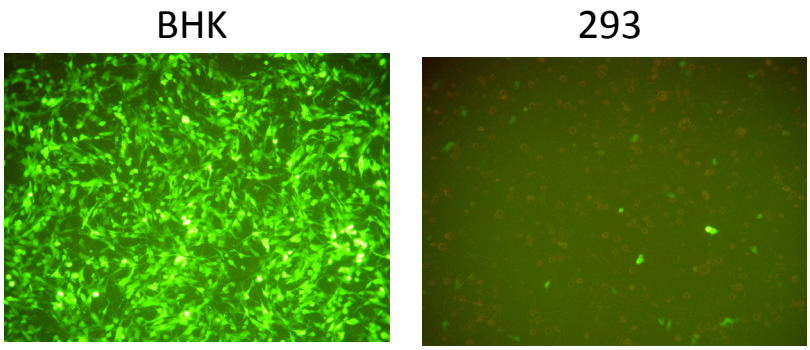

Figure 3.13. Sindbis virus vectors only poorly infect 293 cells. Equal volumes of SINVts-EYFP vector were used to infect BHK or 293 cells for 1 hour at 37°C, then the cells were placed at the permissive temperature of 32°C for 48 hours to induce expression of EYFP.

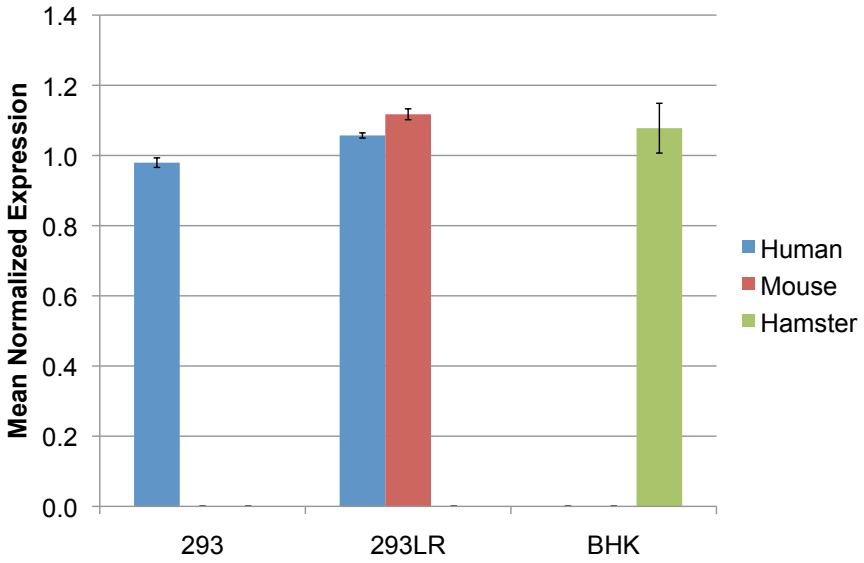

Figure 3.14. Relative expression of laminin receptor by cell type. BHK cells, 293 cells and 293 cells transduced with mouse laminin receptor structurally identical to the BHK laminin receptor (293LR) were assayed for expression of laminin receptor gene (*RPSA)* by RT-qPCR. Blue bars represent the endogenous human laminin receptor in 293 cells, the green bar represents endogenous syrian hamster laminin expression in BHK cells, and the red bar represents expression of the mouse laminin receptor transgene. 293LR cells express both the endogenous and transgene laminin receptor at approximately equal levels, comparable to BHK levels. All primer sets were normalized to actin expression.

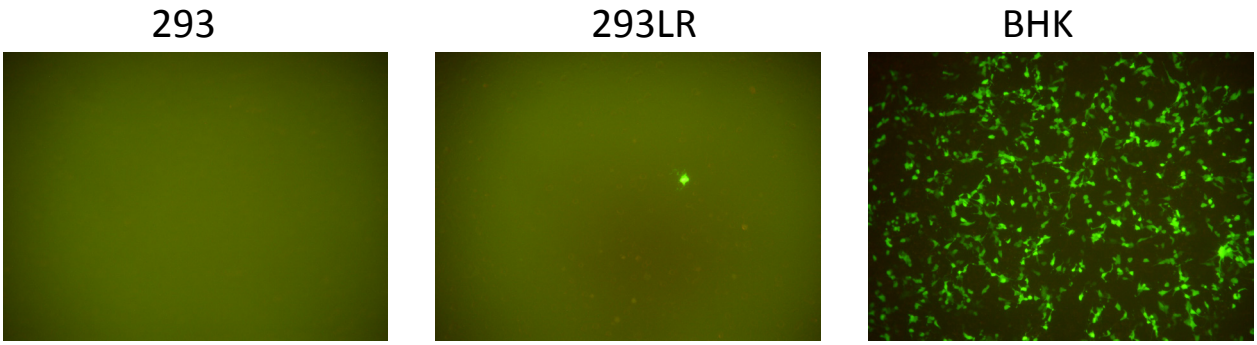

Figure 3.15. Expression of laminin receptor in 293 cells does not increase productive infection. Equal volumes of SINV-EYFP (non-temperature sensitive) vector were used to infect BHK or 293LR (293 cells expressing transgenic mouse laminin receptor) or 293 cells for 24 hours at 37°C. Neither 293 cells or 293LR cells were able to support productive expression from the Sindbis vector.

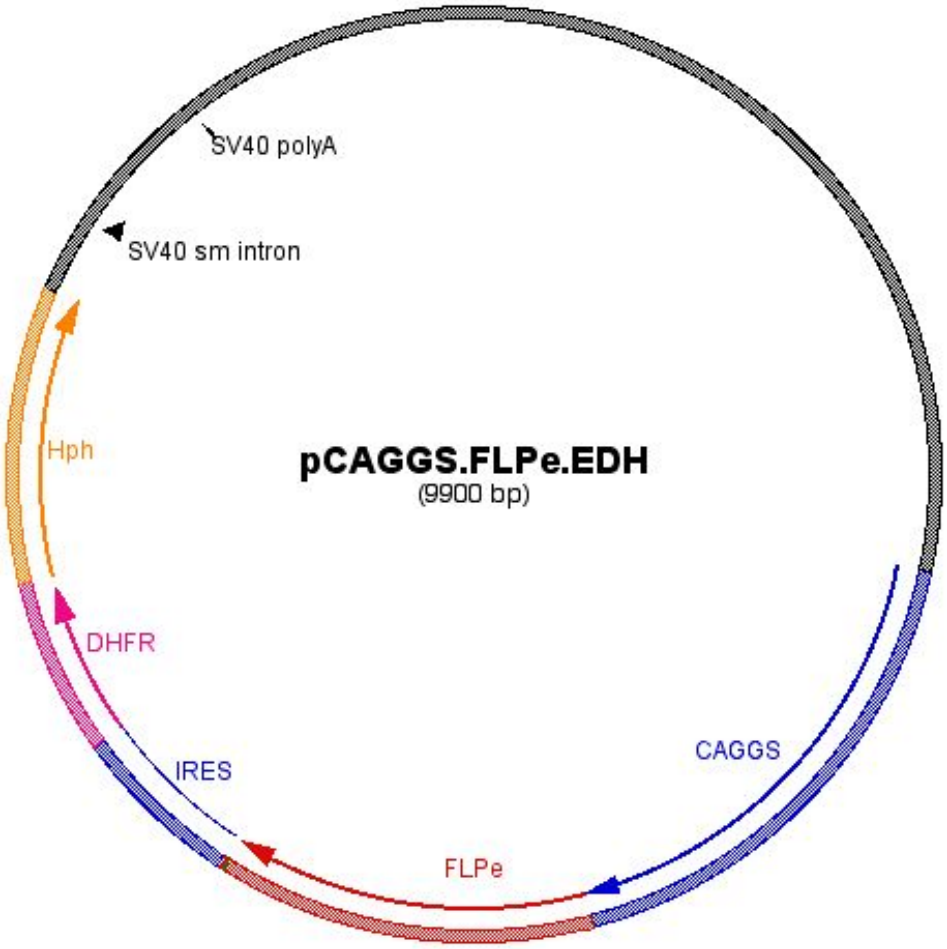

Figure 3A-1. pCAGGS-FLPe.EDH. CMV enhancer/chicken β-actin promoter (CAGGS) driving expression of enhanced FLP (FLPe), followed by the EDH expression cassette. EDH: **E**ncephalomyocarditis virus (ECMV) internal ribosome entry sequence (IRES) for the expression of a **D**HFR-**H**ygromycin fusion gene. The hygromycin selectable marker is fused to dihydrofolate reductase, which inactivates methotrexate in a stoichiometric manner. This plasmid was used for the amplification of FLPe gene copy number in conjunction with methotrexate treatment.

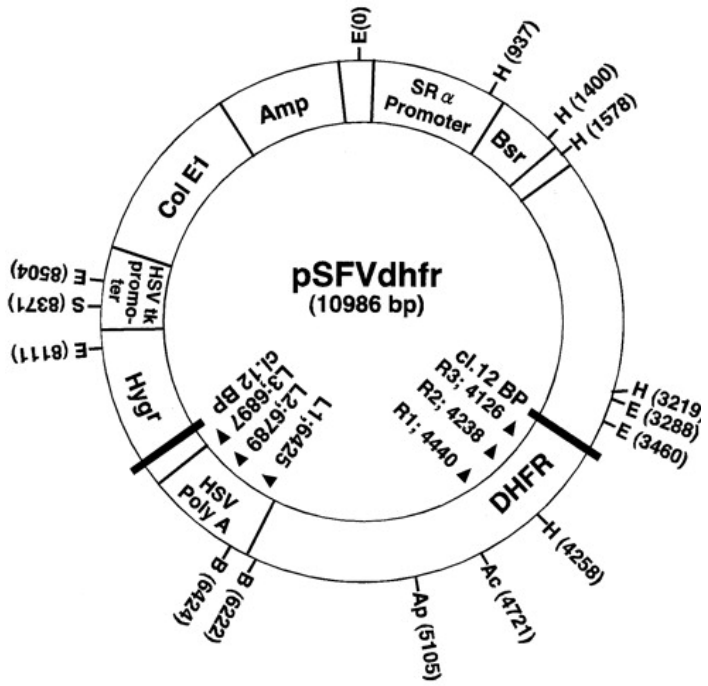

Figure 3A-2. pSFVdhfr. Vector map of pSFVdhfr plamid containing mammalian initiation and matrix attachment regions. This plasmid was co-transfected with pCAGGS-FLPe for amplification of the FLPe gene. Confers hygromycin and blasticidin resistance. **Shimizu N et al. Cancer Res 2003;63:5281-5290.**

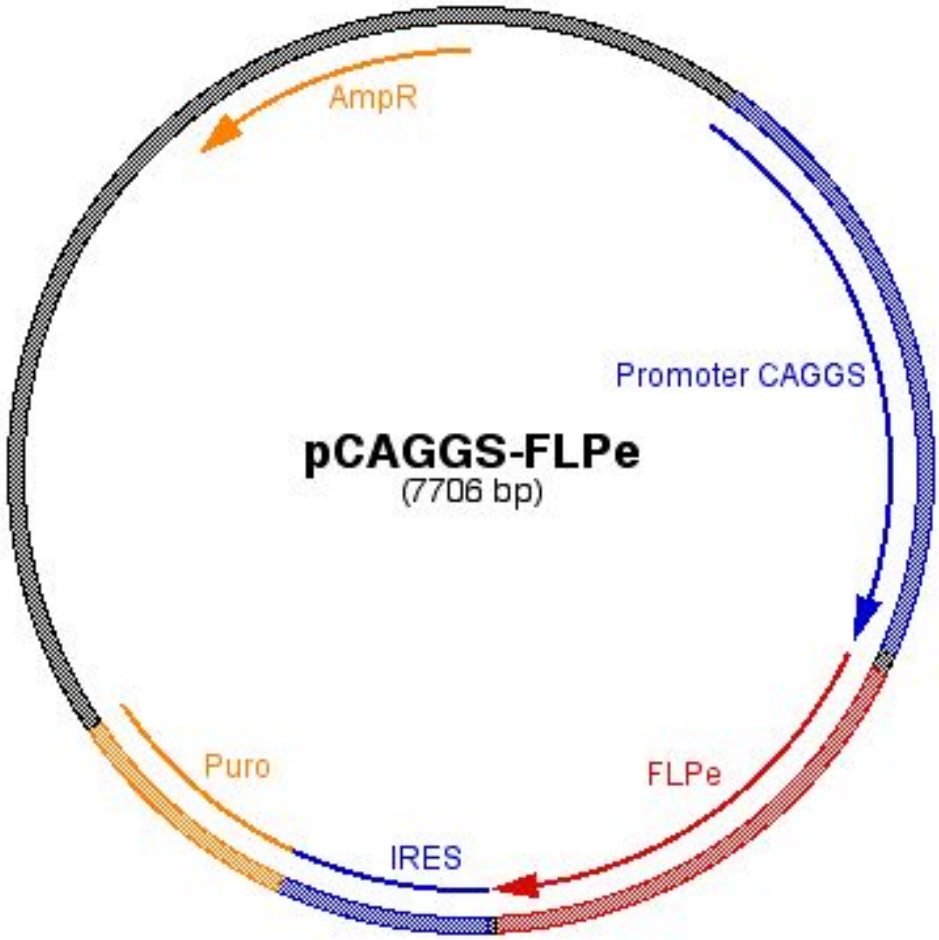

Figure 3A-3. pCAGGS-FLPe. CMV enhancer/chicken β-actin promoter (CAGGS) driving expression of enhanced FLP (FLPe), followed by the encephalomyocarditis virus (ECMV) internal ribosome entry sequence (IRES) for the expression of a puromycin acetyltransferase.

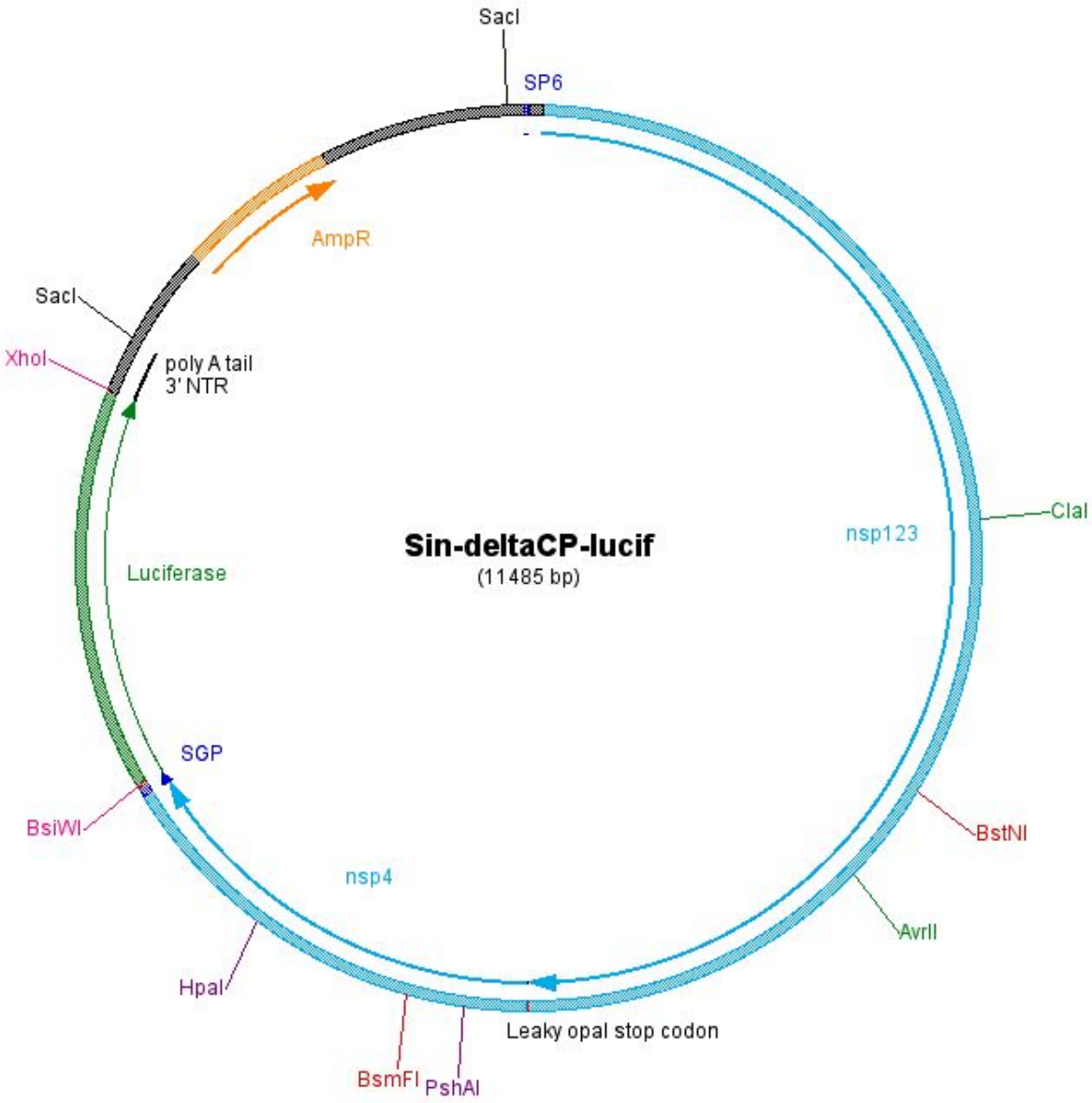

Figure 3A-4. pSin-ΔCP-lucif. Sindbis replicon plasmid for the *in vitro* transcription (IVT) of Sindbis replicon RNA from the SP6 IVT promoter. Digest with *Sac*I removes the backbone for IVT. The full replicase is translated from the nsp1234 message by read-through of the leaky Opal stop codon. The luciferase expression is driven from the subgenomic promoter (SGP) on the bicistronic message, and can be replaced with a gene of interest at the *Bsi*WI and *Xho*I sites. The restriction sites disrupted PCR mutagenesis are shown in red; only the disrupted sites are shown for the sake of clarity.

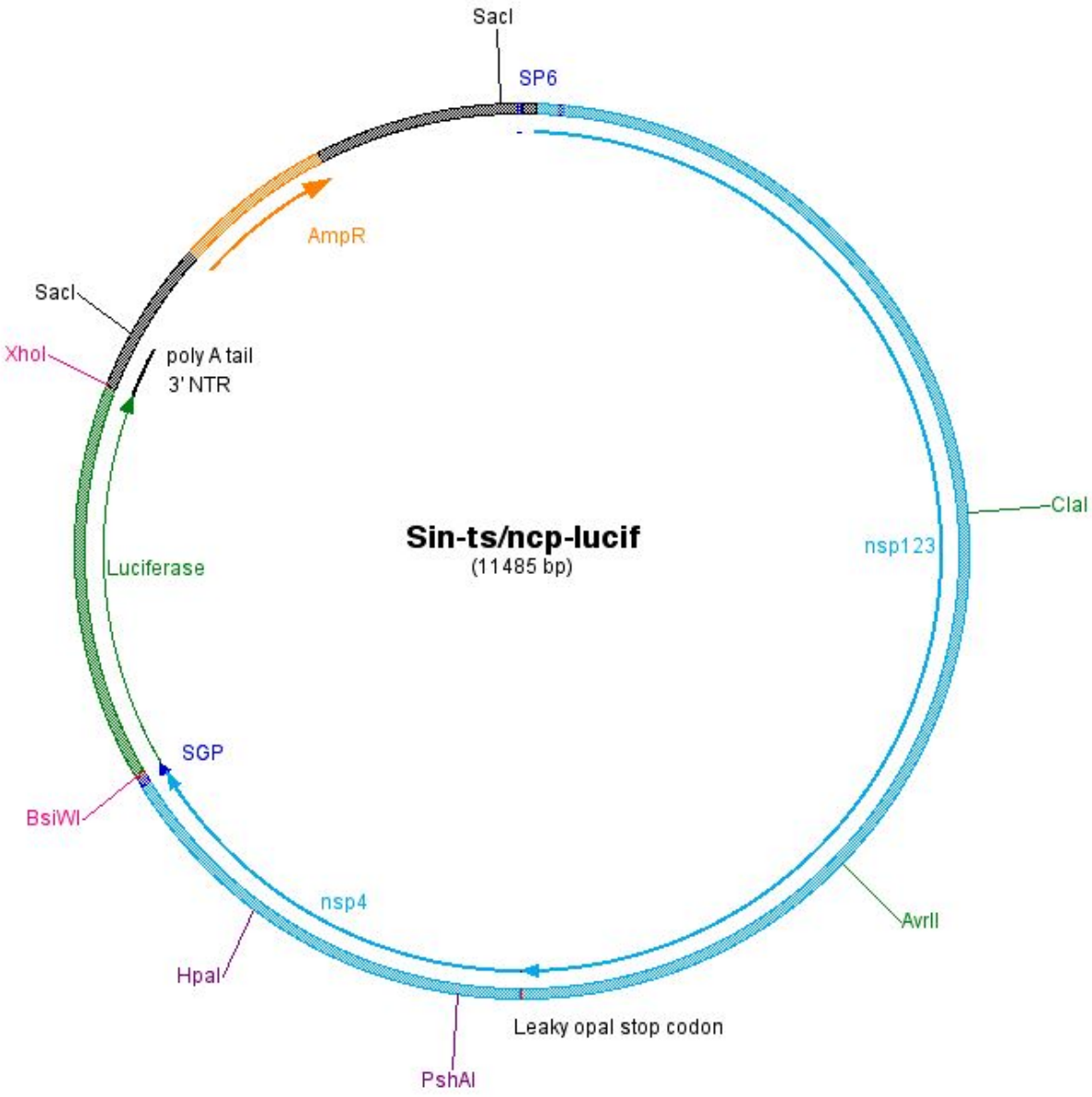

Figure 3A-5. pSin-ts/ncp-lucif. Sindbis replicon plasmid for the *in vitro* transcription (IVT) of the non-cytopathic, temperature sensitive Sindbis replicon RNA from the SP6 IVT promoter. Digest with *Sac*I removes the backbone for IVT. The full replicase is translated from the nsp1234 message by read-through of the leaky Opal stop codon. The luciferase expression is from the subgenomic promoter (SGP) on the bicistronic message, and can be replaced with a gene of interest at the *Bsi*WI and *Xho*I sites. The nsp2 mutation for non-cytopathicity disrupted the *Bst*NI site, and the nsp4 mutation for temperature sensitivity disrupted the *Bsm*FI site. The regions between the *Cla*I and *Avr*II sites (green) and *Psh*AI and *Hpa*I sites (purple) were sequenced, then those fragments were cloned back into the parental plasmid.

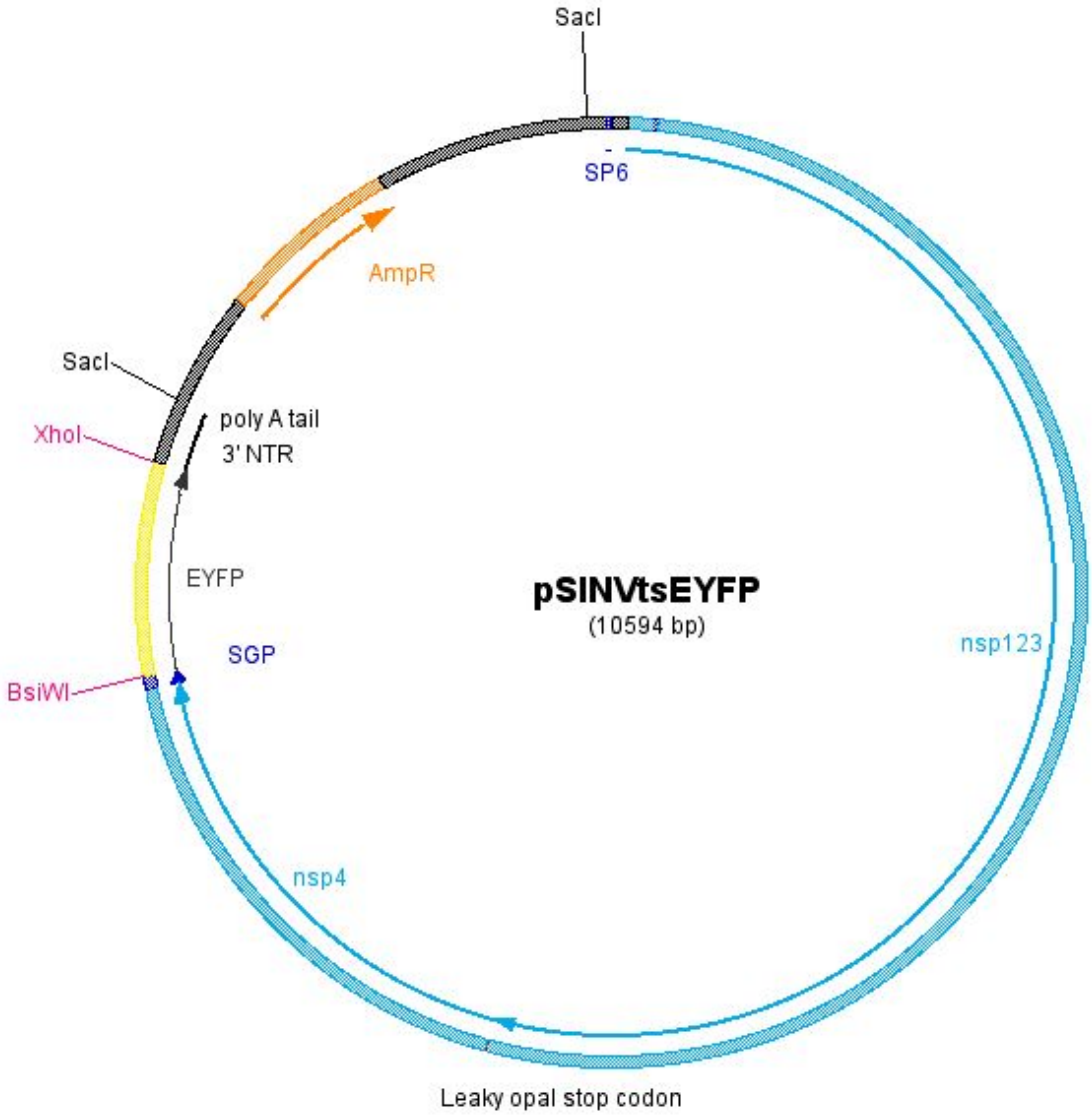

Figure 3A-6. pSINVtsEYFP. Sindbis replicon plasmid for the *in vitro* transcription (IVT) of the non-cytopathic, temperature sensitive Sindbis replicon RNA from the SP6 IVT promoter. Digest with *Sac*I removes the backbone for IVT. The full replicase is translated from the nsp1234 message by read-through of the leaky Opal stop codon. Enhanced yellow fluorescent protein was cloned in at the *Bsi*WI and *Xho*I sites and is expressed from the subgenomic promoter (SGP) on the bicistronic message.

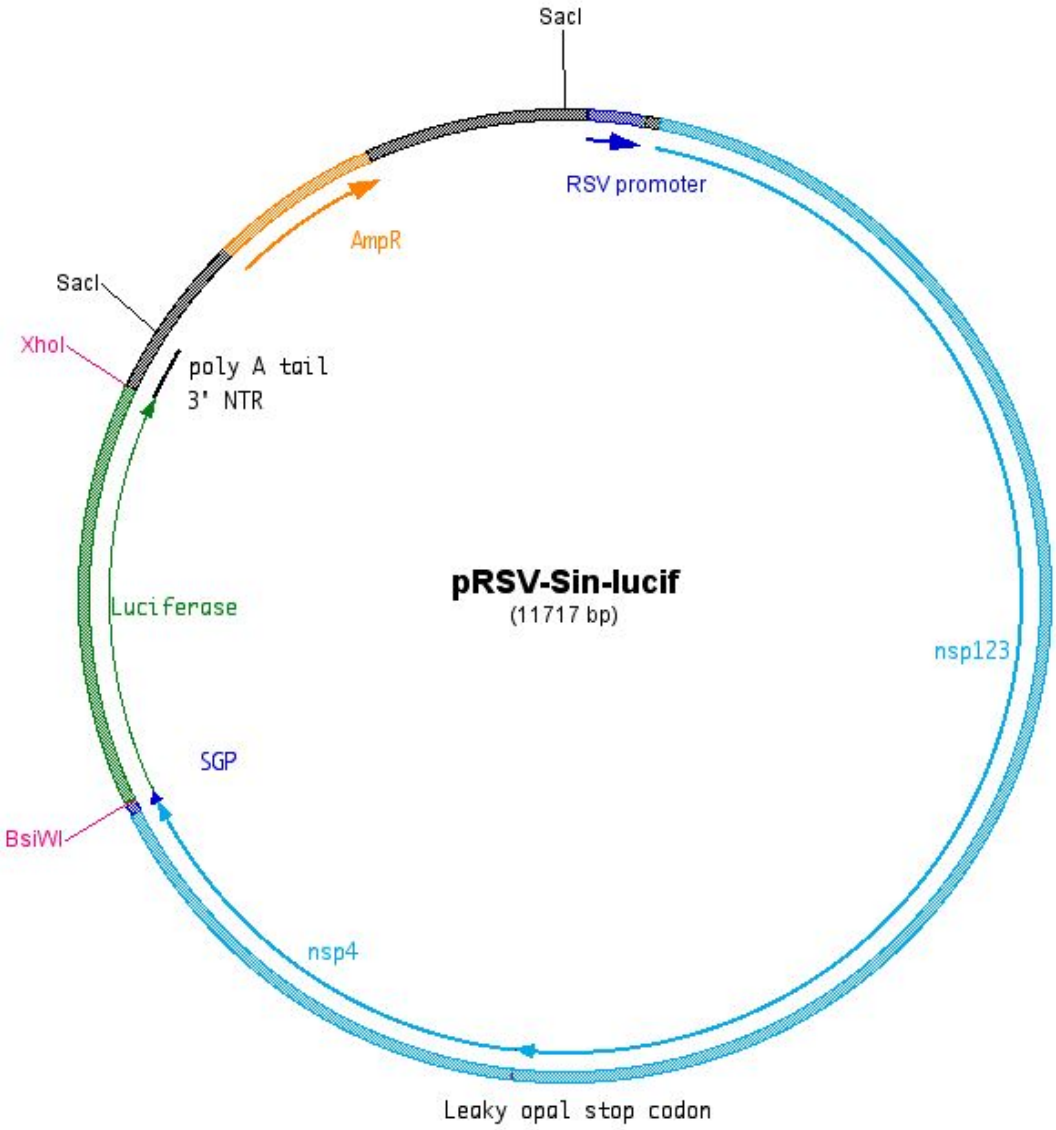

Figure 3A-7. pRSV-Sin-lucif. Sindbis plasmid for expressing the non-cytopathic, temperature sensitive replicase from the mammalian Rous Sarcoma Virus (RSV) promoter. The full replicase is translated from the nsp1234 message by read-through of the leaky Opal stop codon. The luciferase expression is driven from the subgenomic promoter (SGP) on the bicistronic message, and can be replaced with a gene of interest at the *Bsi*WI and *Xho*I sites.

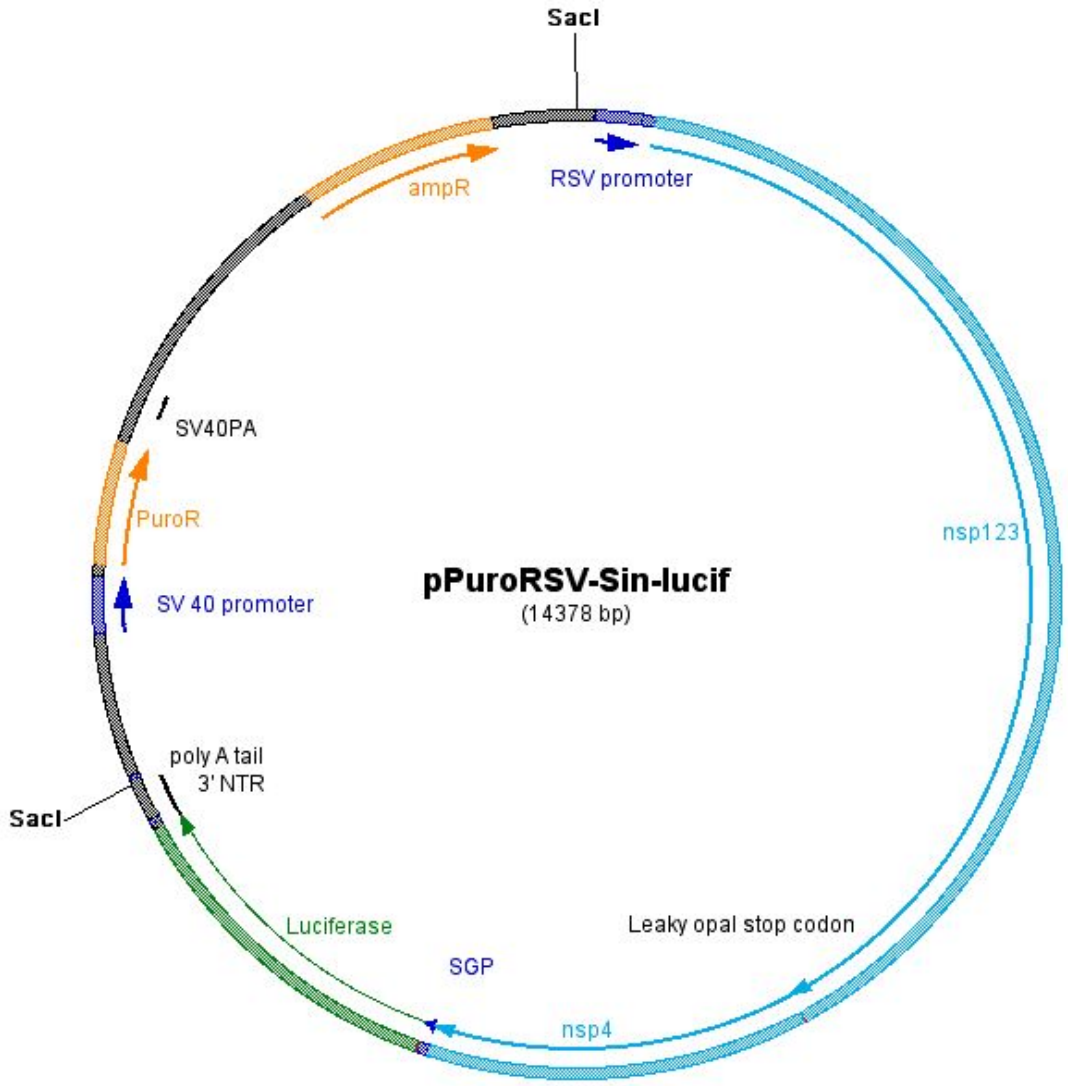

Figure 3A-8. pPuroRSV-Sin-lucif. Sindbis plasmid for selection of clones expressing the non-cytopathic, temperature sensitive replicase from the mammalian Rous Sarcoma Virus (RSV) promoter. This plasmid was created by *Sac*I digest to remove plasmid backbone of pRSV-Sin-lucif, and replacing it with a plasmid expressing puromycin acetyltransferase from the simian virus 40 (SV40 promoter). Luciferase expression is driven from the subgenomic promoter (SGP) on the bicistronic message.

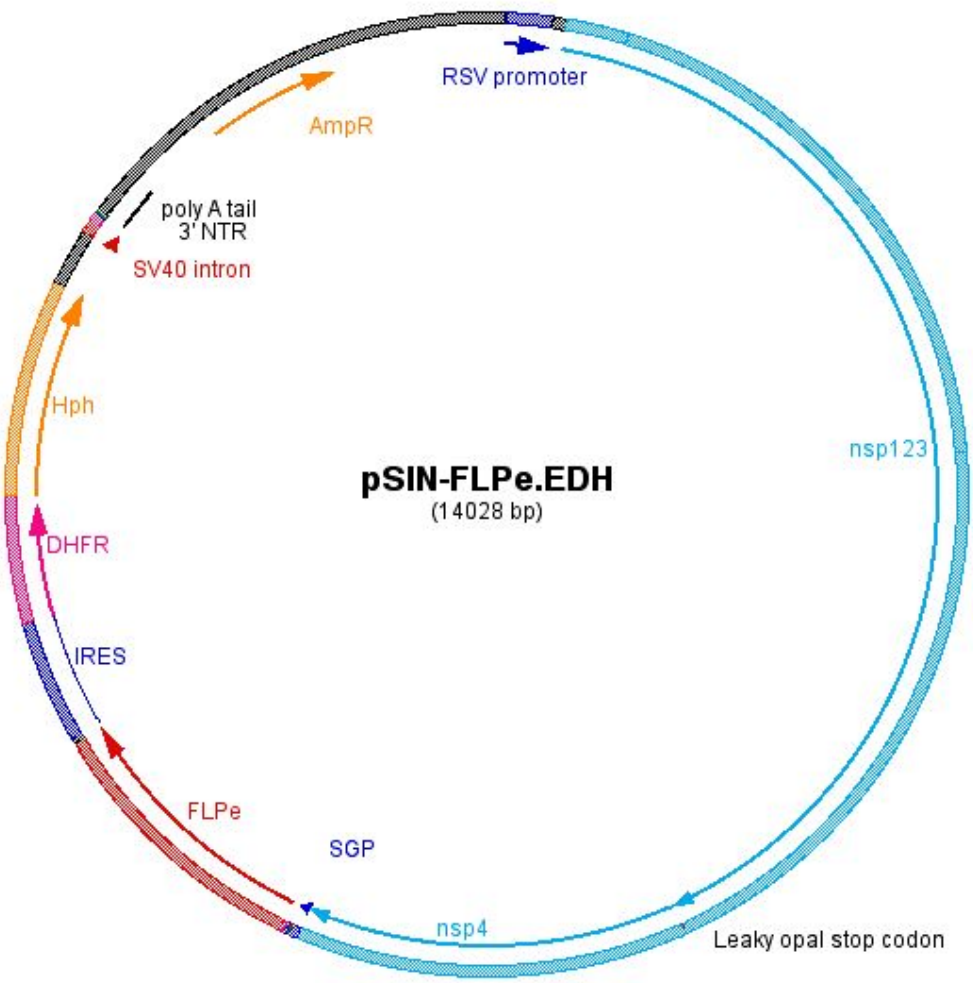

Figure 3A-9. pSIN-FLPe.EDH. Sindbis plasmid for selection of clones expressing the non-cytopathic, temperature sensitive replicase from the mammalian Rous Sarcoma Virus (RSV) promoter, FLPe from the subgenomic promoter, and the DHFR/ hygromycin fusion from the EMCV IRES. This plasmid was created by replacing the luciferase in pRSV-Sin-lucif with the FLPe.EDH bicistronic cassette, including the SV40 intron, from pCAGGS-FLPe.EDH.

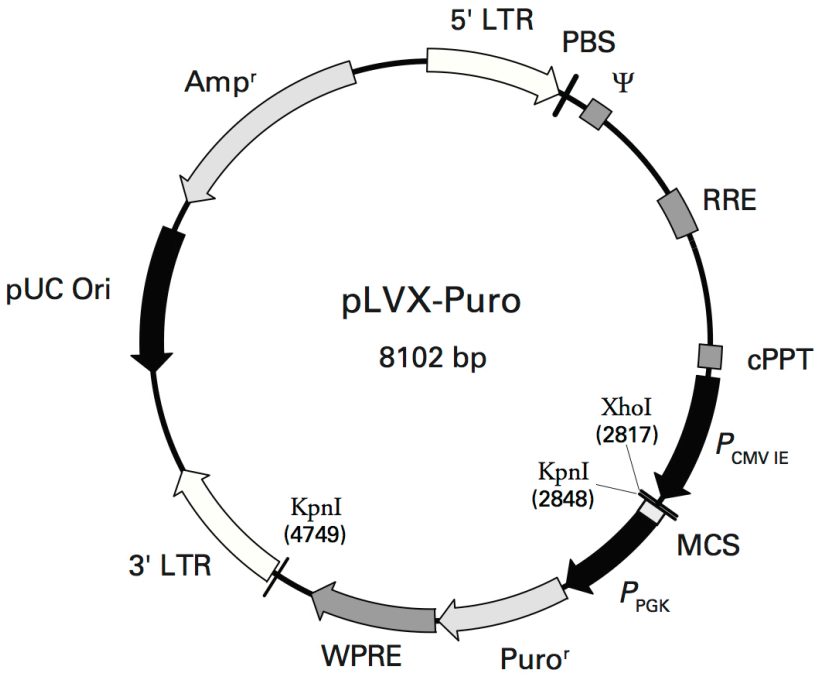

Figure 3A-10. pLVX-Puro. HIV-1-based, lentiviral expression vector. The *RPSA* cDNA was cloned in at the multiple cloning site for expression from the human cytomegalovirus immediate early promoter (PCMV IE). pLVX-Puro contains all of the viral processing elements necessary for the production of replication-incompetent lentivirus. The woodchuck hepatitis virus posttranscriptional regulatory element (WPRE) promotes RNA processing events and enhances nuclear export of viral and transgene RNA, the Rev-response element (RRE), increases viral titers by enhancing the transport of unspliced viral RNA out of the nucleus. A central polypurine tract (cPPT) element increases nuclear importation of the viral genome during target cell infection. In addition to lentiviral elements, pLVX-Puro contains a puromycin resistance gene (Puro^r) under the control of the murine phosphoglycerate kinase (PGK) promoter (P) for the selection of stable transductants. The vector also contains a pUC origin of replication and an *E. coli* ampicillin resistance gene (Amp^r) for propagation and selection in bacteria.

Clontech Laboratories, Inc.
www.clontech.com

REFERENCES

1. Dorigo O et al. (2004) Development of a Novel Helper-Dependent Adenovirus-Epstein-Barr Virus Hybrid System for the Stable Transformation of Mammalian Cells. *J Virol* 78:6556–6566.

2. Gallaher SD, Gil JS, Dorigo O, Berk AJ (2009) Robust In Vivo Transduction of a Genetically Stable Epstein-Barr Virus Episome to Hepatocytes in Mice by a Hybrid Viral Vector. *J Virol* 83:3249–3257.

3. Gil JS, Gallaher SD, Berk AJ (2010) Delivery of an EBV episome by a self-circularizing helper-dependent adenovirus: long-term transgene expression in immunocompetent mice. *Gene Ther* 17:1288–1293.

4. Higgins PJ (1985) Cell cycle compartments of adult mouse hepatocytes identified by flow cytometric analysis of total cellular and nuclear RNA content: Effect of aging on G 1 substates. *Age* 8:122–126.

5. Graf T (2002) Differentiation plasticity of hematopoietic cells. *Blood* 99:3089–3101.

6. Kawabata K, Sakurai F, Koizumi N, Hayakawa T, Mizuguchi H (2006) Adenovirus vector-mediated gene transfer into stem cells. *Mol Pharm* 3:95–103.

7. Gaggar A, Shayakhmetov DM, Lieber A (2003) CD46 is a cellular receptor for group B adenoviruses. *Nat Med* 9:1408–12.

8. Herlitschka SE, Falkner FG, Schlokat U, Dorner F (1996) Overexpression of human prothrombin in permanent cell lines using a dominant selection/amplification fusion marker. *Protein Expr Purif* 8:358–64.

9. Shimizu N, Hashizume T, Shingaki K, Kawamoto J (2003) Amplification of Plasmids Containing a Mammalian Replication Initiation Region Is Mediated by Controllable Conflict between Replication and Transcription. *Cancer Res* 63:5281–5290.

10. Tate CG et al. (2003) Comparison of seven different heterologous protein expression systems for the production of the serotonin transporter. *Biochim Biophys Acta* 1610:141–53.

11. Hahn CS, Hahn YS, Braciale TJ, Rice CM (1992) Infectious Sindbis virus transient expression vectors for studying antigen processing and presentation. *Proc Natl Acad Sci U S A* 89:2679–83.

12. Frolov I et al. (1996) Alphavirus-based expression vectors: strategies and applications. *Proc Natl Acad Sci U S A* 93:11371–7.

13. Boorsma M et al. (2000) A temperature-regulated replicon-based DNA expression system. *Nat Biotechnol* 18:429–32.

14. Boorsma M et al. (2002) Bioprocess applications of a Sindbis virus-based temperature-inducible expression system. *Biotechnol Bioeng* 79:602–9.

15. Hahn YS, Strauss EG, Strauss JH (1989) Mapping of RNA- temperature-sensitive mutants of Sindbis virus: assignment of complementation groups A, B, and G to nonstructural proteins. *J Virol* 63:3142–50.

16. Agapov EV et al. (1998) Noncytopathic Sindbis virus RNA vectors for heterologous gene expression. *Proc Natl Acad Sci U S A* 95:12989–94.

17. Graham FL, Prevec L (1991) Manipulation of adenovirus vectors. *Methods in molecular biology* 7:109–128.

18. Ng P, Graham FL (2002) Construction of first-generation adenoviral vectors. *Methods Mol Med* 69:389–414.

19. Parks RJ et al. (1996) A helper-dependent adenovirus vector system: removal of helper virus by Cre-mediated excision of the viral packaging signal. *Proc Natl Acad Sci U S A* 93:13565–70.

20. Tollefson AE, Kuppuswamy M, Shashkova EV, Doronin K, Wold WSM (2007) in *Adenovirus Methods and Protocols*, Methods in Molecular Medicine., eds Wold WSM, Tollefson AE, Walker JM (Humana Press), pp 223–235. Available at: http://www.springerlink.com/content/h11340k42722156g/abstract/ [Accessed November 3, 2012].

21. Ng P, Beauchamp C, Evelegh C, Parks R, Graham FL (2001) Development of a FLP/frt system for generating helper-dependent adenoviral vectors. *Mol Ther* 3:809–815.

22. Ng P, Parks RJ, Graham FL (2002) Preparation of helper-dependent adenoviral vectors. *Methods Mol Med* 69:371–88.

23. Umana P et al. (2001) Efficient FLPe recombinase enables scalable production of helper-dependent adenoviral vectors with negligible helper-virus contamination. *Nat Biotechnol* 19:582–5.

24. Gallaher SD (2007) In vivo delivery and persistence in mouse of an episomal expression cassette by a helper dependent adenovirus -- Epstein-Barr virus hybrid gene therapy vector. Available at: http://search.proquest.com/docview/304872334/abstract/13A2E44847D6A447447/1?accountid=14512 [Accessed November 4, 2012].

25. Balamotis MA, Huang K, Mitani K (2004) Efficient delivery and stable gene expression in a hematopoietic cell line using a chimeric serotype 35 fiber pseudotyped helper-dependent adenoviral vector. *Virology* 324:229–237.

26. Bredenbeek PJ, Frolov I, Rice CM, Schlesinger S (1993) Sindbis virus expression vectors: packaging of RNA replicons by using defective helper RNAs. *J Virol* 67:6439–6446.

27. Ehrengruber MU, Lundstrom K (2001) in *Current Protocols in Neuroscience* (John Wiley & Sons, Inc.). Available at: http://onlinelibrary.wiley.com/doi/10.1002/0471142301.ns0422s41/abstract [Accessed November 2, 2012].

28. Hernandez R, Sinodis C, Brown DT (2005) in *Current Protocols in Microbiology* (John Wiley & Sons, Inc.). Available at: http://onlinelibrary.wiley.com/doi/10.1002/9780471729259.mc15b01s16/abstract [Accessed November 7, 2012].

29. Stewart SA, Poon B, Jowett JBM, Xie Y, Chen ISY (1999) Lentiviral delivery of HIV-1 Vpr protein induces apoptosis in transformed cells. *PNAS* 96:12039–12043.

30. Naldini L, Blömer U, Gage FH, Trono D, Verma IM (1996) Efficient transfer, integration, and sustained long-term expression of the transgene in adult rat brains injected with a lentiviral vector. *PNAS* 93:11382–11388.

31. Miyoshi H, Blömer U, Takahashi M, Gage FH, Verma IM (1998) Development of a Self-Inactivating Lentivirus Vector. *J Virol* 72:8150–8157.

32. Bubeck P, Winkler M, Bautsch W (1993) Rapid cloning by homologous recombination in vivo. *Nucleic Acids Res* 21:3601–3602.

33. Ng P, Evelegh C, Cummings D, Graham FL (2002) Cre levels limit packaging signal excision efficiency in the Cre/loxP helper-dependent adenoviral vector system. *J Virol* 76:4181–9.

34. Schaft J, Ashery-Padan R, van der Hoeven F, Gruss P, Stewart AF (2001) Efficient FLP recombination in mouse ES cells and oocytes. *Genesis* 31:6–10.

35. Schnell JR, Dyson HJ, Wright PE (2004) Structure, Dynamics, and Catalytic Function of Dihydrofolate Reductase. *Annual Review of Biophysics and Biomolecular Structure* 33:119–140.

36. Alt FW, Kellems RE, Bertino JR, Schimke RT (1978) Selective multiplication of dihydrofolate reductase genes in methotrexate-resistant variants of cultured murine cells. *Journal of Biological Chemistry* 253:1357–1370.

37. Schimke RT (1988) Gene amplification in cultured cells. *J biol Chem* 263. Available at: http://www.jbc.org/content/263/13 [Accessed November 4, 2012].

38. Brown PC, Tlsty TD, Schimke RT (1983) Enhancement of methotrexate resistance and dihydrofolate reductase gene amplification by treatment of mouse 3T6 cells with hydroxyurea. *Mol Cell Biol* 3:1097–1107.

39. Tlsty TD, Brown PC, Schimke RT (1984) UV radiation facilitates methotrexate resistance and amplification of the dihydrofolate reductase gene in cultured 3T6 mouse cells. *Mol Cell Biol* 4:1050–1056.

40. Goz B, Carl PL, Tlsty TD (1989) 1-beta-D-arabinofuranosylcytosine enhancement of resistance to several antineoplastic drugs in mammalian tissue culture cells. *Molecular pharmacology* 36:360–365.

41. Boorsma M et al. (2003) Alphavirus cDNA-based expression vectors: effects of RNA transcription and nuclear export. *Biotechnol Bioeng* 81:553–62.

42. Horowitz B, Prince AM, Horowitz MS, Watklevicz C (1993) Viral safety of solvent-detergent treated blood products. *Dev Biol Stand* 81:147–161.

43. Garmashova N, Gorchakov R, Frolova E, Frolov I (2006) Sindbis Virus Nonstructural Protein nsP2 Is Cytotoxic and Inhibits Cellular Transcription. *J Virol* 80:5686–5696.

44. Wang KS, Kuhn RJ, Strauss EG, Ou S, Strauss JH (1992) High-affinity laminin receptor is a receptor for Sindbis virus in mammalian cells. *J Virol* 66:4992–5001.

45. Akache B et al. (2006) The 37/67-Kilodalton Laminin Receptor Is a Receptor for Adeno-Associated Virus Serotypes 8, 2, 3, and 9. *J Virol* 80:9831–9836.

46. Routes JM, Metz BA, Cook JL (1993) Endogenous expression of E1A in human cells enhances the effect of adenovirus E3 on class I major histocompatibility complex antigen expression. *J Virol* 67:3176–3181.

47. Makrides S, Chitpatima ST, Bandyopadhyay R, Brawerman G (1988) Nucleotide sequence for a major messenger RNA for a 40 kilodalton polypeptide that is under translational control in mouse tumor cells. *Nucleic Acids Res* 16:2349.

48. Takata Y, Kondo S, Goda N, Kanegae Y, Saito I (2011) Comparison of efficiency between FLPe and Cre for recombinase-mediated cassette exchange in vitro and in adenovirus vector production. *Genes to Cells* 16:765–777.

49. Mitani K, Graham FL, Caskey CT, Kochanek S (1995) Rescue, propagation, and partial purification of a helper virus-dependent adenovirus vector. *Proc Natl Acad Sci U S A* 92:3854–3858.

50. Fisher KJ, Choi H, Burda J, Chen SJ, Wilson JM (1996) Recombinant adenovirus deleted of all viral genes for gene therapy of cystic fibrosis. *Virology* 217:11–22.

51. Alemany R et al. (1997) Complementation of helper-dependent adenoviral vectors: size effects and titer fluctuations. *J Virol Methods* 68:147–159.

52. Johnstone RW, Loveland BE, McKenzie IF (1993) Identification and quantification of complement regulator CD46 on normal human tissues. *Immunology* 79:341–347.

53. Anderson BD, Nakamura T, Russell SJ, Peng K-W (2004) High CD46 Receptor Density Determines Preferential Killing of Tumor Cells by Oncolytic Measles Virus. *Cancer Res* 64:4919–4926.

54. Ng SK (2012) in *Protein Expression in Mammalian Cells*, Methods in Molecular Biology., eds Hartley JL, Walker JM (Humana Press), pp 161–172. Available at: http://www.springerlink.com/content/nt95356772273632/abstract/ [Accessed November 8, 2012].

55. Kondo S, Takata Y, Nakano M, Saito I, Kanegae Y (2009) Activities of Various FLP Recombinases Expressed by Adenovirus Vectors in Mammalian Cells. *Journal of Molecular Biology* 390:221–230.

56. Loonstra A et al. (2001) Growth inhibition and DNA damage induced by Cre recombinase in mammalian cells. *Proc Natl Acad Sci U S A* 98:9209–9214.

57. Pfeifer A, Brandon EP, Kootstra N, Gage FH, Verma IM (2001) Delivery of the Cre recombinase by a self-deleting lentiviral vector: Efficient gene targeting in vivo. *PNAS* 98:11450–11455.

58. Baba Y, Nakano M, Yamada Y, Saito I, Kanegae Y (2005) Practical range of effective dose for Cre recombinase-expressing recombinant adenovirus without cell toxicity in mammalian cells. *Microbiol Immunol* 49:559–570.

59. Xiong C et al. (1989) Sindbis virus: an efficient, broad host range vector for gene expression in animal cells. *Science (New York, NY)* 243:1188.

60. Strauss JH, Wang KS, Schmaljohn AL, Kuhn RJ, Strauss EG (1994) Host-cell receptors for Sindbis virus. *Archives of virology Supplementum* 9:473.

61. Schwöbel W, Ahl R (1972) Persistence of Sindbis virus in BHK-21 cell cultures. *Archives of Virology* 38:1–10.

62. Wahlfors JJ, Zullo SA, Loimas S, Nelson DM, Morgan RA (2000) Evaluation of recombinant alphaviruses as vectors in gene therapy. *Gene Ther* 7:472–80.

63. Herweijer H et al. (1995) A Plasmid-Based Self-Amplifying Sindbis Virus Vector. *Human Gene Therapy* 6:1161–1167.

64. Cristea IM et al. (2010) Host Factors Associated with the Sindbis Virus RNA-Dependent RNA Polymerase: Role for G3BP1 and G3BP2 in Virus Replication. *J Virol* 84:6720–6732.

65. Costa M, Ochem A, Staub A, Falaschi A (1999) Human DNA helicase VIII: a DNA and RNA helicase corresponding to the G3BP protein, an element of the ras transduction pathway. *Nucleic Acids Res* 27:817–821.

66. Scheffner M, Knippers R, Stahl H (1989) RNA unwinding activity of SV40 large T antigen. *Cell* 57:955–963.

67. Raykov Z, Legrand V, Homann HE, Rommelaere J (2002) Transient suppression of transgene expression by means of antisense oligonucleotides: a method for the production of toxin-transducing recombinant viruses. *Gene therapy* 9:358–362.